AD-A142 405 DIFFUSION AND ELECTRICAL PROPERTIES OF SULFUR IMPLANTED 1/1
IN GALLIUM ARSENIDE(U) ILLINOIS UNIV AT URBANA
COORDINATED SCIENCE LAB S S CHAN JUL 83 R-992
UNCLASSIFIED N00014-79-C-0424 F/G 20/12 NL

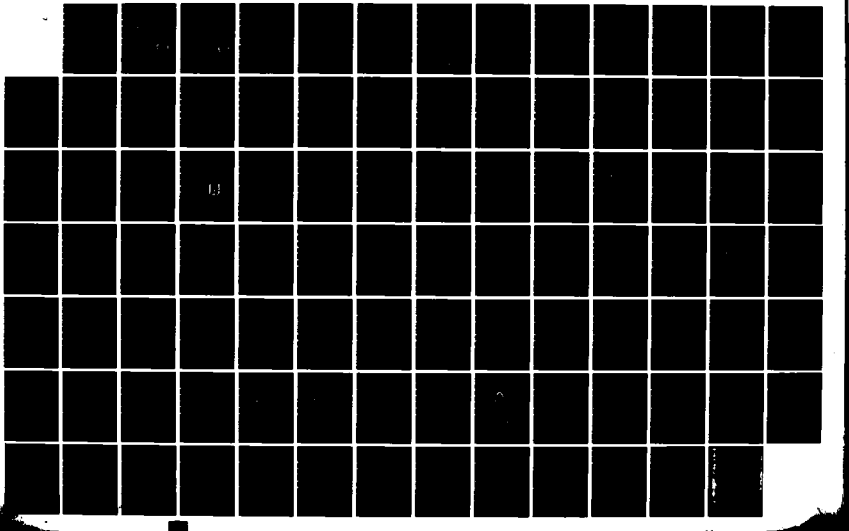

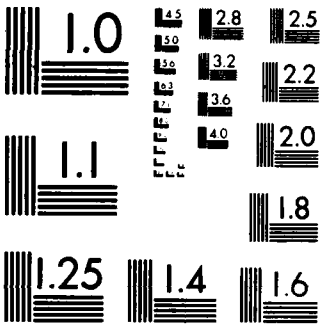

REPORT R-992 JULY 1983 UILU-ENG 83-2213

(12)



# DIFFUSION AND ELECTRICAL PROPERTIES OF SULFUR IMPLANTED IN GALLIUM ARSENIDE

SIU SING CHAN

UNCLASSIFIED

SECURITY CLASSIFICATION OF THIS PAGE (When Data Entered)

| REPORT DOCUMENTATION PAGE | | READ INSTRUCTIONS BEFORE COMPLETING FORM |
|---|---|---|
| 1. REPORT NUMBER | 2. GOVT ACCESSION NO. AD-A142405 | 3. RECIPIENT'S CATALOG NUMBER |
| 4. TITLE (and Subtitle) DIFFUSION AND ELECTRICAL PROPERTIES OF SULFUR IMPLANTED IN GALLIUM ARSENIDE | | 5. TYPE OF REPORT & PERIOD COVERED |
| | | 6. PERFORMING ORG. REPORT NUMBER R-992; UILU-ENG 83-2213 |
| 7. AUTHOR(s) Siu Sing Chan | | 8. CONTRACT OR GRANT NUMBER(s) N00014-79-C-0424 N00014-76-C-0806 |
| 9. PERFORMING ORGANIZATION NAME AND ADDRESS Coordinated Science Laboratory University of Illinois 1101 W. Springfield Ave. Urbana, IL 61801 | | 10. PROGRAM ELEMENT, PROJECT, TASK AREA & WORK UNIT NUMBERS |
| 11. CONTROLLING OFFICE NAME AND ADDRESS Joint Services Electronics Program Office of Naval Research | | 12. REPORT DATE July 1983 |
| | | 13. NUMBER OF PAGES 86 |
| 14. MONITORING AGENCY NAME & ADDRESS(if different from Controlling Office) | | 15. SECURITY CLASS. (of this report) Unclassified |
| | | 15a. DECLASSIFICATION/DOWNGRADING SCHEDULE |

16. DISTRIBUTION STATEMENT (of this Report)

Approved for public release; distribution unlimited.

17. DISTRIBUTION STATEMENT (of the abstract entered in Block 20, if different from Report)



18. SUPPLEMENTARY NOTES

19. KEY WORDS (Continue on reverse side if necessary and identify by block number)

Semiconductors
Dual Implantations
Donors
Sulfur Doping
Impurity Interactions
Defects

20. ABSTRACT (Continue on reverse side if necessary and identify by block number)

The diffusion and electrical properties of implanted sulfur in GaAs have been investigated with secondary ion mass spectrometry (SIMS) and differential resistivity and Hall measurements. Low dose ($7 \times 10^{12}$ cm$^{-2}$, 250 keV) S implants exhibit redistribution behavior upon annealing which approximates gaussian diffusion. Diffusion coefficients estimated from the tails of annealed profiles are high: $9 \times 10^{-13}$ cm$^2$/sec, $1 \times 10^{-12}$ cm$^2$/sec and $8 \times 10^{-12}$ cm$^2$/sec for 700°C, 800°C and 900°C, respectively. The mechanism is believed to be due to defect enhanced diffusion, since these values considerably (continued on reverse side)

DD FORM 1 JAN 73 1473

UNCLASSIFIED

SECURITY CLASSIFICATION OF THIS PAGE (When Data Entered)

20. ABSTRACT (continued)

exceed those reported for S in-diffusion into crystalline GaAs. Increasing the implantation dose decreases the diffusivity of S around the peak of the profile, but penetrating tails are still formed. For electrical measurements, type conversion of the Cr-doped substrates used in this study limits the annealing temperature to 800°C. At this temperature, the electrical activation is at best fair for the low ($7 \times 10^{12}$ $cm^{-2}$, 250 keV) and medium ($7 \times 10^{13}$ $cm^{-2}$, 250 keV) doses, being 26% and 36% respectively. Overall activation efficiency is low (2.3%) for high dose ($10^{15}$ $cm^{-2}$, 250 keV) implants, and although the SIMS profiles reveal little diffusion and a very high S concentration around the original as-implanted peak, almost all of the S in this region is electrically inactive.

The diffusivity of implanted S has been found to be reduced in the presence of a sufficient level of Si doping, whether the latter is introduced during crystal growth or by co-implantation. The reduction is observed up to an annealing temperature of 800°C. However, at 900°C thermal processes again prevail. Dual implants of S and Si have been found to give substantial improvements in peak carrier concentration and activation efficiency as compared to Si implants of an equivalent dose.

Low levels of implantation damage, as produced by $3.5 \times 10^{13}$ $cm^{-2}$, 250 keV Ar co-implants, have been found to result in damage enhanced diffusion of S upon annealing. In the presence of amorphizing Ar co-implants, however, little diffusion is observed up to 900°C. Unfortunately, the electrical activity of the implanted S is entirely lost at the same time. There is some evidence that thermally stable but electrically inactive S-defect complexes are formed which do not diffuse.

# DIFFUSION AND ELECTRICAL PROPERTIES OF SULFUR IMPLANTED IN GALLIUM ARSENIDE

BY

SIU SING CHAN

B.S., University of Illinois, 1976
M.S., University of Illinois, 1980

THESIS

Submitted in partial fulfillment of the requirements
for the degree of Doctor of Philosophy in Electrical Engineering
in the Graduate College of the
University of Illinois at Urbana-Champaign, 1983

Urbana, Illinois

# DIFFUSION AND ELECTRICAL PROPERTIES OF SULFUR IMPLANTED IN GALLIUM ARSENIDE

Siu Sing Chan, Ph.D.
Department of Electrical Engineering
University of Illinois at Urbana-Champaign, 1983

The diffusion and electrical properties of implanted sulfur in GaAs have been investigated with secondary ion mass spectrometry (SIMS) and differential resistivity and Hall measurements. Low dose ($7 \times 10^{12}$ $cm^{-2}$, 250 keV) S implants exhibit redistribution behavior upon annealing which approximates gaussian diffusion. Diffusion coefficients estimated from the tails of annealed profiles are high: $9 \times 10^{-13}$ $cm^2/sec$, $1 \times 10^{-12}$ $cm^2/sec$ and $8 \times 10^{-12}$ $cm^2/sec$ for 700°C, 800°C and 900°C respectively. The mechanism is believed to be due to defect enhanced diffusion, since these values considerably exceed those reported for S in-diffusion into crystalline GaAs. Increasing the implantation dose decreases the diffusivity of S around the peak of the profile, but penetrating tails are still formed. For electrical measurements, type conversion of the Cr-doped substrates used in this study limits the annealing temperature to 800°C. At this temperature, the electrical activation is at best fair for the low ($7 \times 10^{12}$ $cm^{-2}$, 250 keV) and medium ($7 \times 10^{13}$ $cm^{-2}$, 250 keV) doses, being 26% and 36% respectively. Overall activation efficiency is low (2.3%) for high dose ($10^{15}$ $cm^{-2}$, 250 keV) implants, and although the SIMS profiles reveal little diffusion and a very high S concentration around the original as-implanted peak, almost all of the S in this region is electrically inactive.

The diffusivity of implanted S has been found to be reduced in the presence of a sufficient level of Si doping, whether the latter is introduced during crystal growth or by co-implantation. The reduction is observed up to an annealing temperature of 800°C. However, at 900°C thermal processes again prevail. Dual implants of S and Si have been found to give substantial improvements in peak carrier concentration and activation efficiency as compared to Si implants of an equivalent dose.

Low levels of implantation damage, as produced by $3.5 \times 10^{13}$ $cm^{-2}$, 250 keV Ar co-implants, have been found to result in damage enhanced diffusion of S upon annealing. In the presence of amorphizing Ar co-implants, however, little diffusion is observed up to 900°C. Unfortunately, the electrical activity of the implanted S is entirely lost at the same time. There is some evidence that thermally stable but electrically inactive S-defect complexes are formed which do not diffuse.

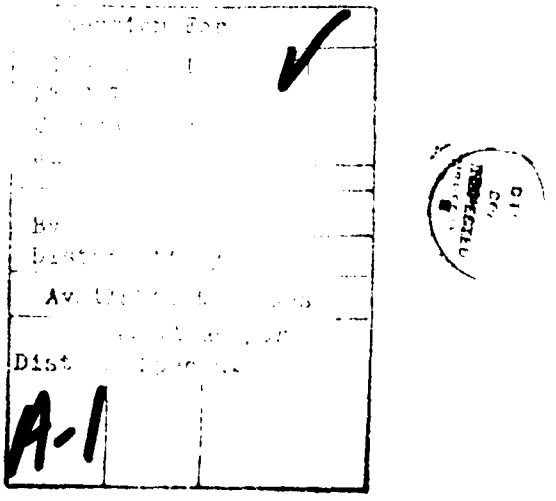

# ACKNOWLEDGEMENTS

The author wishes to express his gratitude to Professor B. G. Streetman for his continued support of this work. He is also deeply indebted to Professor K. Hess for making available facilities which have been crucial.

He also wishes to extend his heartfelt thanks to J. E. Baker and Dr. D. Reed, who have been instrumental in obtaining the SIMS data in this work. Their generosity with their time and expertise is deeply appreciated.

He is grateful to Honeywell, Hughes and Dr. C. G. Kirkpatrick of Rockwell for providing the semi-insulating GaAs used in this work. He also wishes to acknowledge Professor H. Morkoc of the University of Illinois and Professor W. Laidig of North Carolina State University for growing the MBE samples used in this study.

The author wishes to thank his colleagues for helpful discussions, technical assistance and a supportive environment crucial for learning: Dr. M. Keever, Dr. J. D. Oberstar, Dr. M. J. Helix, Dr. K. J. Soda, Dr. J. Y. Tang, Dr. D. S. Day, B. S. Seymour, S. Banerjee, M. Artaki, P. A. Martin, K. Brennan and T. Wang.

The excellent technical services of the Coordinated Science Laboratory are much appreciated. Special thanks are due to O. E. Gardner, whose expertise in electronics has been of immense help to keep the ion implanter and other crucial equipment operable. Thanks are also due to L. Bandy, R. Bales, G. Bouck, W. Beaulin, N. Vassos, W. Lawrence, R. MacFarlane and R. Gladin for their outstanding assistance.

Last, but not least, the author wishes to express his sincere appreciation to his parents and his wife for their constant encouragement and support.

TABLE OF CONTENTS

# 1. INTRODUCTION

As the need for high speed devices and circuits continues to grow, GaAs has received increasing attention as a viable (both technologically and economically) electronic material complementary to Si. The advantages of GaAs lie in its much higher electron mobility and its compatibility with optoelectronic devices. The merits of a planar process have been well demonstrated in Si technology, and in the course of the development of a similar process for GaAs, ion implantation has emerged as an indispensable tool.

Ion implantation is inherently a much more precise and controllable method of selective semiconductor doping than diffusion. To attain the degree of line-width control necessary for high speed or high density devices, ion implantation is a prerequisite. Besides, many useful dopants in GaAs cannot be introduced readily by diffusion because of material constraints.

In spite of its importance in the fabrication of devices which take advantage of the high electron mobility of GaAs, donor implantation in GaAs has not found as much success as acceptor implantations. In order to avoid amphoteric tendencies and possible self-compensation mechanisms, it is generally best to use a column VI element. Unfortunately, S, the lightest column VI donor and therefore the most suitable species for implantation from the viewpoint of projected range control and minimizing radiation damage, has been plagued with redistribution problems during post-implantation annealing as will be discussed in the following chapter. It is the purpose of this study to characterize the diffusion of implanted S in GaAs and its subsequent electrical characteristics so as to understand its applicability in device fabrication.

# 2. BACKGROUND AND OVERVIEW

## 2.1. Implantation Substrates

The best device characteristics and reproducibility are obtained by implantation into high purity, high resistivity layers grown epitaxially on a GaAs substrate. However, despite much work in the area of crystal growth, it is still difficult to produce high quality epitaxial layers on a high-volume production basis. As a result, direct implantation into substrate quality semi-insulating material is gaining popularity as an alternative.

Until fairly recently, most GaAs substrate material has been grown by the horizontal Bridgeman method, where the initial charge of Ga and As and the growing boule are contained in a quartz boat. An unintended reaction between Ga and the quartz results in significant levels of n-type Si doping in the resulting GaAs boule, which must be compensated by the addition of a small amount of Cr to the original Ga charge, to a minimum level equal to the anticipated Si doping [1].

The use of Cr doping to obtain semi-insulating GaAs substrates has some drawbacks. The fairly significant levels of Cr ($10^{16}$- $10^{17}$ $cm^{-3}$) cause a reduction in carrier mobility. In addition, Cr undergoes redistribution upon annealing, and the resulting Cr profiles vary according to the annealing conditions as well as the distribution of defects associated with the implant [2-6]. The redistribution often results in the formation of surface conductive layers due to the depletion of Cr in surface regions to levels below that of the background dopants. In the case of substrates with Cr concentration above its solubility limit at the annealing temperature and in the presence of an encapsulant,

such redistribution has been attributed by Eu et al. [3] to the generation of dislocations at the encapsulant-GaAs interface due to thermal expansion mismatch. These dislocations then serve as nucleation sites leading to Cr precipitation and a subsequent concentration gradient for the Cr which is still in solid solution. The net result is the formation of a Cr depletion region ($\sim$ 1 μm) near the GaAs surface and an accumulation of Cr precipitates at the surface. Residual defects due to incomplete annealing of implantation damage can also serve as additional nucleation sites, giving rise to local accumulations of Cr (due to precipitates) within the depletion region [4]. Kanber et al. reported that by using capless annealing in a $H_2$- $As_4$ ambient and a sufficiently high temperature to eliminate residual implantation damage, Cr redistribution can be completely avoided [4]. An alternative view by Vasudev et al. [5] contends that Cr redistribution is primarily due to gettering by defects, with no particular reference to solid solubility, and that surface defects always occur as a result of annealing, even under capless conditions with As overpressure [7,8]. Cr is gettered by surface defects and residual implantation damage until these are saturated, causing Cr depletion in other regions.

The problem of Cr redistribution is often circumvented by using only "qualified" material for device processing. The procedure of "qualifying" an ingot consists of taking slices from the top and bottom of the ingot, implanting inert gas ions of a similar mass and dose as the intended dopant implants, and annealing the test slices at the same temperature as device processing would require. If no subsequent surface conductivity is found, the Cr redistribution, if any, is not serious enough to affect device characteristics, and the ingot is "qualified".

The problems associated with Cr compensation has spurred efforts which led to the success of growing semi-insulating material with no intentional Cr doping. This is done by Czochralski growth from a melt encapsulated with liquid $B_2O_3$ to prevent As loss in a pyrolytic boron nitride crucible [9-11]. In this so-called LEC (Liquid Encapsulated Czochralski) method, high purity Ga and As are compounded in situ in the growth crucible to form GaAs. Included with the Ga and As elemental charges is a pellet of $B_2O_3$. As the temperature of the crucible is raised, the $B_2O_3$ melts first (melting point $\sim$ 450°C) and encapsulates the rest of the charge. The molten $B_2O_3$ in conjunction with a high pressure $N_2$ ambient prevents As loss during the compounding stage and the subsequent growth stage. Compounding starts at $\sim$ 700°C and when it is complete, a GaAs seed crystal is dipped into the resulting melt and pulled as in a normal Czochralski process. The total avoidance of quartz in the compounding and growth apparatus eliminates the major source of unintentional Si-doping. The predominant shallow residual impurity in this case is C, and the compensation mechanism is apparently due to a deep donor level labeled EL2 with an activation energy of $\sim$ 0.76 eV [12]. The concentration of EL2 depends strongly on the melt stoichiometry during growth [12], and its origin is probably the antisite defect $As_{Ga}$ [13]. However, EL2 also outdiffuses in a similar manner as Cr [14], and only material grown from slightly As-rich melts remains semi-insulating after prolonged heat treatment [15]. Another aspect of concern is the dislocation density (measured by the etch pit density after etching in hot KOH), which is much higher for LEC than in Bridgeman material. The dislocation density is generally at a minimum in the low $10^4$ $cm^{-2}$ range in a concentric annular region at about half radius, and

increases both towards the center and the edge of the wafer to around $10^5$ $cm^{-2}$ [1]. Reports concerning the effects of the dislocation density distribution on the uniformity of device characteristics across the wafer have been conflicting [16-18].

## 2.2. Donors in GaAs

The common shallow donors in GaAs are Si, Sn (column IV) and S, Se, Te (column VI). Sn and Te, being rather heavy, have very limited projected ranges when ion-implanted, and therefore are not commonly used. Most of the early work was focused on Se, which is fairly heavy but still has an appreciable projected range ($\sim$ 0.14 μm at 400 keV). Se has the advantage of being a column VI element, and therefore has no amphoteric effects. In addition, it has a low diffusion coefficient and does not undergo much redistribution during annealing [19]. However, in order to obtain good electrical activation, the implants are generally done at elevated temperatures ($\sim$ 300°C) [20]. Rutherford backscattering (RBS) data on hot Te implants have revealed that by raising the substrate temperature above 150°C, radiation damage can be decreased sharply. Doses that would have amorphized the substrate surface at room temperature result in a level of damage that is only barely measurable by RBS in a hot implant [21]. However, a similar density of compensating defects is still formed [22]. The improvement in activation is due to a larger fraction of the implanted dopant getting to substitutional sites in a less severely damaged crystal. It appears that once the implanted ions are associated with a high density of radiation damage, they are not easily released to become substitutional even after a high temperature anneal [22,23]. Hot implants result in higher percentage improvements of the activation efficiency of heavy

ions (e.g., Se, Te, Sn) than lighter ions (e.g., Si), since the former create more radiation damage [20,24]. Implanting at high temperatures poses some processing complications and precludes the use of photoresist as a mask for selective implantations.

Si, the lightest donor impurity available, is best suited for implantation since it results in the least amount of radiation damage and also the largest range of implantation depths for a given maximum acceleration voltage. In addition, the redistribution of implanted Si during annealing is small, the diffusion coefficient being less than $6 \times 10^{-14}$ $cm^2/sec$ [25]. However, being a column IV element, it exhibits amphoteric tendencies even though it is predominantly a donor. Indeed, GaAs p-n junctions have been fabricated by liquid phase epitaxy in which Si is the dominant dopant on both sides of the junction [26-28]. Implanted Si shows very good electrical activation (> 70%) for low and medium dose implants (< $10^{13}$ $cm^{-2}$) [29,30]. However, at high doses (> $10^{14}$ $cm^{-2}$) the activation efficiencies are significantly lower than those obtainable with similar Se implants [20,29], an observation which is probably due in part to increased self-compensation at high concentrations as a result of the amphoteric tendency of Si.

It would appear from the foregoing discussion that S will be a good alternative to Si and Se when heavily doped n-type implanted layers are needed. With a slightly heavier mass than Si, S will have comparable projected ranges, creates less radiation damage than Se, and will not have the amphoteric tendency of Si. Unfortunately, results of early work show that S undergoes considerable redistribution upon post-implantation annealing and only fair to poor electrical activation [24,31-35]. Some of the disappointing results could have been due to encapsulants of

insufficient quality or annealing temperatures that had been too low. Some more recent efforts using capless annealing in an $H_2$- $As_4$ atmosphere indicate less redistribution [4,36], while other reports using dielectric encapsulation [37,38] continue to describe severe redistribution. Electrical activation in the more recent reports is fairly good for doses up to $10^{13}$ $cm^{-2}$ but falls off very rapidly at the higher doses [30,38,39].

## 2.3. Anomalous Redistribution of Ion-Implanted Impurities

Although the dopant distribution should ideally remain unchanged during annealing (thermal, laser or electron beam) in order to fully realize the advantages of ion implantation, some redistribution by thermal diffusion invariably occurs. It is important to understand the redistribution processes to successfully apply ion implantation to device fabrication.

The discussion here will be limited to redistribution in the cases of thermal annealing. Many factors are present in an implanted layer which often render the redistribution process non-Fickian. The first is the non-uniform distribution of above-equilibrium concentrations of vacancies and self-interstitials. High vacancy concentrations tend to assist substitutional diffusion. In the case of impurities which can exist in the crystal in both substitutional or interstitial forms, the presence of a high concentration of self-interstitials in the implanted region will force a larger fraction of the impurity to become interstitial. Since interstitial diffusion usually proceeds orders of magnitude faster than substitutional diffusion, there will be a local depletion of the impurity from the implanted region in such two-stream diffusion processes [40]. Alternatively, for impurities in III-V compounds diffusing with interstitial-substitutional mechanisms on one sublattice, it is

possible to suppress the formation of impurity interstitials by creating a net excess of vacancies on that sublattice with an implantation of the constituent atoms of the other sublattice [40,41]. Often, a retardation of impurity diffusion will result, since purely substitutional processes are usually much slower. Diffusion of vacancies and self-interstitials because of their own spatial gradients can further modify impurity profiles [40].

A second factor which may lead to anomalous redistribution is the possibility of the formation of vacancy-impurity complexes which may have vastly different diffusivities. Diffusing vacancies may also "carry" impurity atoms along by the formation of complexes. Precipitation or trapping at locations of high defect density is also possible.

A third factor is the possibility of the formation of complexes between the implanted impurity and other impurities already present in the crystal. Here the redistribution characteristics are governed by the chemical affinities of the impurities for one another and the diffusivity of the resulting complex.

In GaAs, many impurities have been found to have significantly altered diffusion properties when ion-implanted, some of the causes of which are still undetermined. Some representative results found in the literature are listed below:

1) MBE-grown Be-doping in GaAs has a diffusion coefficient of $\sim 0.5 - 1 \times 10^{13}$ cm$^2$/sec at 900°C, which is largely concentration independent. On the other hand, ion-implanted Be in high purity GaAs has a diffusion coefficient which is proportional to the square of the Be concentration. At 900°C and an implanted Be concentration of $2 - 3 \times 10^{19}$ cm$^{-3}$, its value

is two orders of magnitude higher than that of MBE-grown Be-doping at the same temperature and concentration [42]. The change in diffusion behavior is not entirely damage related, however. Irradiation of Be-doped MBE GaAs with $He^+$ ions and subsequent annealing fail to cause any significant changes in the diffusion behavior of Be [42].

2) Implanted Se has been found to exhibit radiation-enhanced diffusion when the substrate temperature is maintained above 150°C during implantation [43]. The profile broadening is observed even without any post-implantation annealing and is largely independent of substrate type, implantation dose, time and energy. Raising the substrate temperature above the 150°C threshold only brings about small increases in profile broadening. In some respects the effect is similar to radiation enhancement of B diffusion in Si at low temperature, which is governed by vacancy migration during the irradiation of the substrate [44].

3) Zn, which is believed to be transported in GaAs and $GaAs_{0.6}P_{0.4}$ by an interstitial-substitutional mechanism, has been found to have a greatly retarded diffusion coefficient when it is co-implanted with As or P in $GaAs_{0.6}P_{0.4}$ than when it is co-implanted with Ga or implanted alone [45]. The As or P introduced by the co-implant is believed to cause a greater fraction of the implanted Zn to occupy substitutional lattice positions where it diffuses much more slowly.

4) A high density of radiation damage near the projected range of a heavy dose implant into Cr-doped GaAs can cause a local accumulation of Cr to form when the sample is subsequently annealed.

The cause of the Cr accumulation is a precipitation or gettering effect of a high density of defects as described in section 2.1. Analogous effects of radiation damage in Si have been used for Au gettering [46].

5) Zn indiffusing from an external vapor source at 700°C has been observed to diffuse towards a deep $H^+$ pre-implant with an enhanced rate and ultimately forms a buried accumulation which significantly exceeds the concentration of Zn anywhere in the sample. The Zn accumulation has a profile which closely resembles the shape of the $H^+$ pre-implant and is absent if $He^+$ has been used instead of $H^+$ [47]. It appears that the accumulation is the result of an Zn-H interaction.

6) Cr-doped GaAs which is oxygen-implanted and subsequently annealed has a Cr distribution with a local accumulation which is correlated with the oxygen distribution. The local Cr accumulation is absent if the oxygen implant is replaced by a Ne implant of the same dose and energy [48]. It appears that a Cr-O coupling disturbs the usual Cr redistribution process and causes the formation of the local Cr buildup.

Because of the multiplicity of ways in which the impurity redistribution processes can be anomalously affected, they must be thoroughly studied along with their electrical effects in order to appropriately design device fabrication processes. Some anomalous effects may even lend themselves to advantageous applications.

## 2.4. Motivation of This Study

Although S is a simple substitutional donor in GaAs, there is some evidence that it diffuses via a complex involving the gallium divacancy ($V_{Ga}V_{Ga}$) [49]. Concentration dependent effects have also been observed in surface indiffusion experiments [49]. Wilson and Jamba [37] showed that S redistribution during post-implantation annealing is much reduced if the GaAs substrate is pre-amorphized by equal doses of Ga and As ions before the S implantation. It appears that the diffusion properties of implanted S need further study, especially in the context of interactions with defects and the subsequent electrical properties, in order to ascertain its applicability to device fabrication.

It has been pointed out by Yoder [50] that the redistribution of implanted S appears to be inhibited by the presence of an equal or larger concentration of implanted Si. The total activation efficiency and carrier mobility are improved at the same time [51]. Since S donors occupy As sites while Si donors occupy Ga sites, it is conceivable that the presence of S enhances the fraction of Si that becomes donors by depleting the availability of As vacancies for the formation of Si acceptors. Yoder further suggests that the reduction of S redistribution is due to the formation of a nearest-neighbor complex with Si which is too large to diffuse [50].

More data are needed to confirm the existence of the proposed S-Si complex and its diffusion properties. Since the S and Si impurities have to be sufficiently close to one another for complex formation, the concentration dependence of any possible interactions has to be investigated. Finally, the thermal stability and electrical characteristics of the proposed complex must be determined to ascertain possible applications.

# 3. EXPERIMENTAL PROCEDURES

## 3.1. Scope of This Study

The diffusion of implanted S in GaAs is studied under the following conditions:

1) S implanted alone
2) Implanted S in the presence of Si co-implants
3) S implanted into Si-doped epitaxial layers
4) Implanted S in the presence of Ar co-implants.

Si has been chosen for studying possible impurity interactions with implanted S because of favorable indications from the work of Oakes and Degenford [51], which is also pointed out by Yoder [50]. The Ar co-implants are used to study the effects of various degrees of crystal damage on S diffusion.

Most of the implantation substrates used are semi-insulating Cr-doped Bridgeman or LEC wafers with Cr concentrations of approximately $2 \times 10^{16}$ $cm^{-3}$. Qualification tests with $10^{14}$ $cm^{-2}$ Ar bombardment and rf plasma $Si_3N_4$ encapsulation indicate no surface conductivity up to 800°C annealing. Some conductivity begins to appear at 850°C and type conversion is severe at 900°C. Si-doped epitaxial layers used in this study are MBE grown on Si-doped substrates.

Atomic distributions of S and other chemical species are measured using secondary ion mass spectrometry (SIMS). Electrical activation and mobility data are taken whenever they complement the SIMS data.

## 3.2. Ion Implantation

Implantations are done with an Accelerators, Inc. model 300-MP ion implanter. S and Si ion beams are generated by $SF_6$ and $SiF_4$ plasmas

respectively in a cold cathode source. Whenever possible, the $^{34}S$ isotope instead of the more abundant $^{32}S$ isotope is used to avoid $O_2$ interference in SIMS measurements. Ar beams are obtained with an Ar plasma in a hot cathode source. All implants are done at room temperature with the substrates tilted 7° from the ion beam normal to avoid channeling effects.

As an ion impinges on a substrate, the stopping mechanisms are characterized by the nuclear stopping power $S_{N,k}(E)$ and the electronic stopping power $S_{e,k}(E)$ of each type of elements of the substrate (k being the label for various types of elements). Both the nuclear and electronic stopping powers are functions of the incident ion energy.

Nuclear stopping to a good approximation can be considered as independent classical elastic scattering processes due to the screened Coulomb potential of lattice nuclei. The result of the energy transfer from incident ions to lattice nuclei is the displacement of the latter from their equilibrium positions, i.e., radiation damage. Electronic stopping is due to the interaction between the incident ion and the electronic structure of the target. The electrons may be approximated by a free electron gas, and the incident ion loses energy by the excitation of plasma resonances [52]. Alternatively, the energy transfer may be viewed as the formation and ultimate breakup of "quasi-molecules" as the incident ions and target atoms exchange outer electrons and attempt to form molecules [53]. Electronic stopping does not result in radiation damage. Nuclear stopping dominates over electronic stopping for heavy ions and at low ion energies, while the reverse is true for light ions and at high ion energies.

The distribution of implanted impurities is well approximated in most cases by the theory of Lindhard, Scharff and Schiott (LSS) [54].

Here the target is considered to be amorphous with a uniform distribution of each type of host element. The spatial rate of energy loss is given by

$$\frac{dE}{dx} = - \sum_k N_k [S_{N,k}(E) + S_{e,k}(E)]$$

where $N_k$ is the density of the kth type of substrate element. For crystalline substrates, the amorphous approximation is quite good if the crystal is tilted a few degrees away from major crystal axes, where ion channels occur because of the periodic structure of the crystal. The total distance R traveled before an ion is stopped is given by

$$R = \int_o^E \frac{dE}{\sum_k N_k [S_{N,k}(E) + S_{e,k}(E)]}$$

However, the quantity of interest is usually the distance traveled perpendicular to the substrate surface, or the projected range $R_p$. Since the stopping of the ions is essentially a random process, there is a spread (standard deviation $\Delta R_p$) in their spatial distribution. The distribution profile in LSS theory can be approximated by a gaussian

$$N(x) = \frac{N_\square}{\Delta R_p \sqrt{2\pi}} \exp\left[ - \frac{(x - R_p)^2}{2\Delta R_p^{\,2}} \right]$$

where $N_\square$ is the implantation dose (i.e., ions/cm$^2$). The peak concentration of the distribution is given by

$$N_p = \frac{N_\square}{\Delta R_p \sqrt{2\pi}} \simeq \frac{0.4 N_\square}{\Delta R_p}$$

Values of $R_p$ and $\Delta R_p$ for various ion/substrate combinations at different

ion energies have been tabulated [55].

Acceleration energies for dual implants in this study have been chosen such that the LSS projected ranges approximately overlap. $^{34}S$ implants are done at 250 keV ($R_p$ = 0.193 μm), $^{28}Si$ at 220 keV ($R_p$ = 0.195 μm), and $^{40}Ar$ at 250 keV ($R_p$ = 0.17 μm).

## 3.3. Encapsulation and Annealing

Typical temperatures needed to anneal out radiation damage due to ion implantation in GaAs are in the range of 700°C-900°C. Since unprotected GaAs surfaces undergo severe degradation due to As loss at temperatures starting from 600°C [56], a scheme of surface protection is necessary. Surface degradation can be prevented by annealing in a $H_2$- $As_4$ atmosphere [3,36,57,58], achieving at the same time minimal surface stress and reduced Cr redistribution. However, a more traditional approach is to encapsulate the GaAs surface with an appropriate dielectric. Various schemes of transient annealing with laser beams [59-61], electron beams [62,63] or incoherent radiation [64,65] have also been devised but even in these cases most of the better results are still observed when dielectric encapsulation is used in conjunction.

The two most popular encapsulants are $SiO_2$ and $Si_3N_4$. $SiO_2$ films have the advantages of simple deposition procedures and excellent film adhesion properties. However, it has been demonstrated that $SiO_2$ allows Ga outdiffusion from the GaAs surface upon annealing and creates a deep level detectable by photoluminescence, whereas $Si_3N_4$ preserves the material integrity of GaAs during similar heat treatment [66]. Electrically, ion-implanted p-n junctions fabricated with $SiO_2$ encapsulation have been shown to have orders of magnitude higher leakage currents than

when $Si_3N_4$ is used [67]. $Si_3N_4$ has therefore been chosen as the encapsulant throughout this work.

It is important to avoid oxygen contamination in the process of depositing $Si_3N_4$, since it will lead to the formation of silicon oxynitride, which has many of the undesirable properties of $SiO_2$ [66,67]. A plasma-enhanced chemical vapor deposition method is used to obtain the $Si_3N_4$ caps in this work. The apparatus is shown in Fig. 3.1. The samples to be encapsulated are placed on a resistive heater made from ultra-pure graphite in a pyrex reaction chamber. To ensure the elimination of oxygen contamination of the films, the pyrex chamber is evacuated to pressures below $3 \times 10^{-6}$ torr. Ultra-high purity $N_2$ is then admitted into the chamber from the top at the rate of 50 standard cc per minute (sccm) and an rf plasma is ignited for 15 min. The purpose of this preliminary $N_2$ plasma is to remove any residual air adsorbed on the walls of the chamber by ion bombardment. To avoid bombardment of the sample surfaces at the same time, a stainless steel shutter is extended over the samples by means of a linear motion feedthrough. Protection of the sample surfaces at this stage is necessary for good mechanical adhesion of the deposited films. At the end of the 15 min period, the stainless steel shutter is retracted, and a 2% mixture of $SiH_4$ in ultra-high purity Ar is admitted through the side port via the gas dispersion ring at the rate of 11 sccm. The samples are rapidly heated to 320°C and the rf plasma is again ignited to start the deposition.

The deposition rate as well as the Si:N ratio in the films are functions of the gas flow rates, which are chosen to yield stoichiometric silicon nitride [68]. The typical film thickness used is 0.1 μm, and the deposition time is about 15 min.

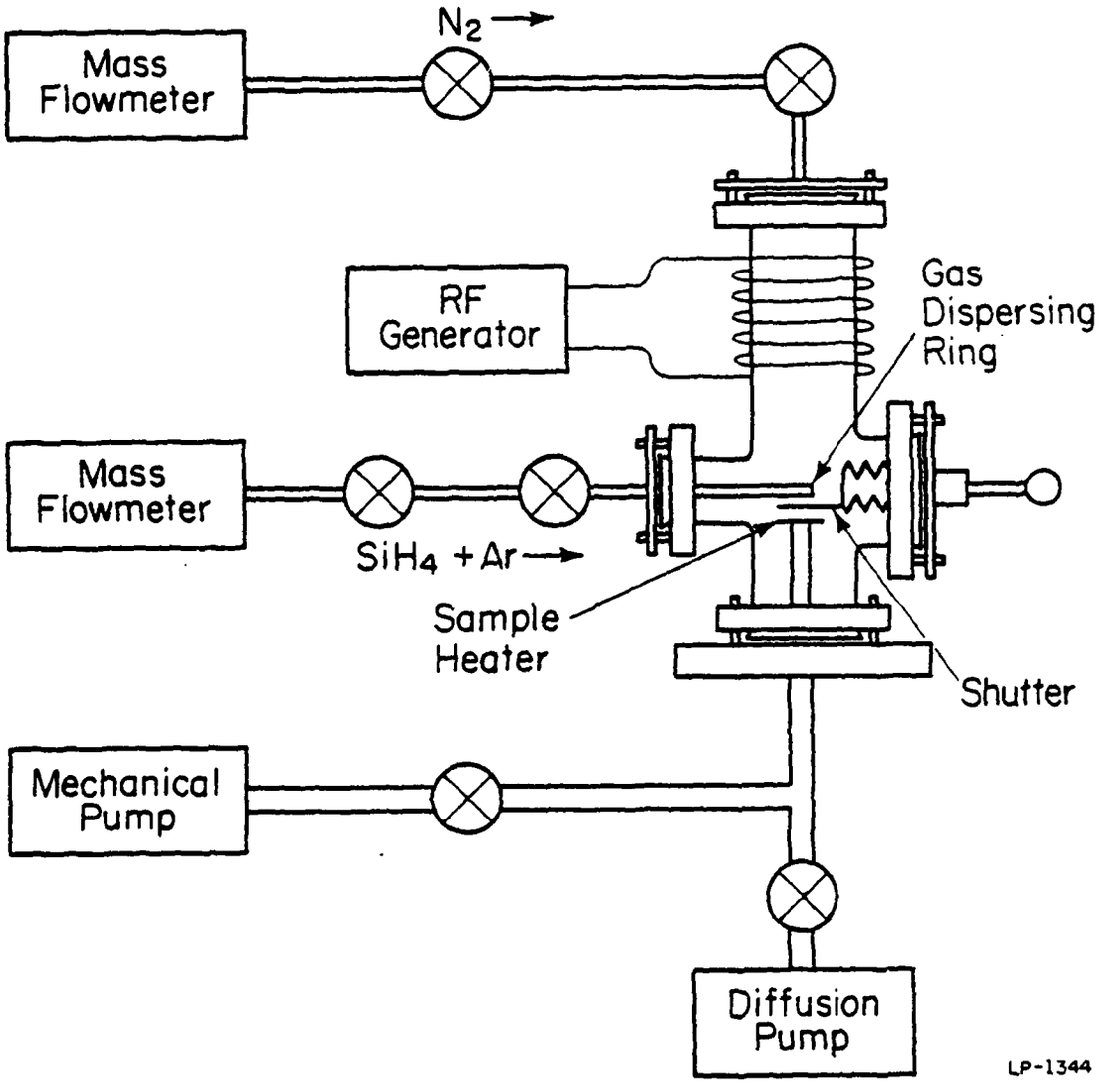


Fig. 3.1 Schematic diagram of the rf-plasma $Si_3N_4$ deposition system [68].

Thermal annealing is done in a 12" TransTemp gold-coated tube furnace in a stream of forming gas (4% $H_2$ in ultra-high purity $N_2$). All anneals in this study are 30 min.

## 3.4. Atomic Profiling

Atomic distributions of an implanted species before and after annealing are measured with secondary ion mass spectrometry (SIMS) using a Cameca IMS-3f, a schematic of which is shown in Fig. 3.2. In this system a beam of primary ions in the 1 - 30 keV range is directed onto the sample surface and causes sputtering. Most of the material ejected from the surface is in the form of neutral atoms, but a fraction of it will be ionized. These secondary ions are extracted by an electrostatic lens and mass analyzed with a magnet. A depth profile is obtained by monitoring the secondary ion intensity as the primary beam sputters a crater into the surface at a constant rate. The depth calibration is obtained by measuring the depth of the crater after the experiment using a surface profiler.

In practice, the primary ion species is chosen to enhance the secondary ion yield of the elements of interest. In the case of electronegative elements which tend to form negative ions, a cesium ($Cs^+$) beam is used [70,71]. In the case of electropositive elements, an $O_2^+$ beam is best [72]. The primary beam is rastered over a much larger area than is needed for analysis, and by proper electronic or mechanical aperturing, only the secondary ions coming from the flat bottom of the crater are analyzed. This is done to eliminate the degradation of depth resolution due to the often non-vertical sides of the crater [70].

In this work, $^{34}S$, $^{32}S$ and $^{29}Si$ are detected using a $Cs^+$ primary

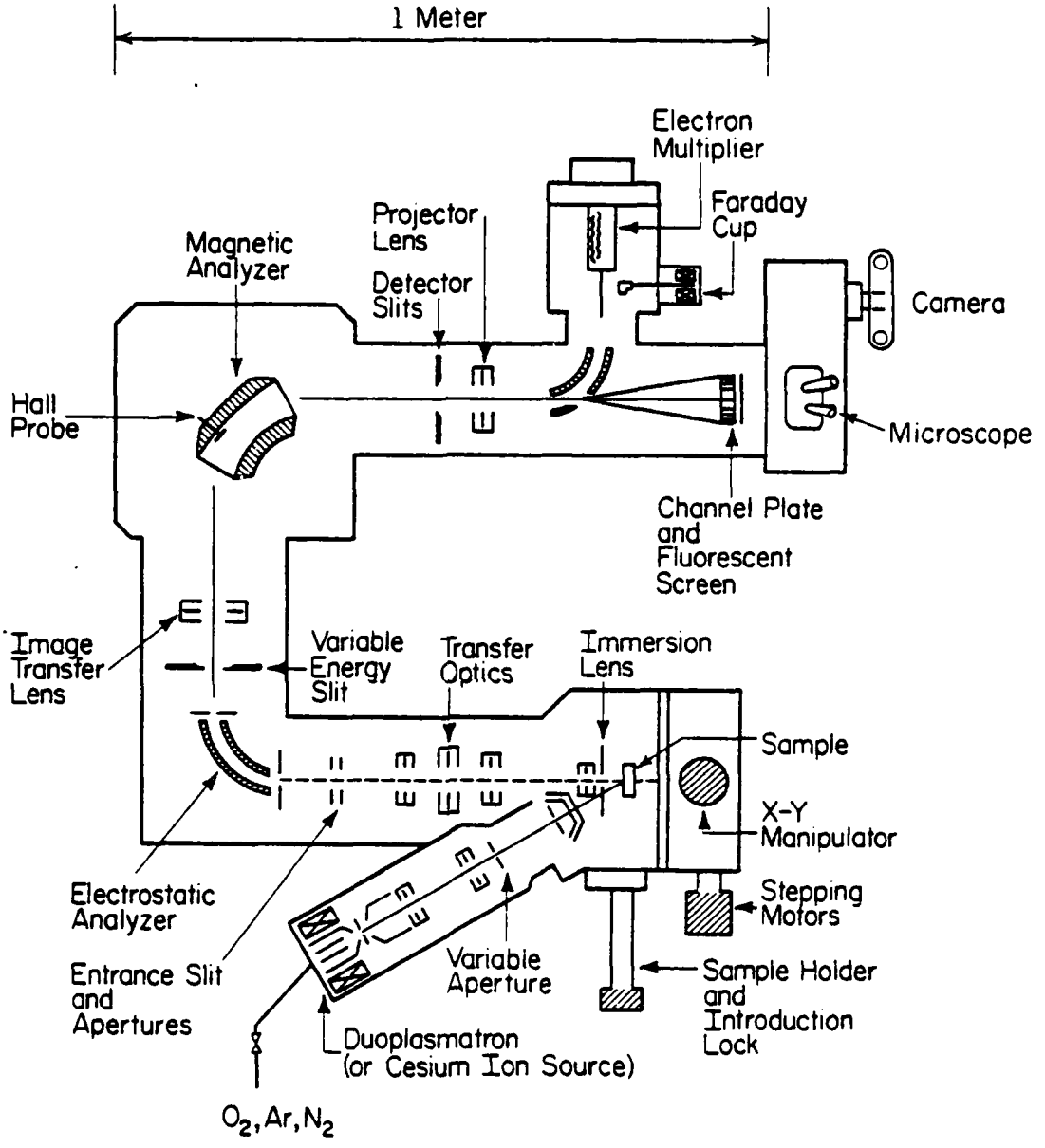


Fig. 3.2 Schematic diagram of the Cameca IMS-3f direct imaging secondary ion mass spectrometer (after Cameca [69]).

beam, and $^{52}Cr$ is detected using an $O_2^+$ beam. The beam is rastered over an area of 250 um × 250 μm. The secondary Ga or As ion count from the substrate matrix is monitored at the same time and found to be quite constant, indicating a uniform sputtering rate. The resulting crater depths are measured with a Sloan Dektak mechanical stylus to an accuracy of ±5-6%. In the case of implanted samples which have undergone no annealing, the calibration constant for converting secondary ion counts to absolute impurity concentrations is obtained by integrating the raw SIMS profile (after correcting for background effects) and setting it equal to the implantation dose. For annealed samples, outdiffusion into the cap is a distinct possibility, and the calibration constants in these cases are obtained from those of unannealed samples by correlating the Ga or As matrix counts. The assumptions made are as follows:
1) since the concentrations of Ga and As are constant for all samples, a change in the matrix count is caused by slight variations in the alignment between the sample and the beam optics as different samples are moved under the primary beam for analysis; 2) such variations in alignment affect all secondary ion counts by the same amount. Hence the calibration constants for annealed samples are obtained by scaling the calibration constant for the unannealed sample by the amount the matrix counts have changed. However, it has been found (for reasons that are still undetermined) that the above assumptions are not always valid, and it is best to adjust the samples until the matrix counts are about the same to obtain consistent results. Cr concentrations are obtained similarly by calibrating against unannealed Cr-implanted samples.

## 3.5. Electrical Profiling

Electrical profiling is done to determine the fraction of the implanted dopant that has become electrically active. This is achieved by a series of resistivity and Hall measurements accompanied by successive layer removal.

### 3.5.1. Sample preparation

The most convenient geometry for resistivity and Hall effect measurements is the van der Pauw geometry [73], in which the sample is a disc of arbitrary shape with four ohmic contacts at arbitrary points on its periphery. In this work the van der Pauw geometry is approximated by a clover-leaf pattern (Fig. 3.3).

Upon removal of the $Si_3N_4$ encapsulant after annealing, a square array of four Au-Sn contact pads (96% Au, 4% Sn) is evaporated onto each sample through a shadow mask. The contacts are annealed in a hydrogen atmosphere for 15 sec at 400°C. By mounting the samples face down on an appropriate stainless steel mask with glycol phthalate, grooves are made between contact pads with an abrasive air jet in a configuration as shown in the inset of Fig. 3.3. Since the deepest conductive layers due to the implants are about 1 μm thick, the grooves made in this fashion always extend well into the semi-insulating substrate. Thus the contact pads are electrically isolated from one another except through the central region of the sample among the four grooves. Since the interior ends of the grooves are very close together, this central region may be considered as a van der Pauw disc, with the contact pads connected by short strips of the implanted layer to its periphery.

Each sample is then mounted with an insulating varnish (GE 7031) on a nylon disc, which fits into a nylon sample holder (Fig. 3.3). The

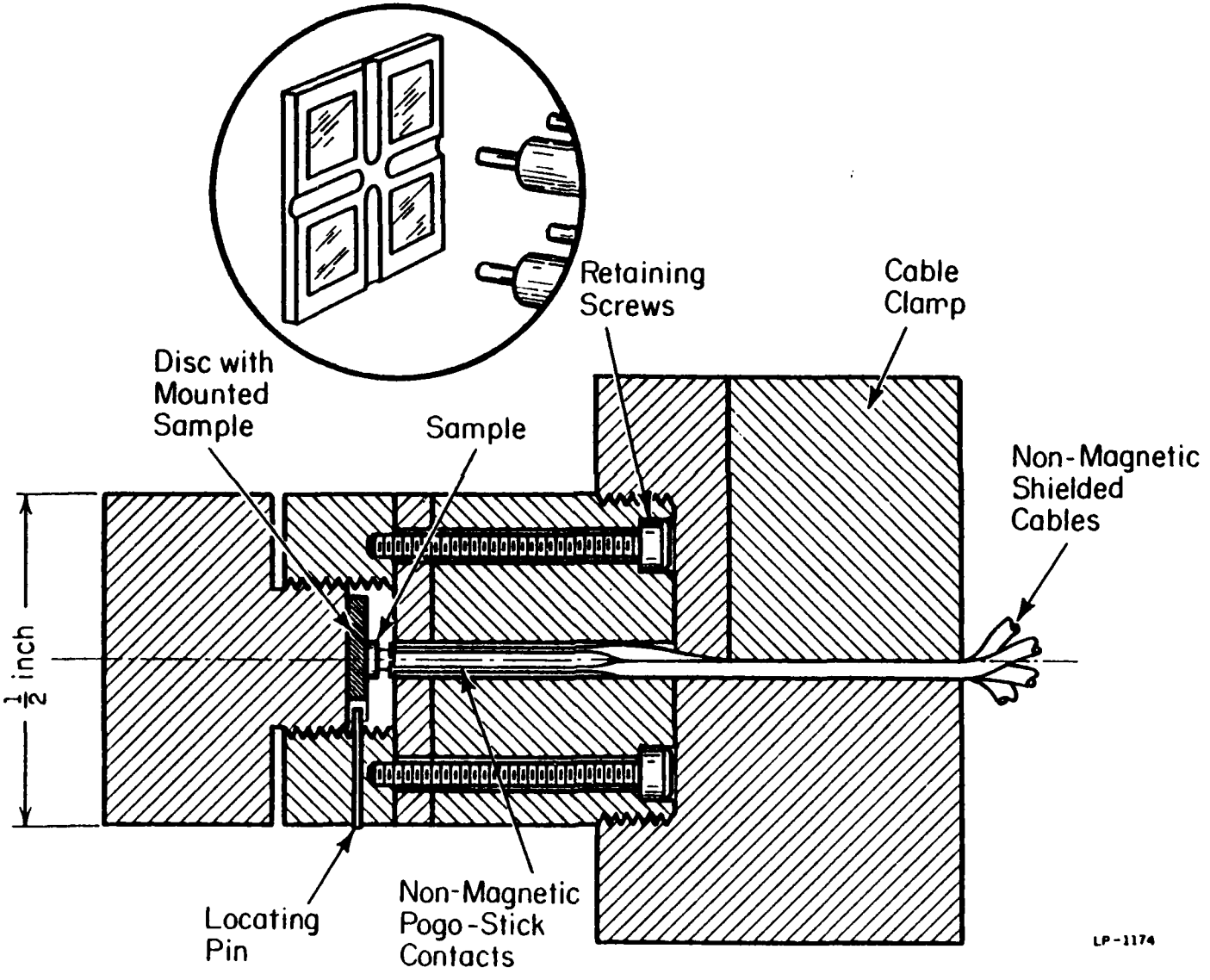


Fig. 3.3 Cross-sectional view of the sample holder used for van der Pauw resistivity and Hall measurements. The inset shows the sample geometry and spring-loaded contacts in the holder [42].

sample is positioned on the disc such that the contact pads make contact with four non-magnetic spring-loaded "pogo-stick" probes. A notch in the nylon disc fits onto a locking pin in the sample holder so that the sample can be easily realigned with the "pogo-stick" probes in the event that it had been removed from the holder and subsequently reinserted. An ac magnetic field is applied perpendicular to the sample by inserting the sample into a small solenoidal ac magnet.

Layer removal is accomplished with a chemical etch consisting of a 1:1:200 mixture of 30% $H_2O_2$, concentrated $H_2SO_4$ and deionized water. The etch rate is approximately 300 Å/min. The exact etch rate and hence the thicknesses of the removed layers in each case are monitored by protecting small regions of the samples near the edges with black Apiezon wax and measuring the resulting step heights with a Sloan Dektak mechanical stylus.

### 3.5.2. Double ac resistivity and Hall measurements [74]

With the van der Pauw geometry and conventional dc excitation, the Hall voltage appears as a small correction to a large background voltage (due to the non-aligned contacts) upon the application of the magnetic field, rendering it difficult to be measured to the accuracy needed for profiling. The difficulty is further complicated by various thermoelectric and misalignment effects which must be averaged out by permutation of field and current.

In the double ac method, the current and the magnetic field are driven at well-separated frequencies. The Hall voltage occurs at the heterodyne frequencies, and can be measured with phase lock-in techniques with excellent sensitivity and noise rejection. As a result, only small magnetic fields (several hundred gauss) are necessary. Permutation of field and current is carried out automatically, and hence only one

measurement is necessary. The double ac method is therefore very convenient and well suited for electrical profiling, where small changes in the Hall voltage must be detected repeatedly as surface layers are removed by chemical etching. Voltages in resistivity measurements occur at the same frequency as the current excitation.

A block diagram of the double ac Hall system used in this work is shown in Fig. 3.4 [74]. A circuit schematic is also included (Fig. 3.5) [42]. The sample current is driven by oscillator $f_1$ at a frequency of 1 kHz. The 200 gauss (rms) solenoidal magnet is driven by oscillator $f_2$ and a power amplifier at a frequency of 250 Hz. The resistivity voltages occur at 1 kHz and the Hall voltage is detected at $f_1 - f_2 = 750$ Hz. These signals are measured by a PAR 186A lock-in amplifier. The reference signal for the measurement of the Hall voltage is generated from oscillators $f_1$ and $f_2$ with a mixer and a three-stage tuned active filter.

The sheet resistivity $\rho$ and sheet Hall coefficient $R_H$ of the implanted layers are given by [73]

$$\rho = \frac{\pi}{\ell n 2} \left(\frac{R_{ABCD} + R_{BCDA}}{2}\right) f\left(\frac{R_{ABCD}}{R_{BCDA}}\right)$$

$$R_H = \frac{\sqrt{2}\ \Delta R_{BDAC}}{B_o(\text{rms})}$$

Labeling the contacts on the sample consecutively by A, B, C and D, $R_{ABCD}$ is defined by

$$R_{ABCD} = \frac{V_{CD}}{I_{AB}}$$

where $V_{CD}$ is the voltage of contact D over that of contact C due to a

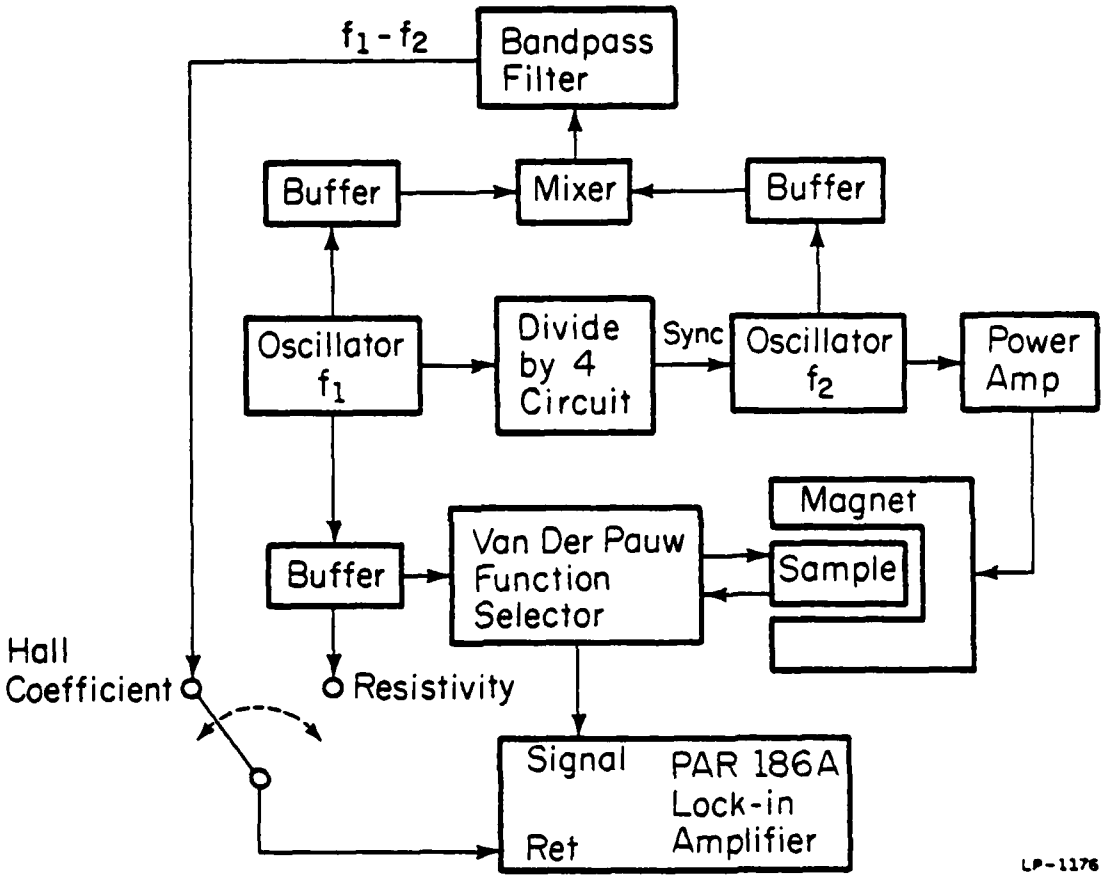


Fig. 3.4 Block diagram of the double ac Hall system [74].

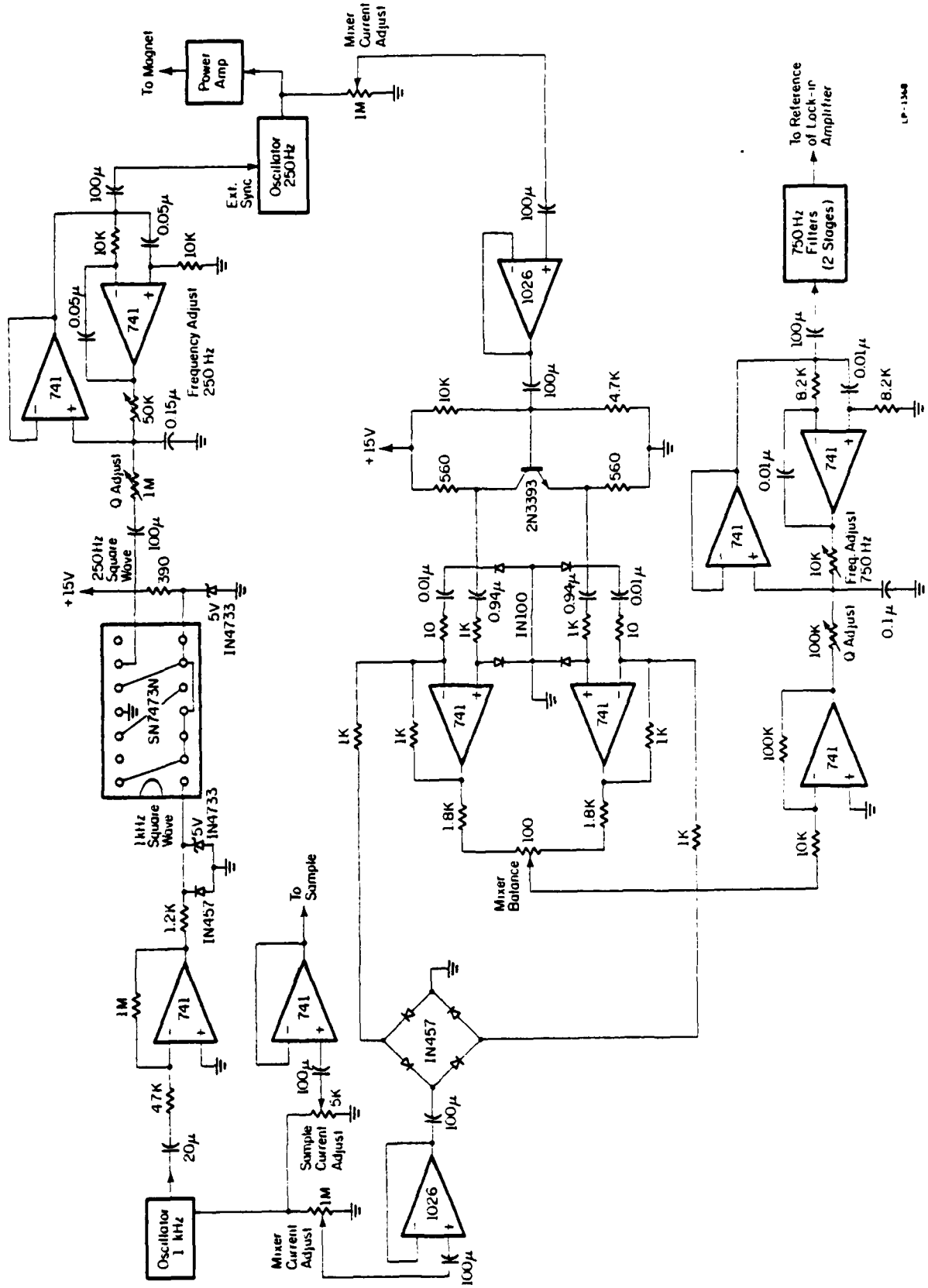


Fig. 3.5 Circuit diagram of the double ac Hall system [42].

current $I_{AB}$ entering the sample at contact A and leaving at contact B. Similarly $R_{BCDA}$ and $\Delta R_{BDAC}$ are defined by

$$R_{BCDA} = \frac{V_{DA}}{I_{BC}}$$

$$\Delta R_{BDAC} = \frac{\Delta V_{AC}}{I_{BD}}$$

The voltages associated with $R_{ABCD}$ and $R_{BCDA}$ are related to resistivity and are therefore measured at the same frequency as the current. The voltage $\Delta V_{AC}$ associated with $\Delta R_{BDAC}$ is the Hall voltage due to the magnetic field $B_o$ and is measured at the difference (heterodyne) frequency. The function $f(R_{ABCD}/R_{BCDA})$ has been evaluated by van der Pauw [73].

If $\rho_j$, $R_{H,j}$ are the values of $\rho$ and $R_H$ before a layer of thickness $d_j$ is removed and $\rho_{j-1}$, $R_{H,j-1}$ are the corresponding values after layer removal, the average mobility $\mu_j$ and average carrier concentration $n_j$ in the removed layer are given by [75]

$$\mu_j = \frac{R_{H,j}}{\rho_j} + \frac{R_{H,j-1}}{\rho_{j-1}} - \frac{R_{H,j-1} - R_{H,j}}{\rho_{j-1} - \rho_j}$$

$$n_j = \frac{\frac{1}{\rho_j} - \frac{1}{\rho_{j-1}}}{qd_j\mu_j}$$

where q is the magnitude of the electronic charge. The Hall coefficient factor has been assumed to be 1 due to practical difficulties of determining the dominant scattering mechanisms in the presence of residual implantation damage. The error associated with this assumption is likely to be less significant than the experimental uncertainties [42].

# 4. SINGLE SULFUR IMPLANTS

## 4.1. Diffusion Properties of Single S Implants

Sulfur has been implanted to doses of $7 \times 10^{12}$ $cm^{-2}$ (low), $7 \times 10^{13}$ $cm^{-2}$ (medium) and $10^{15}$ $cm^{-2}$ (high) at 250 keV into Cr-doped GaAs (substrates held at room temperature). For low and medium dose implants, $^{34}S$ has been used to enhance SIMS detectability. For the high dose implant, $^{32}S$ has been used to avoid excessively long implantation times. Annealing is done with $Si_3N_4$ encapsulation at 700°C, 800°C and 900°C for 30 min.

Shown in Figs. 4.1-4.3 are the SIMS profiles of the atomic distributions of S as a function of dose and annealing temperature. A note of caution must be added before the interpretation of these profiles is discussed. Thin native oxide films on the samples (inevitably formed as a result of atmospheric exposure) always cause an enhancement of the secondary ion yield which is quite unrelated to the actual concentration of the chemical species being monitored [72]. Also, it takes a short time before the sputtering rate and the primary ion incorporation into the surface reach their steady state. As a result, the background Ga or As matrix count has a period of instability corresponding to approximately the first 500 Å of the profile, and the impurity profiles show a shoulder in the same region. These artifacts should be disregarded in the interpretation of SIMS data.

In the case of unannealed samples, the peaks of the S distributions occur at 0.21 μm ± 0.02 μm from the surface, which compare fairly well with the projected range of 0.19 μm for $^{34}S$ calculated from LSS theory. The range differences between $^{34}S$ and $^{32}S$ due to the difference in mass

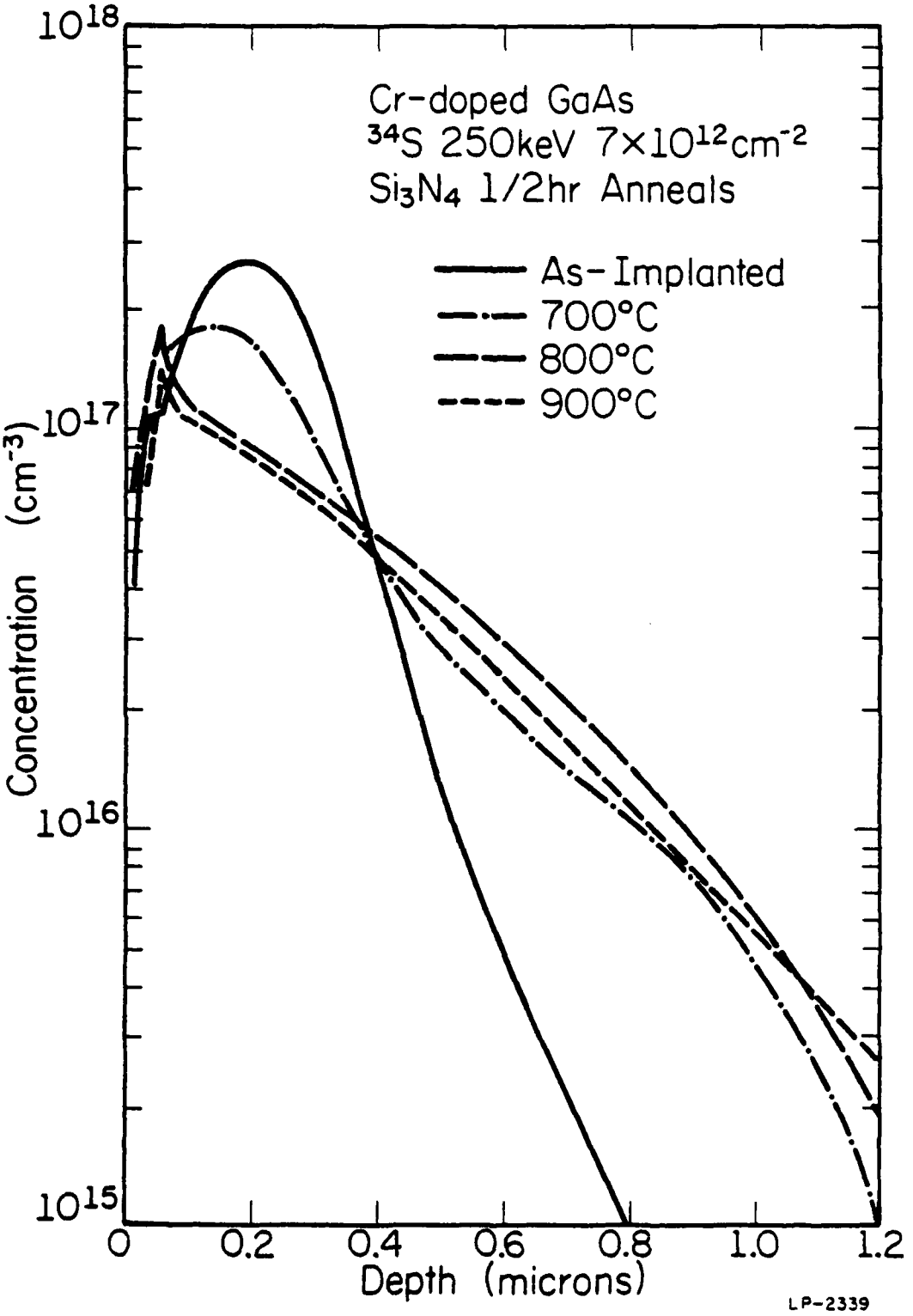


Fig. 4.1 SIMS profiles of $^{34}S$ due to a $7 \times 10^{12}$ $cm^{-2}$ implant annealed at 700°C, 800°C and 900°C.

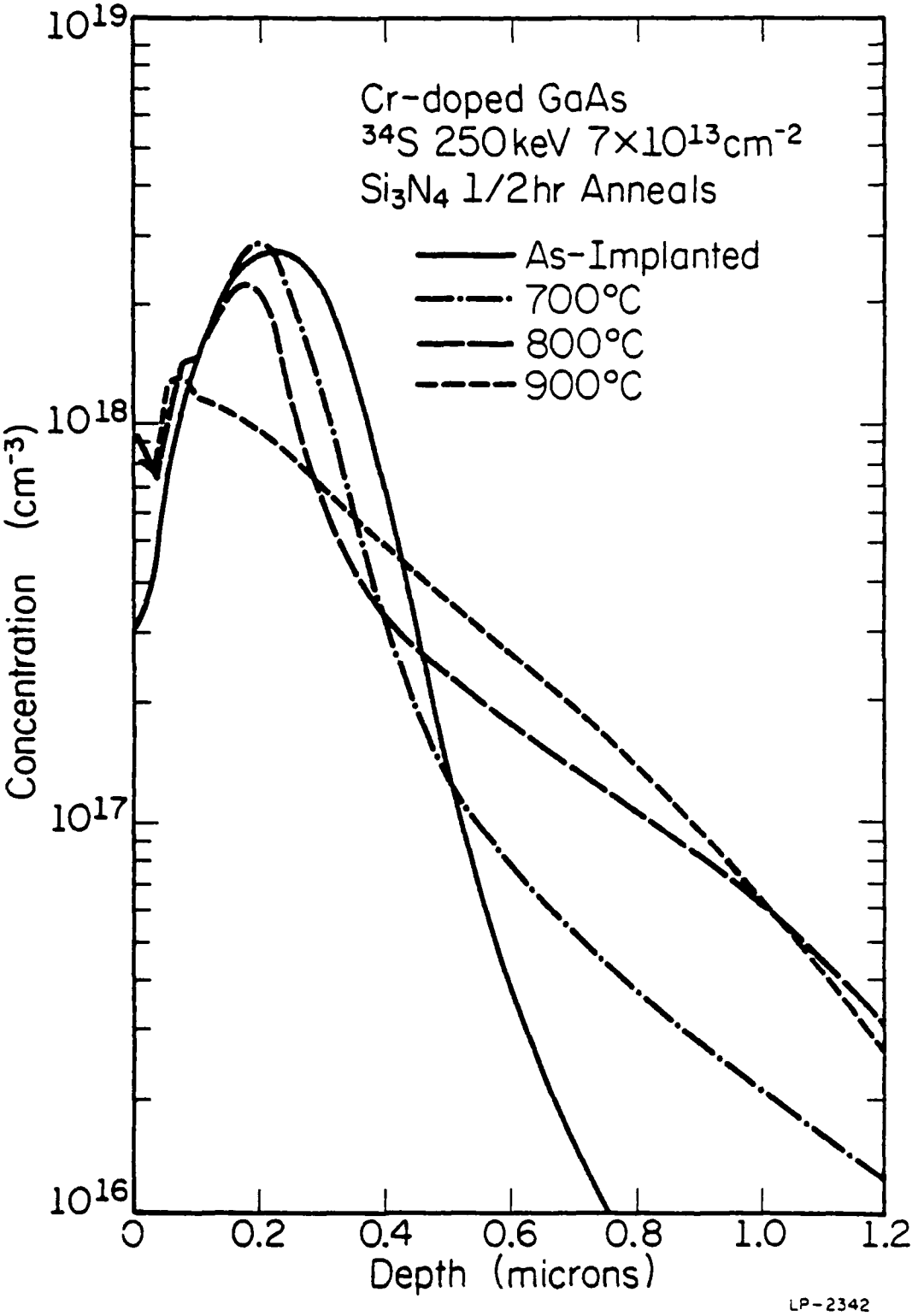


Fig. 4.2 SIMS profiles of $^{34}S$ due to a $7 \times 10^{13}$ $cm^{-2}$ implant annealed at 700°C, 800°C and 900°C.

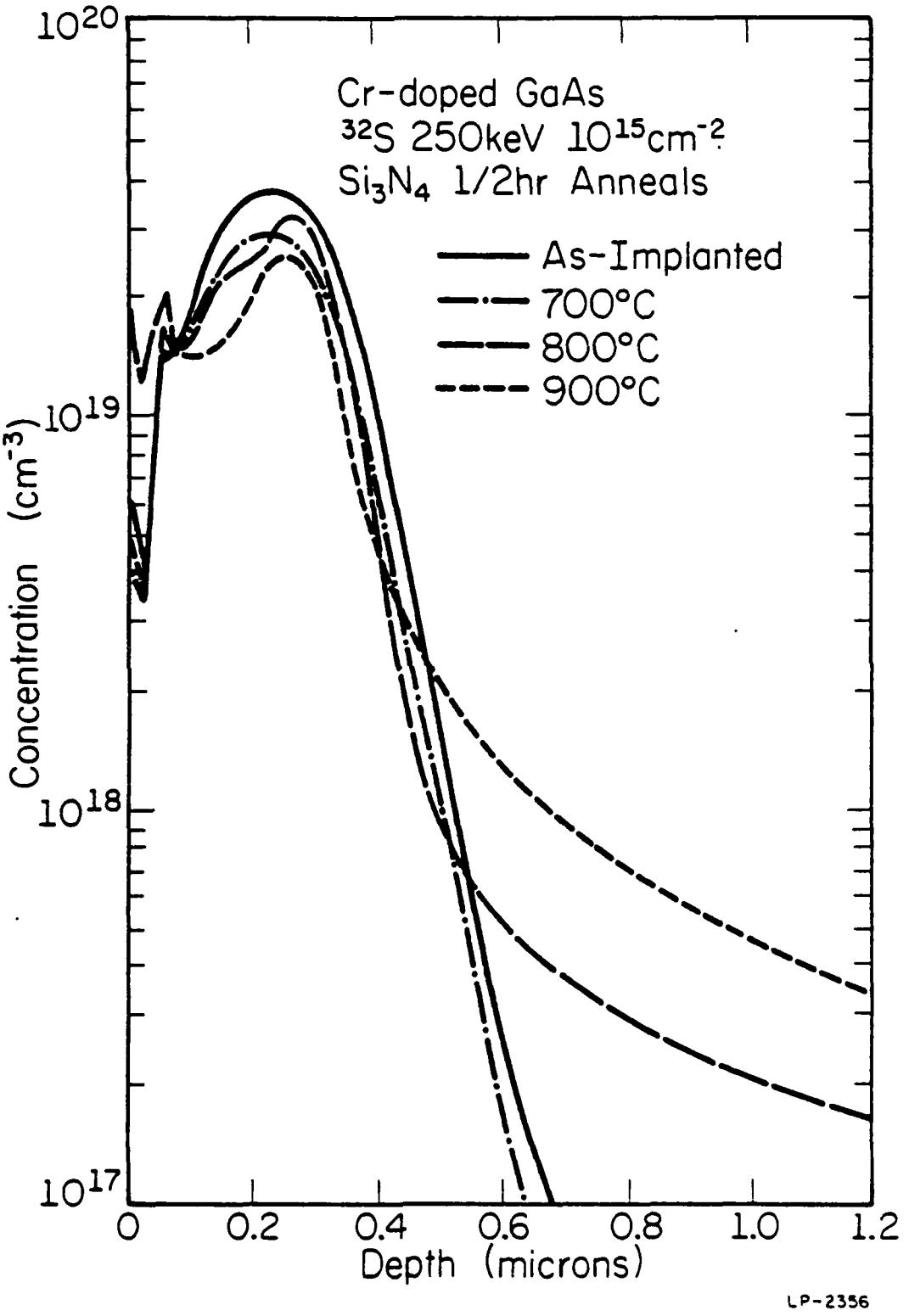


Fig. 4.3 SIMS profiles of $^{32}S$ due to a $10^{15}$ $cm^{-2}$ implant annealed at 700°C, 800°C and 900°C.

is smaller than the uncertainties of depth measurements and is therefore neglected. The shape of the as-implanted distributions is skewed for all three doses, with tails which are deeper than expected from LSS statistics. The values of $\sigma_1$, $\sigma_2$, $\sigma_3$ corresponding to the respective distances between the peak of the as-implanted distributions and the $e^{-0.5}$, $e^{-2}$ and $e^{-4.5}$ points are tabulated as follows:

| dose ($cm^{-2}$) | $\sigma_1$ (μm) | $\sigma_2$ (μm) | $\sigma_3$ (μm) |
|---|---|---|---|
| $7 \times 10^{12}$ | 0.11 | 0.12 | 0.22 |
| $7 \times 10^{13}$ | 0.105 | 0.11 | 0.225 |
| $10^{15}$ | 0.105 | 0.095 | 0.12 |

According to LSS theory, $\sigma_1 = \sigma_2 = \sigma_3 = \Delta R_p = 0.07$ μm. The measured unannealed profiles closely approximate a gaussian with $\Delta R_p \approx 0.11$ μm relatively close to the peak. The tail of the distribution in regions where the profiles deviate from a gaussian is considerably deeper for the low and medium dose implants than for the high dose implant. Similar observations have also been reported for Se implants in GaAs and have been attributed to possible interscitial migration of Se in crystalline GaAs during implantation when the total dose does not exceed the amorphization threshold [37]. From this it may be concluded that the amorphization threshold for S implants in GaAs is probably between $7 \times 10^{13}$ $cm^{-2}$ and $10^{15}$ $cm^{-2}$.

Upon annealing, the three doses result in rather different redistribution. One common feature, however, is the high diffusivity of S, evident in the formation of deep tails which in the case of 900°C anneals extend to depths well over 1 μm. In the low dose case,

redistribution is evident even at 700°C. However, the shape of the as-implanted profile is still roughly preserved and the tail region approximates a gaussian for depths greater than 0.9 μm. At 800°C and 900°C, the shape of the as-implanted profile is completely lost and the profiles look surprisingly similar. Both profiles are approximately gaussian, but the 900°C profile penetrates somewhat deeper. Diffusion coefficients at the tails of the profiles have been estimated by fitting a gaussian to the profiles in these regions. The diffusion coefficient D is given by

$$Dt = \sigma^2 - (\Delta R_p)^2$$

where $\sigma$ is the standard deviation of the fitted gaussian and t is the total annealing (diffusion) time. D has been found to be $9 \times 10^{-13} cm^2/sec$, $10^{-12}$ $cm^2/sec$, and $8 \times 10^{-12}$ $cm^2/sec$ for 700°C, 800°C, 900°C, respectively. The corresponding integrated areas under the profiles are $5.9 \times 10^{12}$ $cm^{-2}$, $5.2 \times 10^{12}$ $cm^{-2}$ and $4.4 \times 10^{12}$ $cm^{-2}$, indicating increasing outdiffusion of S into the $Si_3N_4$ cap, contrary to the reports of Yeo et al. [38] and Kwor et al. [39].

For the medium dose, annealing at 700°C and 800°C results in somewhat less redistribution. The as-implanted peak persists in both cases, although its position is slightly shifted towards the surface. The 700°C anneal results in a tail that is much more penetrating than a gaussian. The 800°C anneal gives an exponential tail which eventually turns into a gaussian at depths greater than 1 μm. For the 900°C anneal, the profile flattens out entirely. It is approximately exponential up to 0.7 μm and becomes a gaussian after 0.9 μm. Again, outdiffusion into the cap is significant, the integrated areas under the profiles being $6 \times 10^{13}$ $cm^{-2}$, $5.6 \times 10^{13}$ $cm^{-2}$ and $4.8 \times 10^{13}$ $cm^{-2}$ for annealing temperatures of 700°C,

800°C and 900°C, respectively (as compared to the implantation dose of $7 \times 10^{13}$ $cm^{-2}$). The diffusion coefficients estimated from the gaussian part of the diffusion tails are $2 \times 10^{-12}$ $cm^2/sec$ at 800°C and $10^{-11}$ $cm^2/sec$ at 900°C, which are reasonably close to the values estimated from the low dose case.

The high dose implant suffers the least redistribution. The shape of the as-implanted peak survives even the 900°C anneal with minor distortions. However, penetrating tails are still formed at 800°C and 900°C which decrease much slower than a gaussian or even an exponential. Outdiffusion into the cap is somewhat less. Estimation of the diffusion coefficient at the tails of the profiles is not attempted since they do not exhibit a simple gaussian shape.

One trend is apparent in these experiments: the redistribution of implanted S decreases at higher doses. The diffusivity remains high at the tails of the profiles, but the region in the vicinity of the as-implanted peak exhibits less diffusion effects as the dose is increased. This seems to imply that the diffusion of implanted S is decreased by a sufficient density of implantation damage, which is consistent with the observation of Wilson and Jamba [37], who noted that the redistribution of implanted S is significantly reduced if the implant is performed into a pre-amorphized GaAs substrate.

The observed diffusion coefficients at the tails of the profiles are consistent with those reported by Sansbury and Gibbons [31] for implanted S, but are almost an order of magnitude higher than the results of Kendall [76] and 2-3 orders of magnitude higher than that of Young and Pearson [49] from sulfur indiffusion experiments. There is some evidence that the diffusion of S in crystalline GaAs involves a Ga divacancy ($V_{Ga}V_{Ga}$)

[49], and it is conceivable that vacancies diffusing out of the region of implantation damage can significantly alter the diffusivity of S in the tail regions of the annealed profiles.

The redistribution effects are apparently not related to the type of GaAs used, since similar S implants into unintentionally doped MBE GaAs have been found to exhibit the same diffusion properties upon annealing.

The SIMS detection limit is approximately 2-3 × $10^{16}$ $cm^{-3}$ for $^{32}S$ and 1 × $10^{15}$ $cm^{-3}$ for $^{34}S$ with a $Cs^+$ primary beam.

## 4.2. Electrical Properties of Single S Implants

Shown in Figs. 4.4-4.9 are the carrier concentration and mobility profiles due to the various implants and annealing temperatures up to 800°C. The Cr-doped substrates type convert upon annealing at 900°C, yielding a surface layer with a very significant conductivity even in the absence of a dopant implant, and hence no electrical characterization can be done at this temperature.

For all three doses investigated, the electrical activation is always higher for 800°C annealing than for 700°C. This indicates that lattice recovery from implantation damage improves at the higher temperature. Indeed, even at 800°C a significant amount of residual damage apparently still remains, since work on Be implantation in GaAs shows that annealing at 900°C is necessary for optimal recovery [77,78].

For the low dose implant, the carrier concentration profile has a similar shape as the SIMS profile both for 700°C and 800°C annealing, with activation efficiencies of 12% and [illegible] respectively (neglecting the fraction of the implanted S that has outdiffused into the cap). The corresponding peak carrier concentrations are 3.7 × $10^{16}$ $cm^{-3}$ and 7 × $10^{16}$ $cm^{-3}$. Both carrier profiles are rather shallow and the carrier

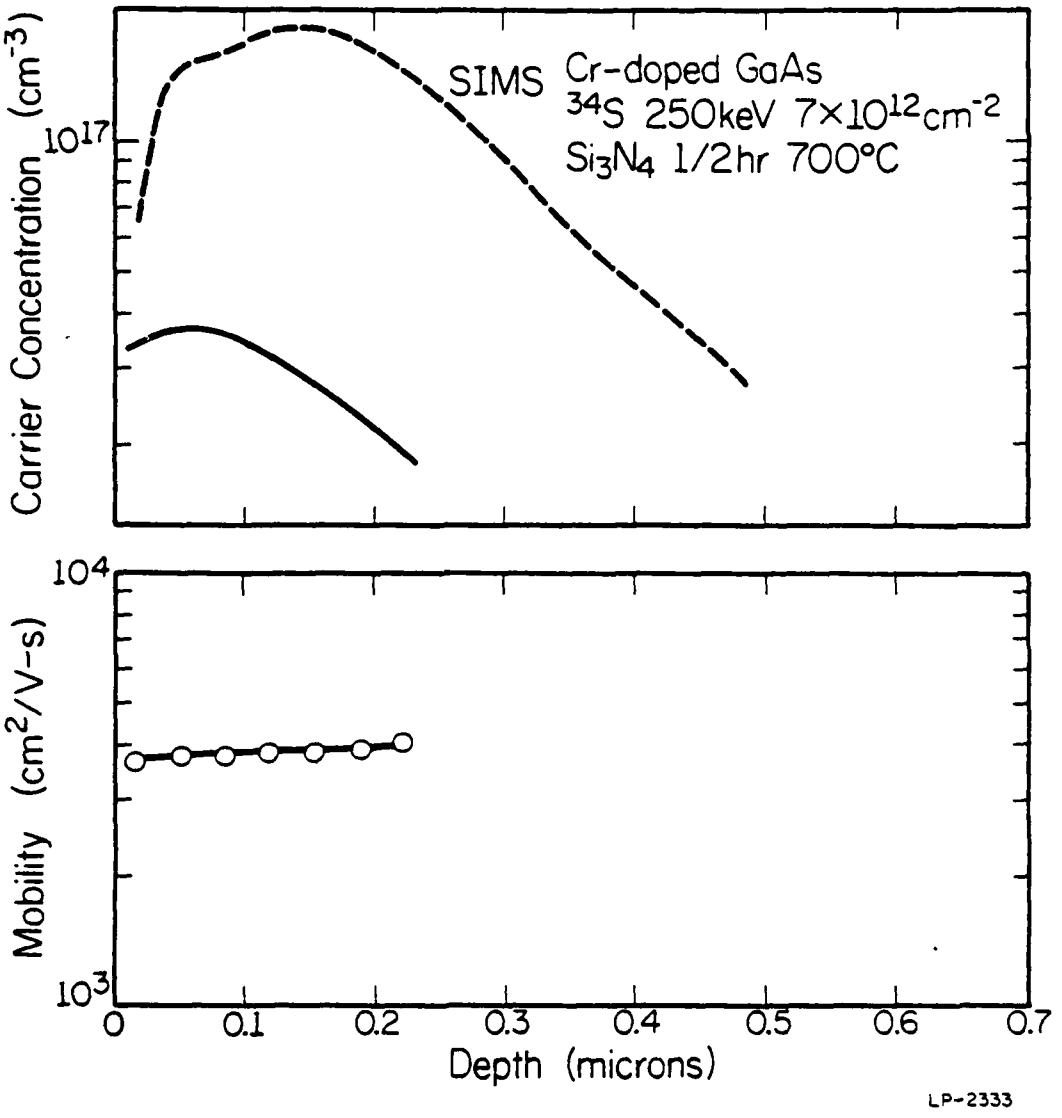


Fig. 4.4 Carrier concentration and mobility profiles due to a $7 \times 10^{12}$ $cm^{-2}$ $^{34}S$ implant at 250 keV annealed at 700°C. The SIMS profile is also shown for comparison.

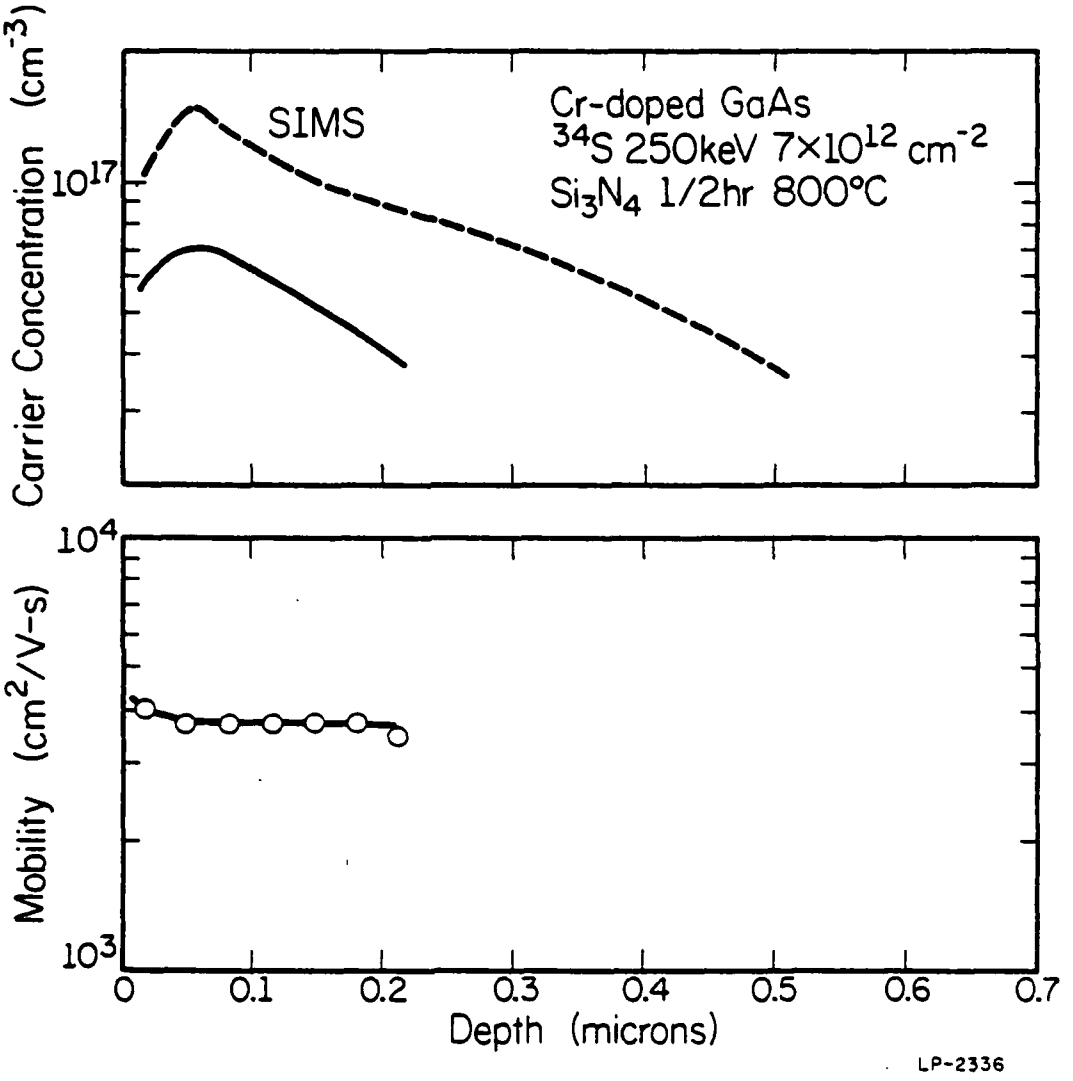


Fig. 4.5 Carrier concentration and mobility profiles due to a $7 \times 10^{12}$ cm$^{-2}$ $^{34}$S implant at 250 keV annealed at 800°C. The SIMS profile is also shown for comparison.

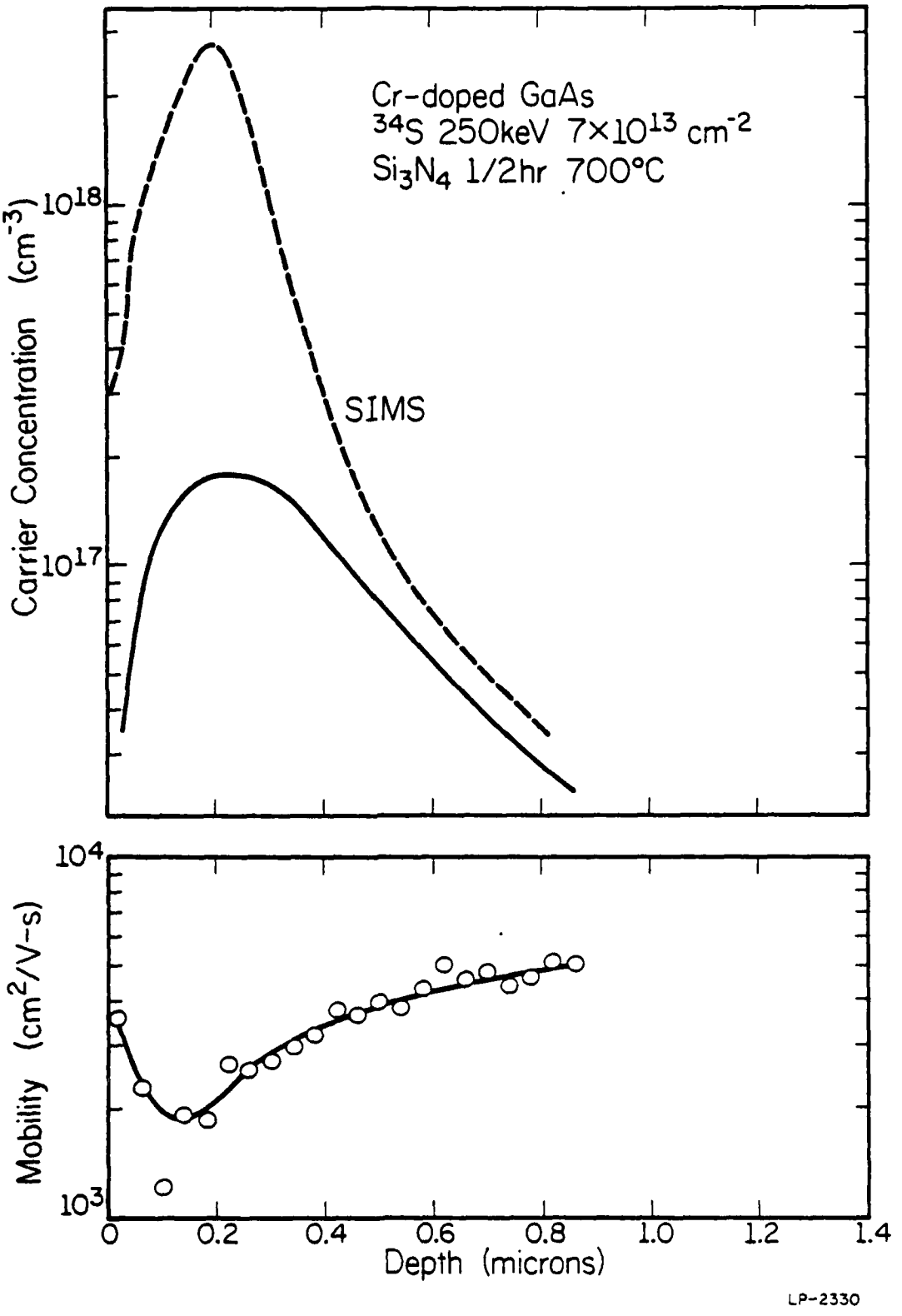


Fig. 4.6 Carrier concentration and mobility profiles due to a $7 \times 10^{13}$ cm$^{-2}$ $^{34}$S implant at 250 keV annealed at 700°C. The SIMS profile is also shown for comparison.

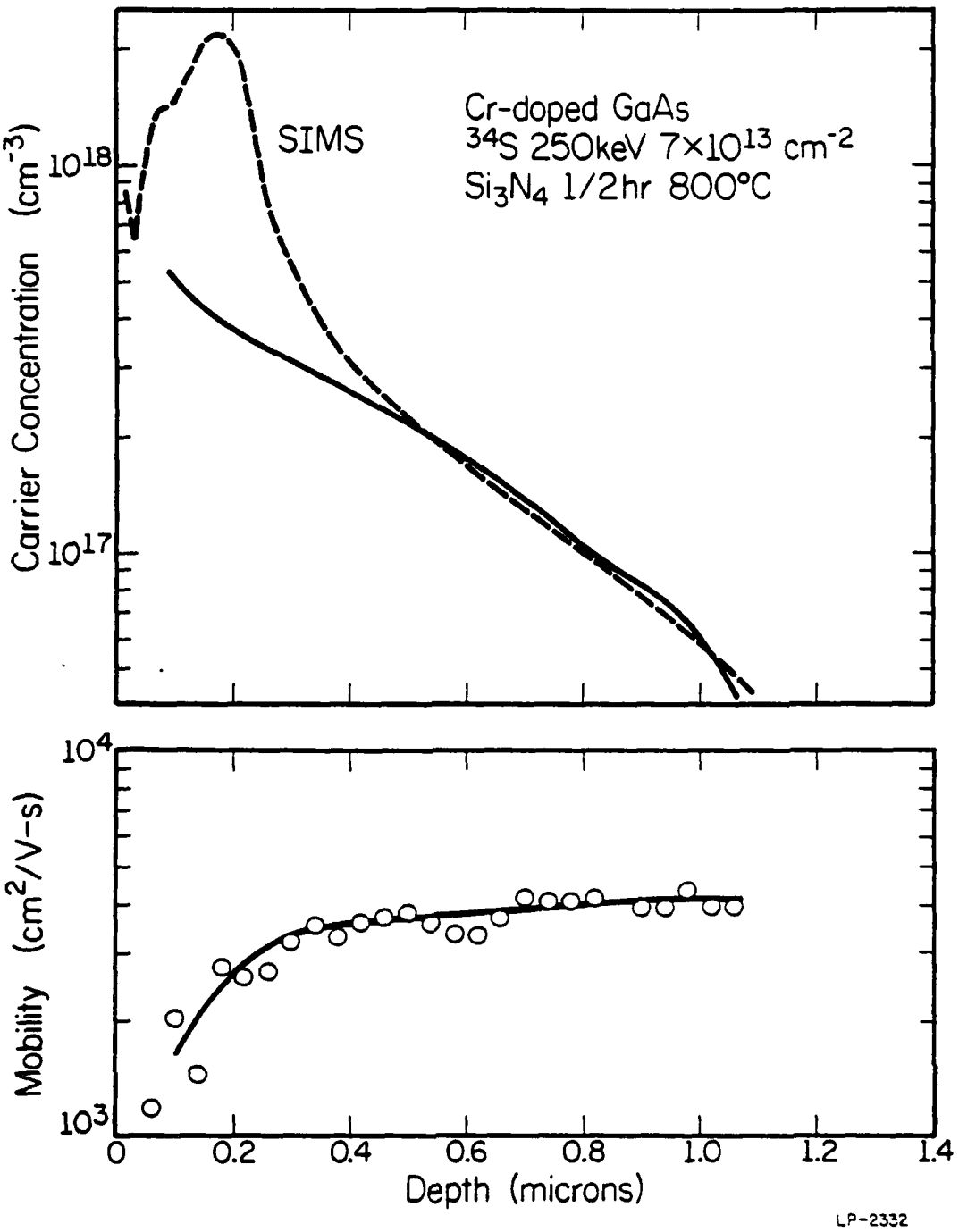


Fig. 4.7 Carrier concentration and mobility profiles due to a $7 \times 10^{13}$ cm$^{-2}$ $^{34}S$ implant at 250 keV annealed at 800°C. The SIMS profile is also shown for comparison.

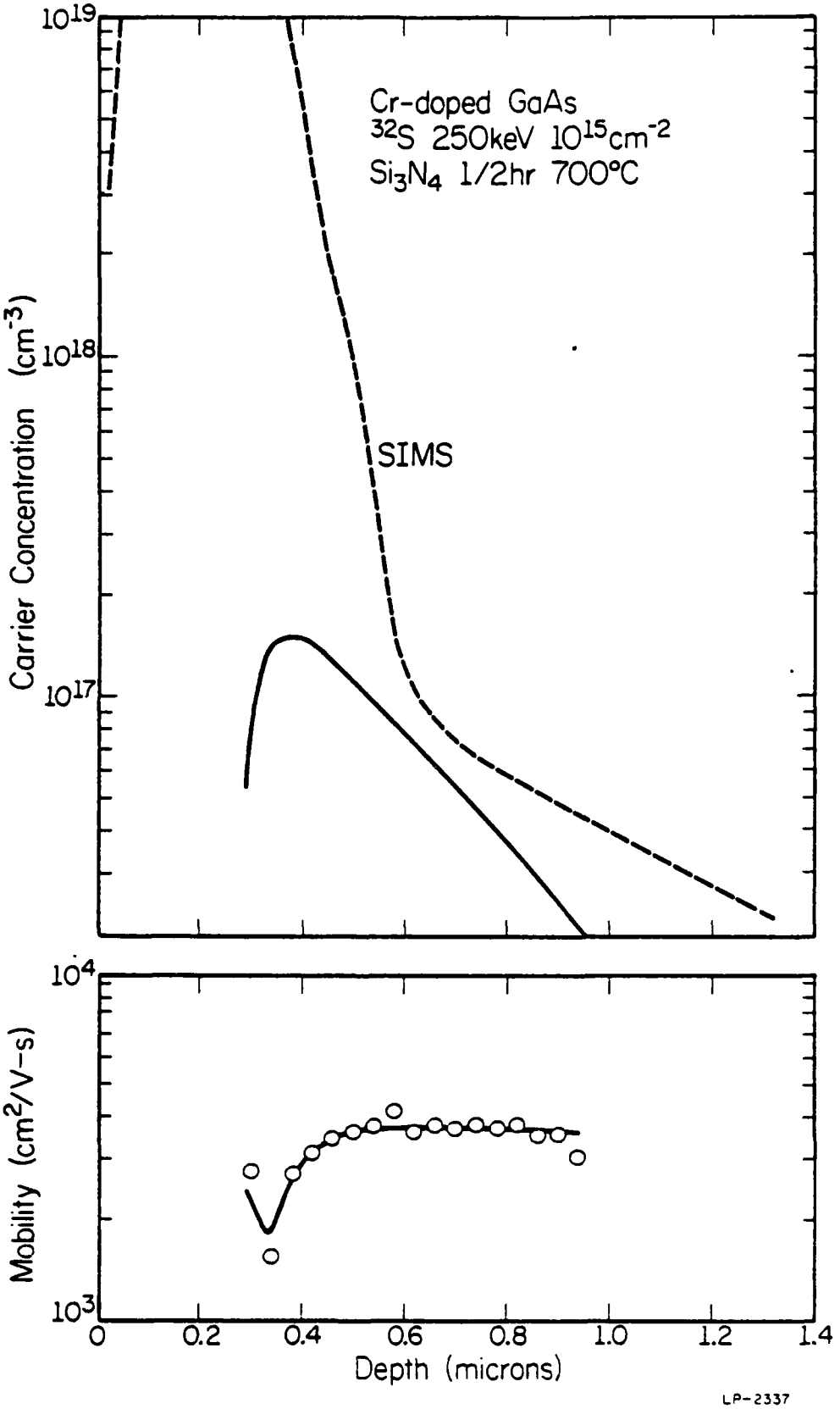


Fig. 4.8 Carrier concentration and mobility profiles due to a $10^{15}$ cm$^{-2}$ $^{32}$S implant at 250 keV annealed at 700°C. The SIMS profile is also shown for comparison.

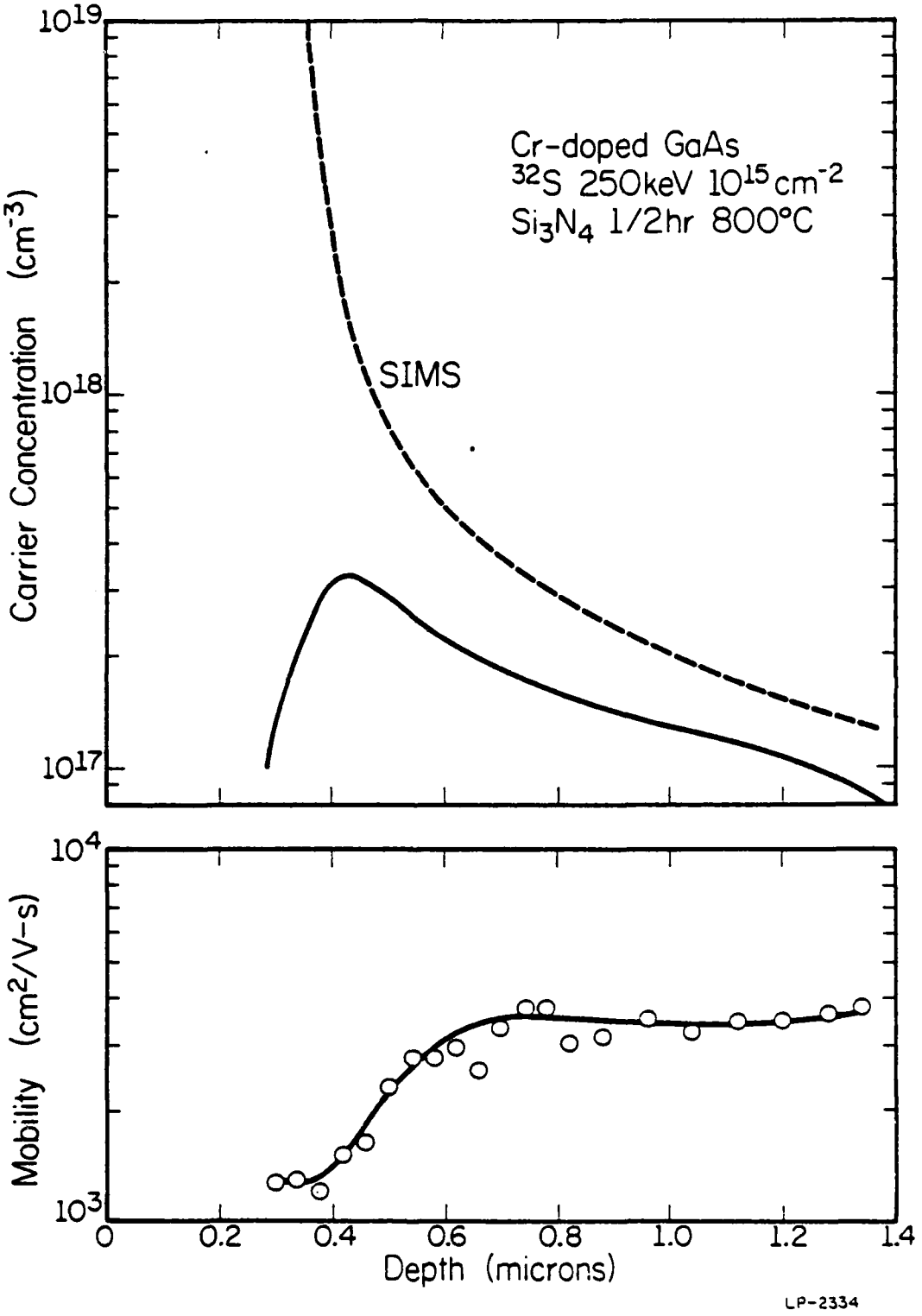


Fig. 4.9 Carrier concentration and mobility profiles due to a $10^{15}$ $cm^{-2}$ $^{32}S$ implant at 250 keV annealed at 800°C. The SIMS profile is also shown for comparison.

concentrations are not measurable after a depth of 0.22 μm. Mobilities are high (3800 $cm^2$/V-sec for 700°C and 3700 $cm^2$/V-sec for 800°C) and do not change much throughout the carrier profile. The low activation efficiency is partly due to the background Cr concentration of $\sim 2 \times 10^{16}$ $cm^{-3}$, which is quite significant compared to the atomic S concentration throughout the distribution, and also due to the less than optimum annealing temperature.

The medium dose implant shows good activation and high mobilities (close to 4000 $cm^2$/V-sec) at the tail of the atomic distributions for both 700°C and 800°C annealing. However, in the vicinity of the peaks of the atomic distributions, a substantial fraction of the implanted S is electrically inactive while the carrier mobilities are also low. This indicates that significant amounts of residual damage remain after annealing at these temperatures. The overall electrical activation is 13% at 700°C annealing and increases to 36% at 800°C.

For the high dose implant, the carrier profiles lie almost entirely in the tail regions of the atomic profiles for both annealing temperatures. There is a surface inactive layer of about 0.3 μm in both cases, and very little of the implanted S in the peak regions of the atomic profiles is electrically active. The overall activation efficiency is very low, being 0.7% for 700°C and 2.3% for 800°C. Again, the poor electrical activation near the peak of the atomic profiles is accompanied by low carrier mobilities for both annealing temperatures, while the mobility values in the tail regions are rather good ($\sim$ 3500 $cm^2$/V-sec). On comparing the electrical profiles of the high and medium dose implants, it appears at this point that the additional implantation damage in the high dose implant (which probably amorphizes

a surface layer of the substrate) fails to be effectively annealed out at either 700°C or 800°C, and actually causes a reduction in carrier concentration and the production of surface inactive layers. Other factors may also be present, however, as will be discussed in the next chapter.

## 4.3. Summary

It appears that implanted S is a very rapid diffuser during the annealing process. High dose implants result in less redistribution in the regions where most of the implantation damage is expected to reside (i.e., around the peak), suggesting gettering of S in the damage. Electrical activation upon annealing at 800°C is only fair in the low and medium dose cases, and is poor in the high dose case. A higher temperature is apparently necessary to anneal out all the implantation damage, but is unfortunately prohibited by type conversion of the Cr-doped substrates in cases where electrical measurements are desired.

# 5. INTERACTIONS OF IMPLANTED S WITH Si AND DEFECTS

## 5.1. S and Si Dual Implants

Possible impurity interactions between S and Si in GaAs have been investigated because of preliminary evidence of such interactions pointed out by Yoder [50] and Oakes and Degenford [51]. Various doses of Si have been co-implanted at 220 keV with low ($7 \times 10^{12}$ cm$^{-2}$) and medium ($7 \times 10^{13}$ cm$^{-2}$) doses of S at 250 keV. These ion energies are chosen so that the range statistics of the two species are approximately the same and the relative concentrations of S and Si are almost constant throughout the implanted layer. The Si dose has been varied from 0.5 to 7 times the corresponding S dose.

Shown in Figs. 5.1-5.3 are the SIMS profiles of a $7 \times 10^{13}$ cm$^{-2}$ S implant in the presence of a $3 \times 10^{14}$ cm$^{-2}$ Si co-implant after annealing at 700°C, 800°C and 900°C. Shown also for comparison are the S distributions due to single S implants and also the Cr profiles in the dual implants. It can be seen immediately that the Si co-implant substantially reduces the diffusion of S upon annealing at all temperatures, and roughly preserves the as-implanted shape of the S profiles. However, at 900°C a secondary peak of undetermined origin also appears. Out-diffusion into the cap is appreciably reduced in all cases.

The above results are actually typical of a series of experiments in which the dose of the S implant is kept constant at $7 \times 10^{13}$ cm$^{-2}$ while the Si dose is varied from $1 \times 10^{14}$ cm$^{-2}$ to $5 \times 10^{14}$ cm$^{-2}$. In each case a reduction of S diffusion is observed and a secondary peak appears for 900°C annealing. The corresponding Si distribution, however, remains almost unchanged after annealing (Fig. 5.4).

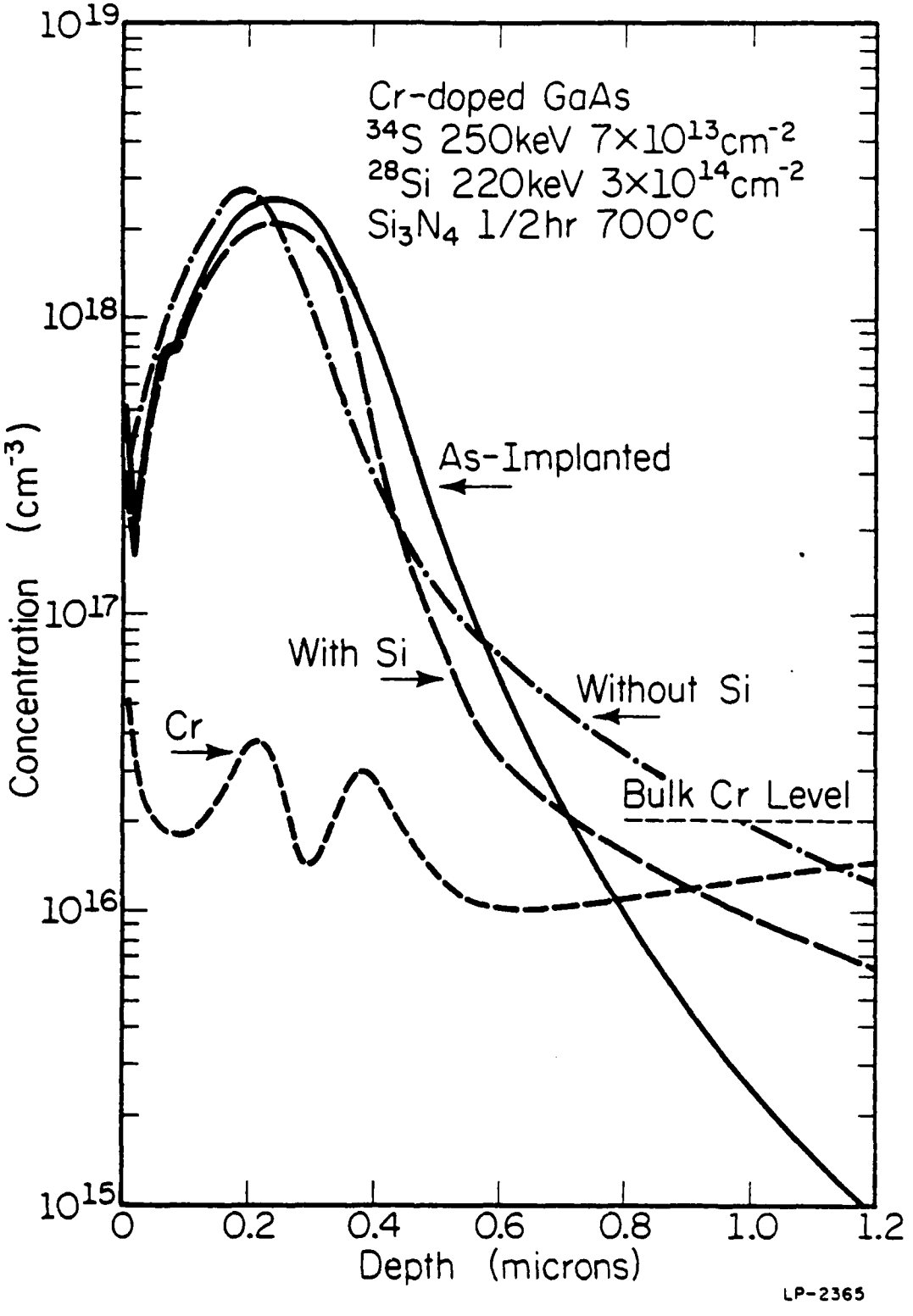


Fig. 5.1 SIMS profile of $^{34}S$ due to a $7 \times 10^{13}$ cm$^{-2}$, 250 keV $^{34}S$ implant in the presence of a $3 \times 10^{14}$ cm$^{-2}$, 220 keV $^{28}Si$ co-implant and annealed at 700°C ("With Si"). Shown also for comparison are the SIMS profile of $^{34}S$ if the $^{28}Si$ co-implant is absent ("Without Si") and the Cr distribution in the dual implants.

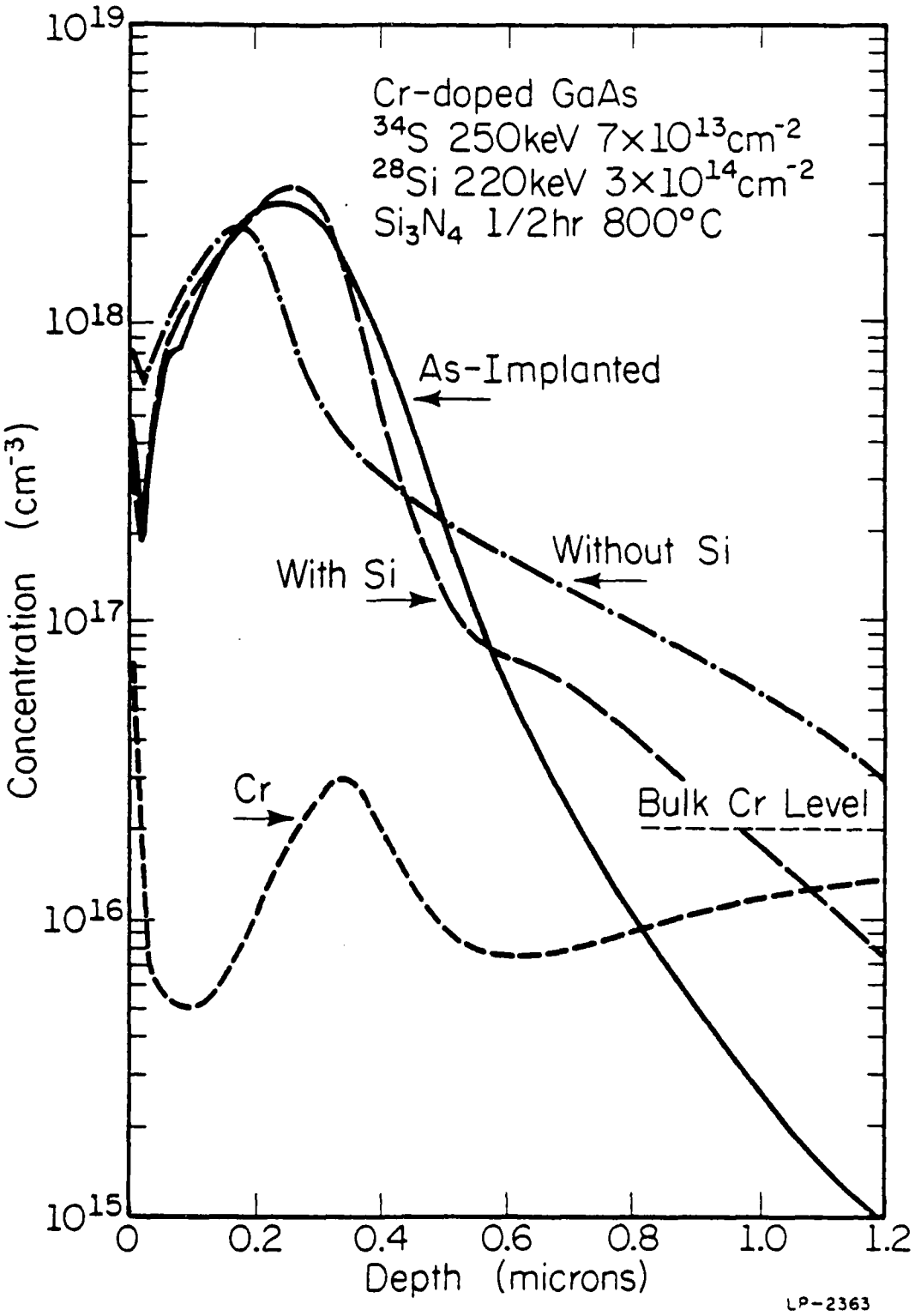


Fig. 5.2 SIMS profile of $^{34}S$ due to a $7 \times 10^{13}$ cm$^{-2}$, 250 keV $^{34}S$ implant in the presence of a $3 \times 10^{14}$ cm$^{-2}$, 220 keV $^{28}Si$ co-implant and annealed at 800°C ("With Si"). Shown also for comparison are the SIMS profile of $^{34}S$ if the $^{28}Si$ co-implant is absent ("Without Si") and the Cr distribution in the dual implants.

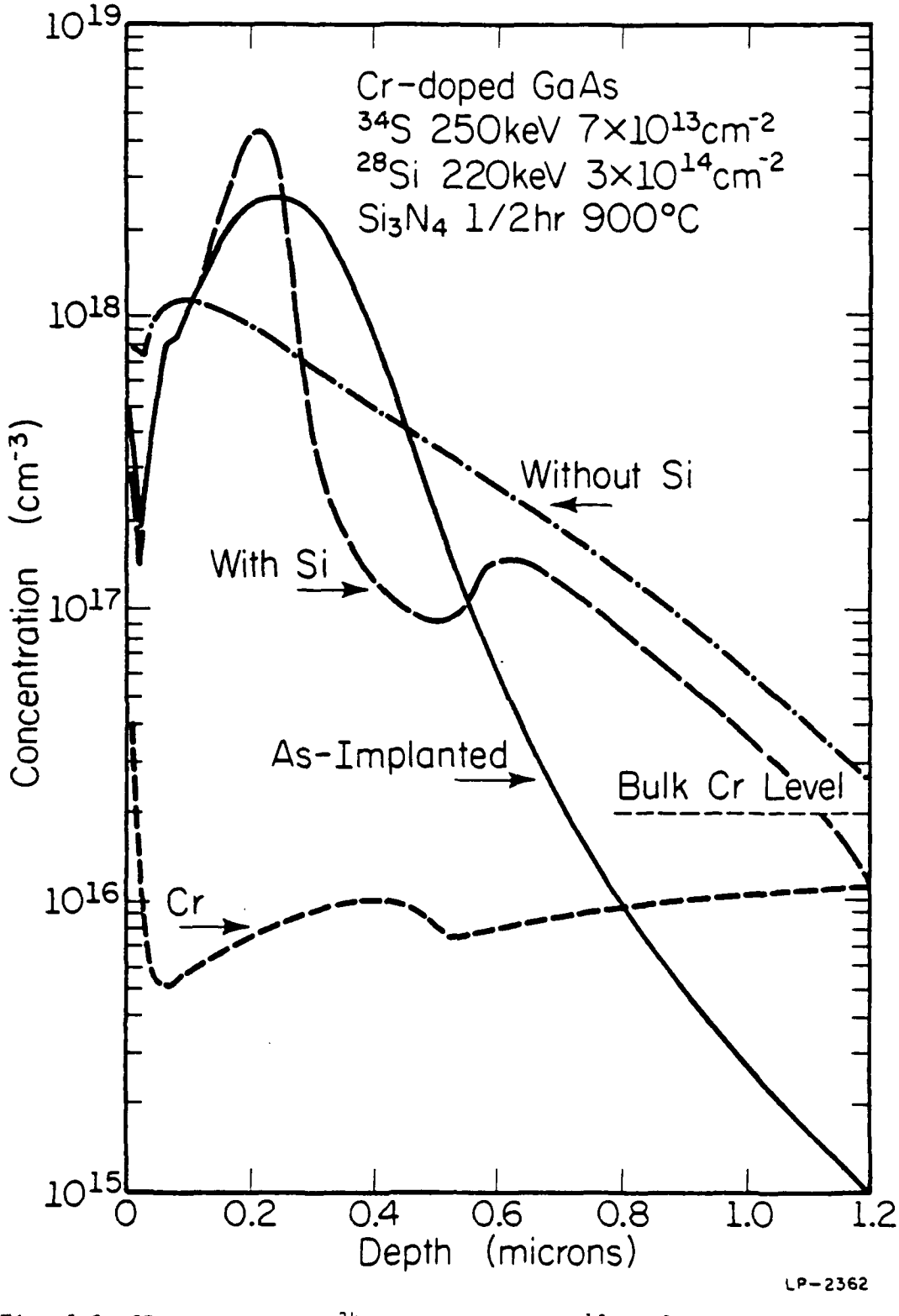


Fig. 5.3 SIMS profile of $^{34}S$ due to a $7 \times 10^{13}$ $cm^{-2}$, 250 keV $^{34}S$ implant in the presence of a $3 \times 10^{14}$ $cm^{-2}$, 220 keV $^{28}Si$ co-implant and annealed at 900°C ("With Si"). Shown also for comparison are the SIMS profiles of $^{34}S$ if the $^{28}Si$ co-implant is absent ("Without Si") and the Cr distribution in the dual implants.

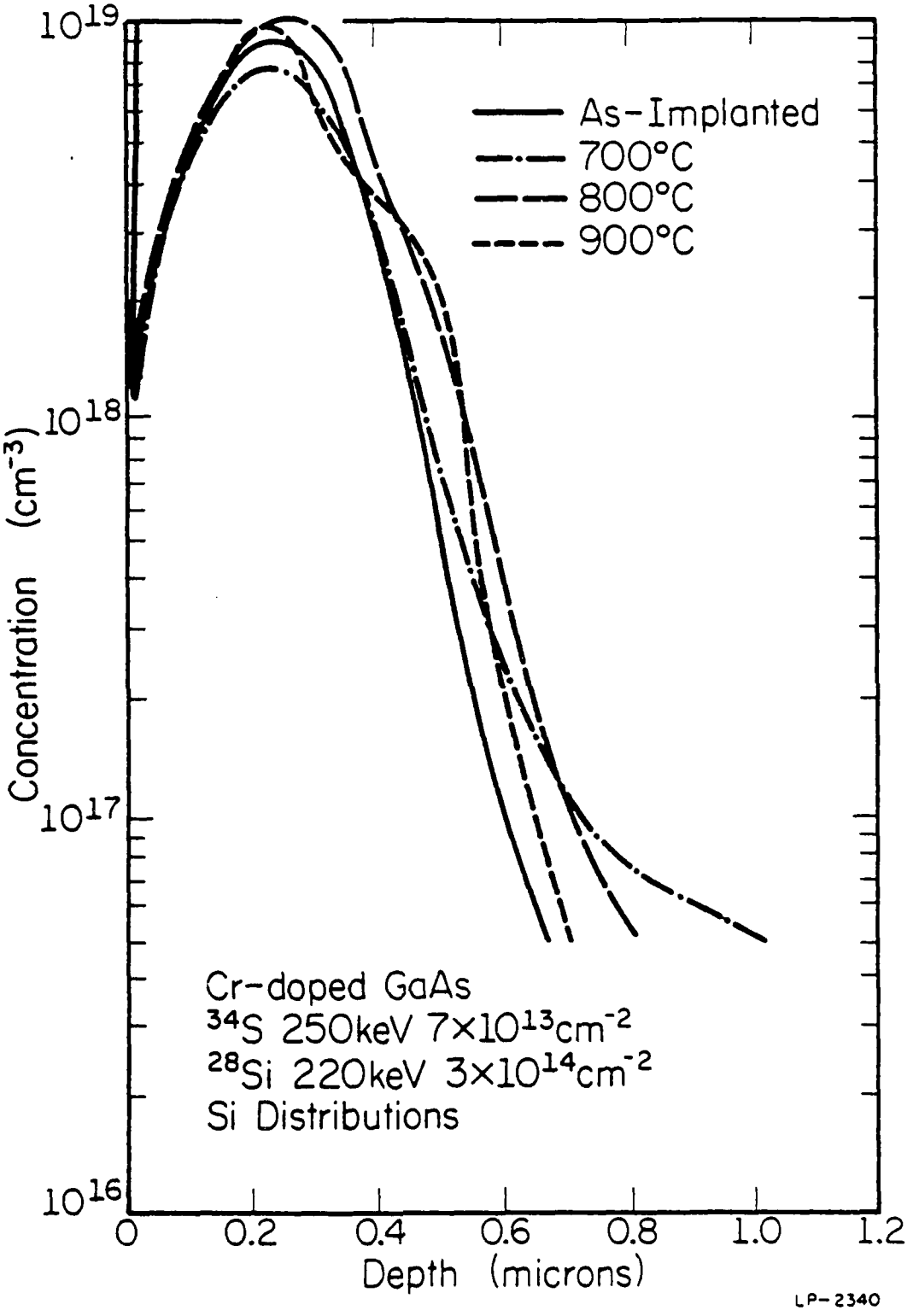


Fig. 5.4 SIMS profiles of $^{29}Si$ in dual implants of $7 \times 10^{13}$ $cm^{-2}$ $^{34}S$ at 250 keV with $3 \times 10^{14}$ $cm^{-2}$ $^{29}Si$ at 220 keV after annealing at 700°C, 800°C and 900°C.

Reducing the Si dose below that of the S implant brings about an entirely different behavior. Figs. 5.5-5.7 show the S distributions due to a $7 \times 10^{13}$ $cm^{-2}$ S implant and a $3.5 \times 10^{13}$ $cm^{-2}$ Si co-implant after annealing. For 700°C annealing, the amount of S diffusion is basically the same as for a single S implant of the same dose. For 800°C, there is somewhat more S redistribution with the Si co-implant than that for the single S implant. For 900°C, the extent of S redistribution with the Si co-implant is much more pronounced than in the single S implant. Damage enhanced diffusion is actually observed here (900°C): the implanted S is swept out of the original implanted region leaving it slightly depleted relative to the deeper regions. The Si distribution is again found to be little changed by annealing.

The behavior of the Cr originally present in the substrates is found to be quite independent of the dose of the Si co-implant. For both the high Si dose (Figs. 5.1-5.3) and the low Si dose (Figs. 5.5-5.7), annealing at 700°C yields a local double Cr peak structure in the region with the most implantation damage, a phenomenon attributed to Cr gettering by residual damage [5] or Cr precipitation at nucleation sites provided by residual damage [4]. At 800°C, the two local Cr peaks merge into one and there is a Cr depletion region on either side of the peak. The Cr level does not rise back to its bulk concentration until 2 μm below the surface. At 900°C the local Cr peak disappears altogether, presumably due to sufficient recovery of the crystal from implantation damage, and a broad ($\sim$ 3 μm) Cr depletion region is formed. A very shallow (< 0.03 μm) surface accumulation region is found in all cases, but this can be a SIMS surface artifact.

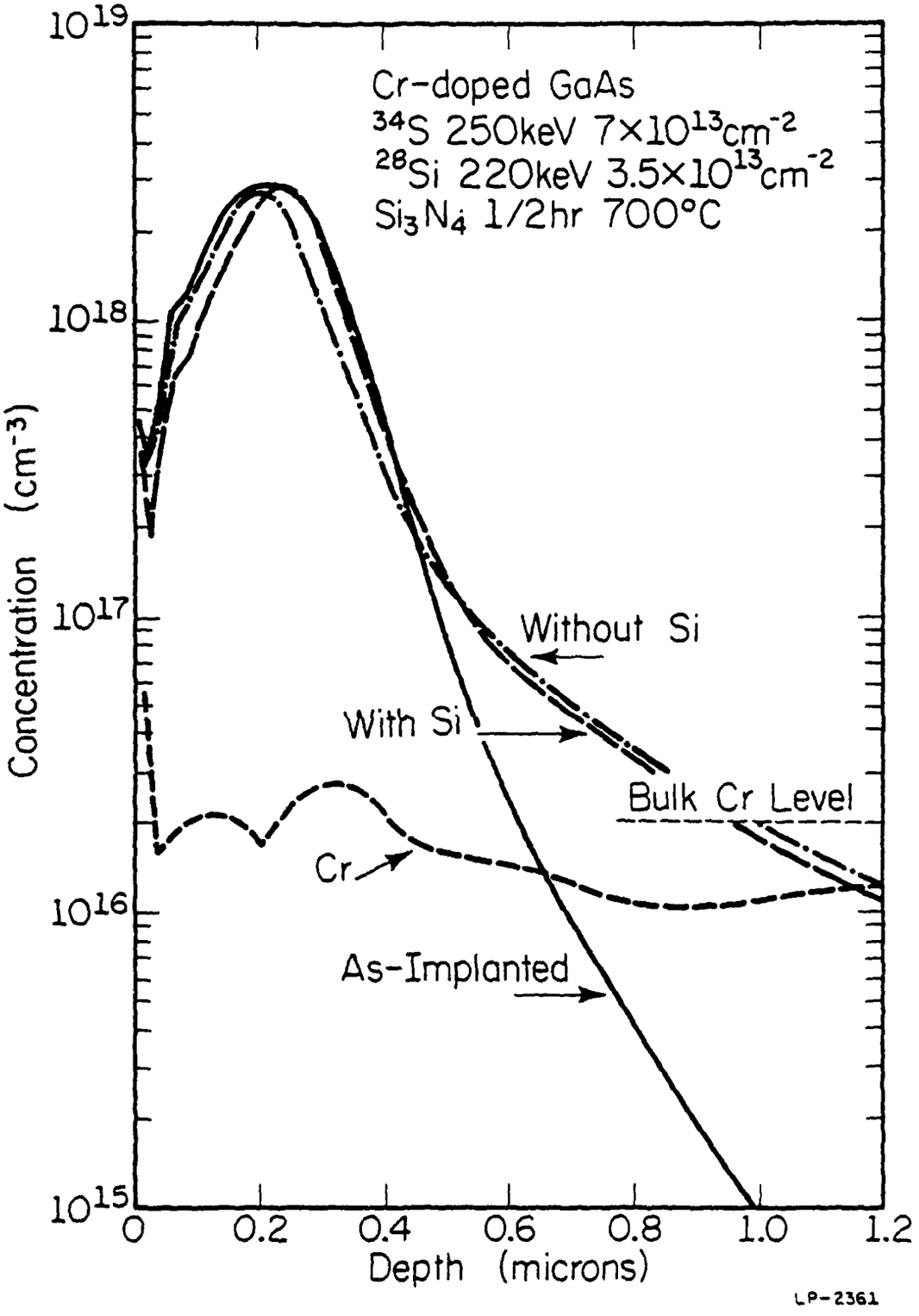


Fig. 5.5 SIMS profile of $^{34}S$ due to a $7 \times 10^{13}$ $cm^{-2}$, 250 keV $^{34}S$ implant in the presence of a $3.5 \times 10^{13}$ $cm^{-2}$, 220 keV $^{28}Si$ co-implant and annealed at 700°C ("With Si"). Shown also for comparison are the SIMS profiles of $^{34}S$ if the $^{28}Si$ co-implant is absent ("Without Si") and the Cr distribution in the dual implants.

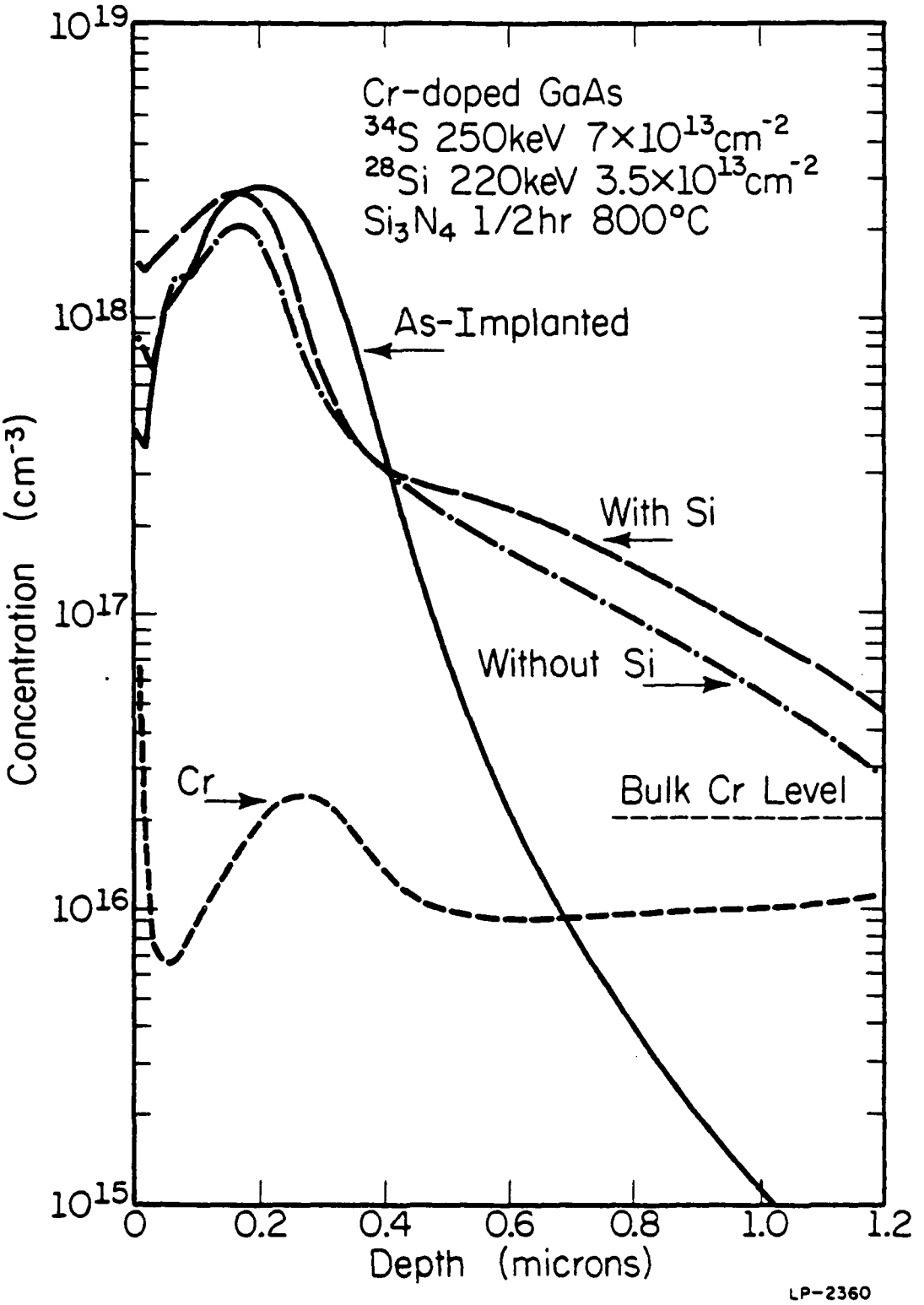


Fig. 5.6 SIMS profile of $^{34}S$ due to a $7 \times 10^{13}$ $cm^{-2}$, 250 keV $^{34}S$ implant in the presence of a $3.5 \times 10^{13}$ $cm^{-2}$, 220 keV $^{28}Si$ co-implant and annealed at 800°C ("With Si"). Shown also for comparison are the SIMS profiles of $^{34}S$ if the $^{28}Si$ co-implant is absent ("Without Si") and the Cr distribution in the dual implants.

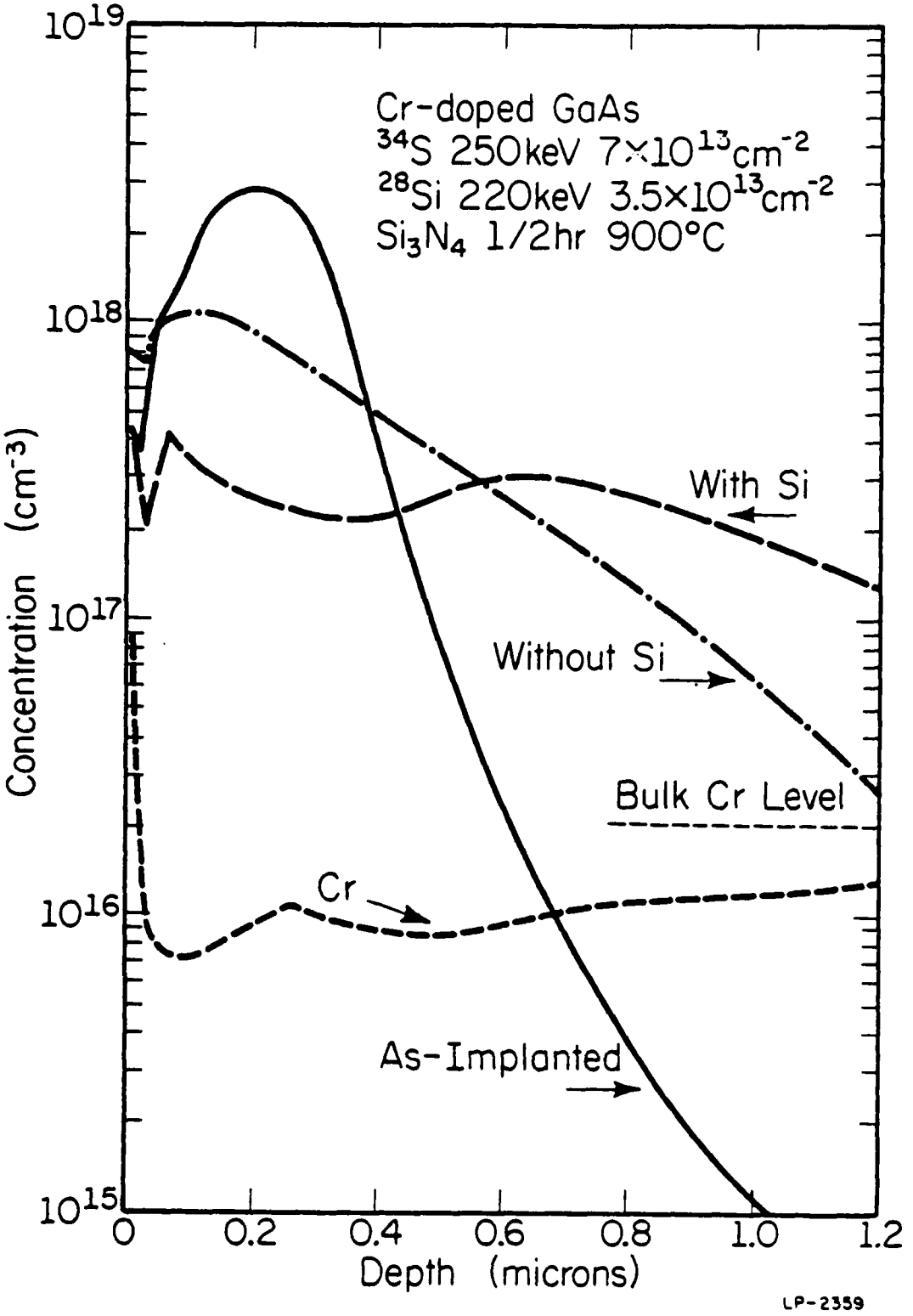


Fig. 5.7 SIMS profile of $^{34}S$ due to a $7 \times 10^{13}$ $cm^{-2}$, 250 keV $^{34}S$ implant in the presence of a $3.5 \times 10^{13}$ $cm^{-2}$, 220 keV $^{28}Si$ co-implant and annealed at 900°C ("With Si"). Shown also for comparison are the SIMS profiles of $^{34}S$ if the $^{28}Si$ co-implant is absent ("Without Si") and the Cr distribution in the dual implants.

The similar Cr behavior associated with both the high dose and low dose Si dual implants indicates that the modified diffusion properties of S are directly related to the presence of implanted Si. However, it remains to be determined whether the effect is due to interactions of S with Si or the additional radiation damage associated with the Si co-implant.

The concentration dependence of possible S-Si interactions has also been investigated. A dual implant of $7 \times 10^{12}$ $cm^{-2}$ S and $3 \times 10^{13}$ $cm^{-2}$ Si has been performed to see if the decrease in the diffusivity of S persists after both the S and Si concentrations are reduced by a factor of 10. Figures 5.8-5.10 show the SIMS profiles of S in such cases as compared to single $7 \times 10^{12}$ $cm^{-2}$ implants annealed under similar conditions. At 700°C and 800°C annealing, S diffusion effects appear to be less in the vicinity of the peak regions of the as-implanted distributions. However, deeper into the substrate, where both the Si and S concentrations fall, little difference between the diffusion behavior of S in the dual implant and the single S implant is observed. At 900°C, defect enhanced diffusion again occurs.

## 5.2. S Implants into Si-Doped MBE GaAs

S implants at 250 keV and $7 \times 10^{13}$ $cm^{-2}$ have been performed into heavily Si-doped MBE layers ($N_d \simeq 2.2 \times 10^{18}$ $cm^{-3}$) to determine the effects of Si-doping on the diffusion of implanted S in the absence of Si implant damage. Upon annealing at 800°C, the S redistribution is clearly less severe than if there is no Si-doping, but is still quite considerable (Fig. 5.11). Outdiffusion of S into the cap is also reduced (sheet concentration = $6 \times 10^{13}$ $cm^{-2}$). The diffusion tail in this case

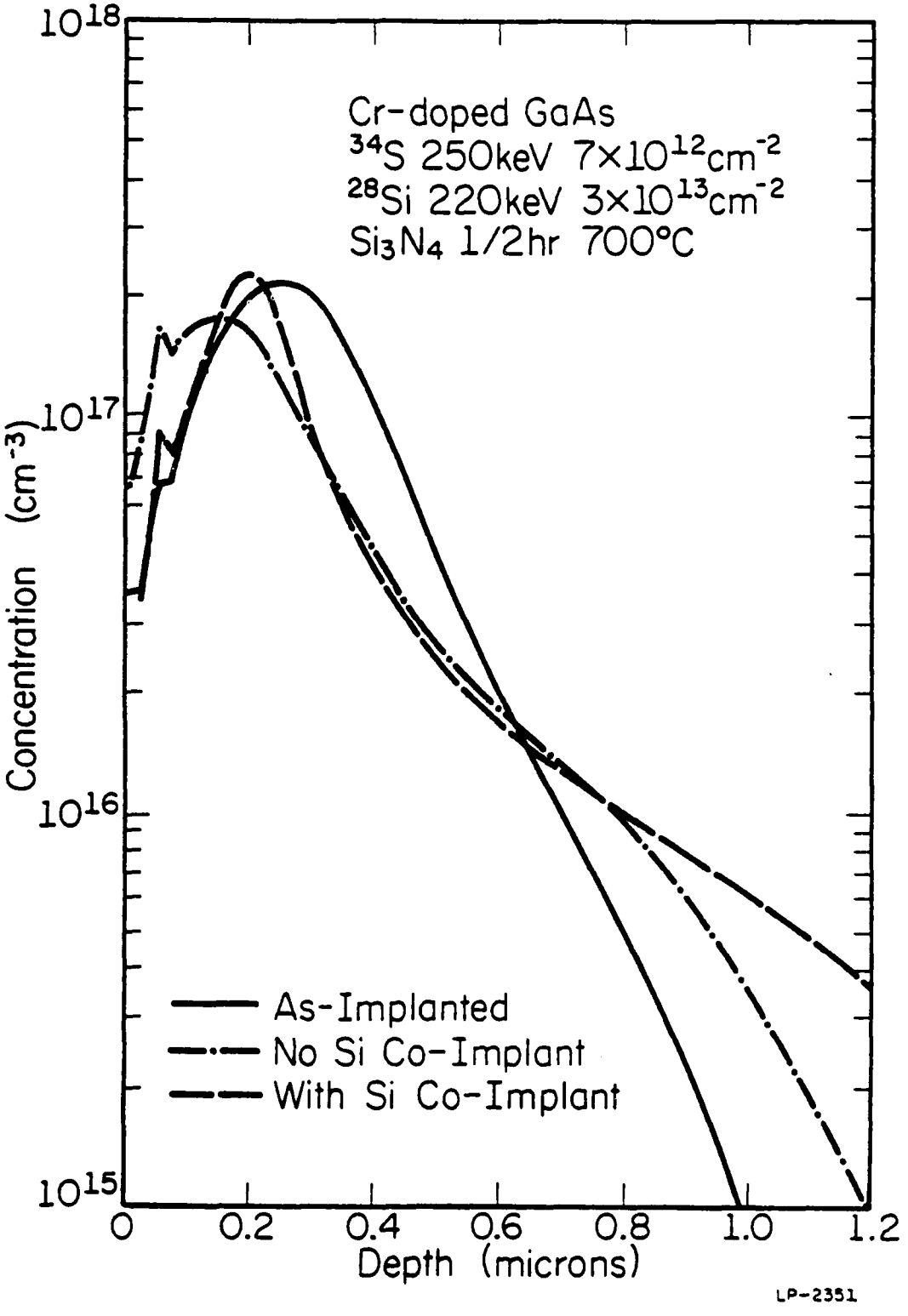


Fig. 5.8 SIMS profile of $^{34}S$ due to a $7 \times 10^{12}$ $cm^{-2}$, 250 keV $^{34}S$ implant in the presence of a $3 \times 10^{13}$ $cm^{-2}$, 220 keV $^{28}Si$ co-implant and annealed at 700°C ("With Si"). Shown also for comparison is the SIMS profile of $^{34}S$ if the $^{28}Si$ co-implant is absent ("Without Si").

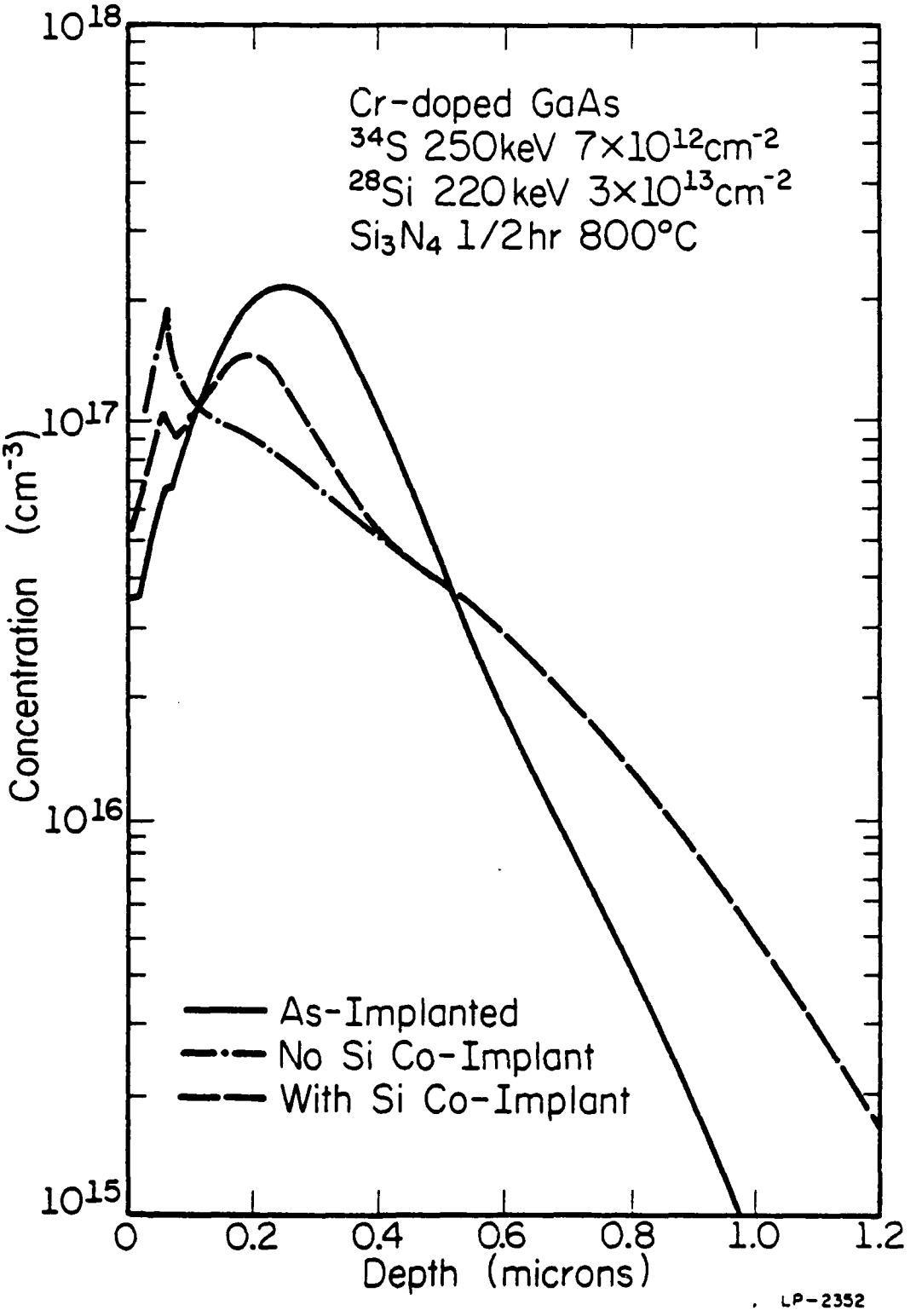


Fig. 5.9 SIMS profile of $^{34}S$ due to a $7 \times 10^{12}$ $cm^{-2}$, 250 keV $^{34}S$ implant in the presence of a $3 \times 10^{13}$ $cm^{-2}$, 220 keV $^{28}Si$ co-implant and annealed at 800°C ("With Si"). Shown also for comparison is the SIMS profile of $^{34}S$ if the $^{28}Si$ co-implant is absent ("Without Si").

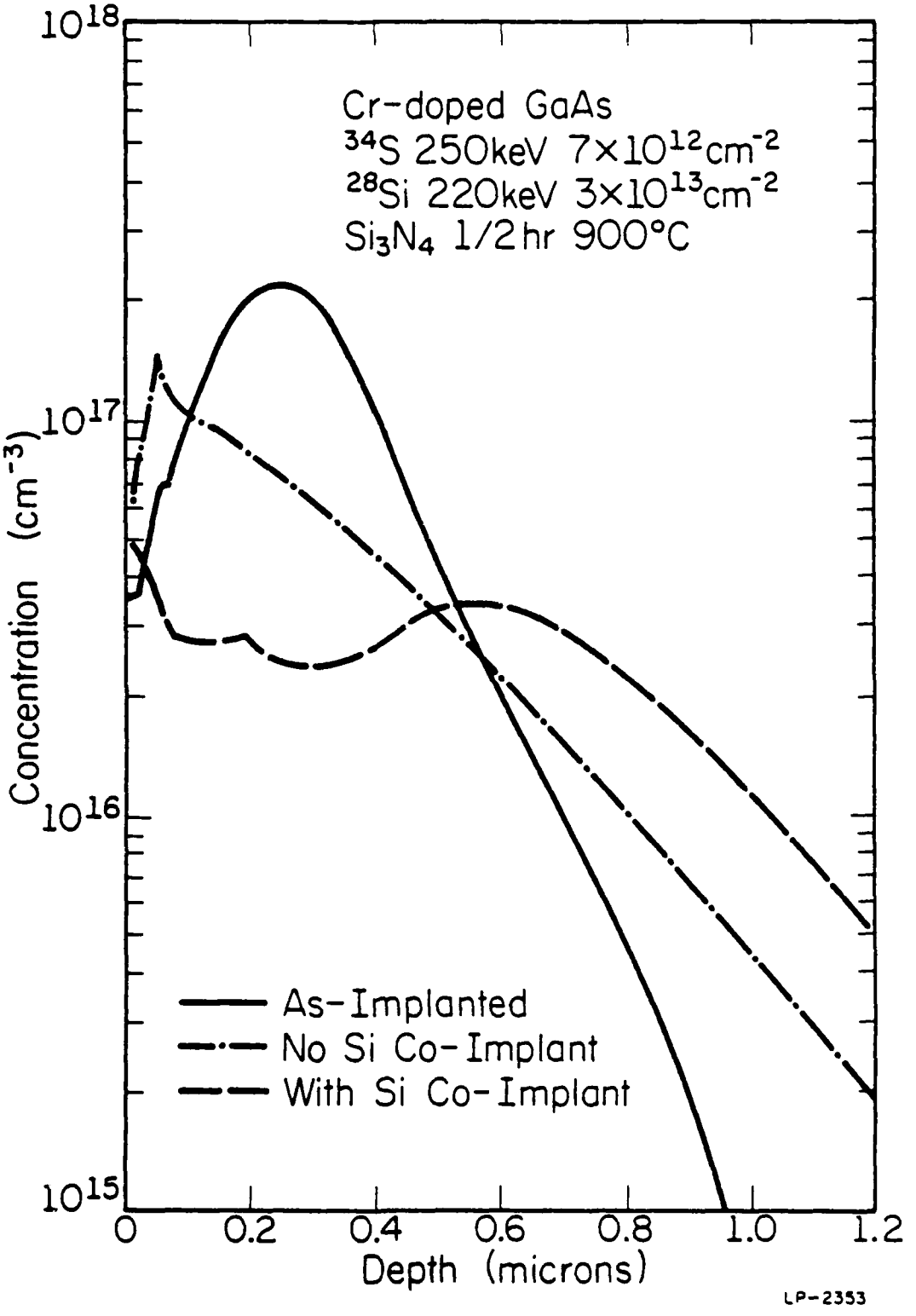


Fig. 5.10 SIMS profile of $^{34}S$ due to a $7 \times 10^{12}$ $cm^{-2}$, 250 keV $^{34}S$ implant in the presence of a $3 \times 10^{13}$ $cm^{-2}$, 220 keV $^{28}Si$ co-implant and annealed at 900°C ("With Si"). Shown also for comparison is the SIMS profile of $^{34}S$ if the $^{28}Si$ co-implant is absent ("Without Si").

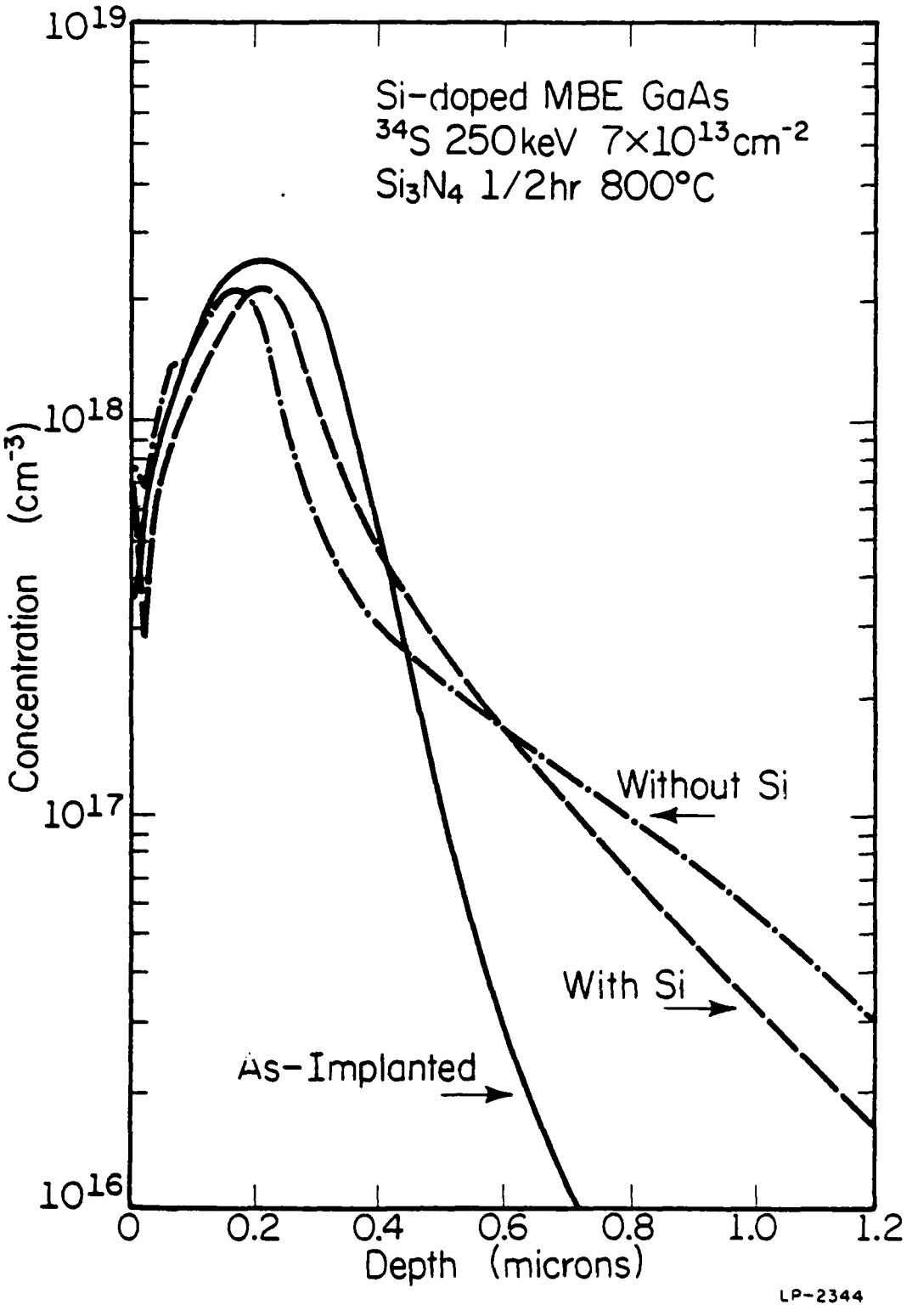


Fig. 5.11 SIMS profile of $^{34}S$ due to a $7 \times 10^{13}$ $cm^{-2}$ $^{34}S$ implant into heavily Si-doped (Nd ≈ $2.2 \times 10^{18}$ $cm^{-3}$) MBE GaAs annealed at 800°C ("With Si"). Shown also for comparison is the SIMS profile of $^{34}S$ if the Si-doping is absent ("Without Si").

is almost exponential, raising the possibility of a mechanism which slows down the fast diffusing S by trapping it with the Si-doping [79,80]. When the annealing temperature is further raised to 900°C, thermal processes again dominate and the S diffusion is actually more pronounced than if the Si-doping is absent (Fig. 5.12).

The effect of the Si is dependent on its concentration. Similar experiments performed in an MBE layer doped with $1 \times 10^{18}$ $cm^{-3}$ Si show no modification of the diffusivity of S for 800°C annealing. This supports the view that a short range interaction between S and Si, e.g., the formation of a nearest-neighbor complex as suggested by Yoder [50], is responsible for reducing the redistribution of S due to diffusion. Reducing the concentration of Si would reduce the probability of a near distance encounter required for complex formation. At sufficiently high temperatures, such complexing effects will vanish because of increasing domination by thermal events, as is observed here.

Si is known to be a slow diffuser in GaAs. The possible S-Si complex may be a slow diffuser simply because of the difficulty of moving Si through the GaAs lattice or because the complex has a physical size too large to diffuse very effectively.

## 5.3. S and Ar Dual Implants

From Fig. 5.3, it appears that other factors besides Si-doping must also be involved in reducing S diffusivity in S + Si dual implants with a sufficiently large Si dose. The effects of Si-doping alone would have resulted in the total loss of the shape of the as-implanted S profile at 900°C annealing (Fig. 5.12), while the dual implants show a S distribution which is still approximately peaked at the projected range and the

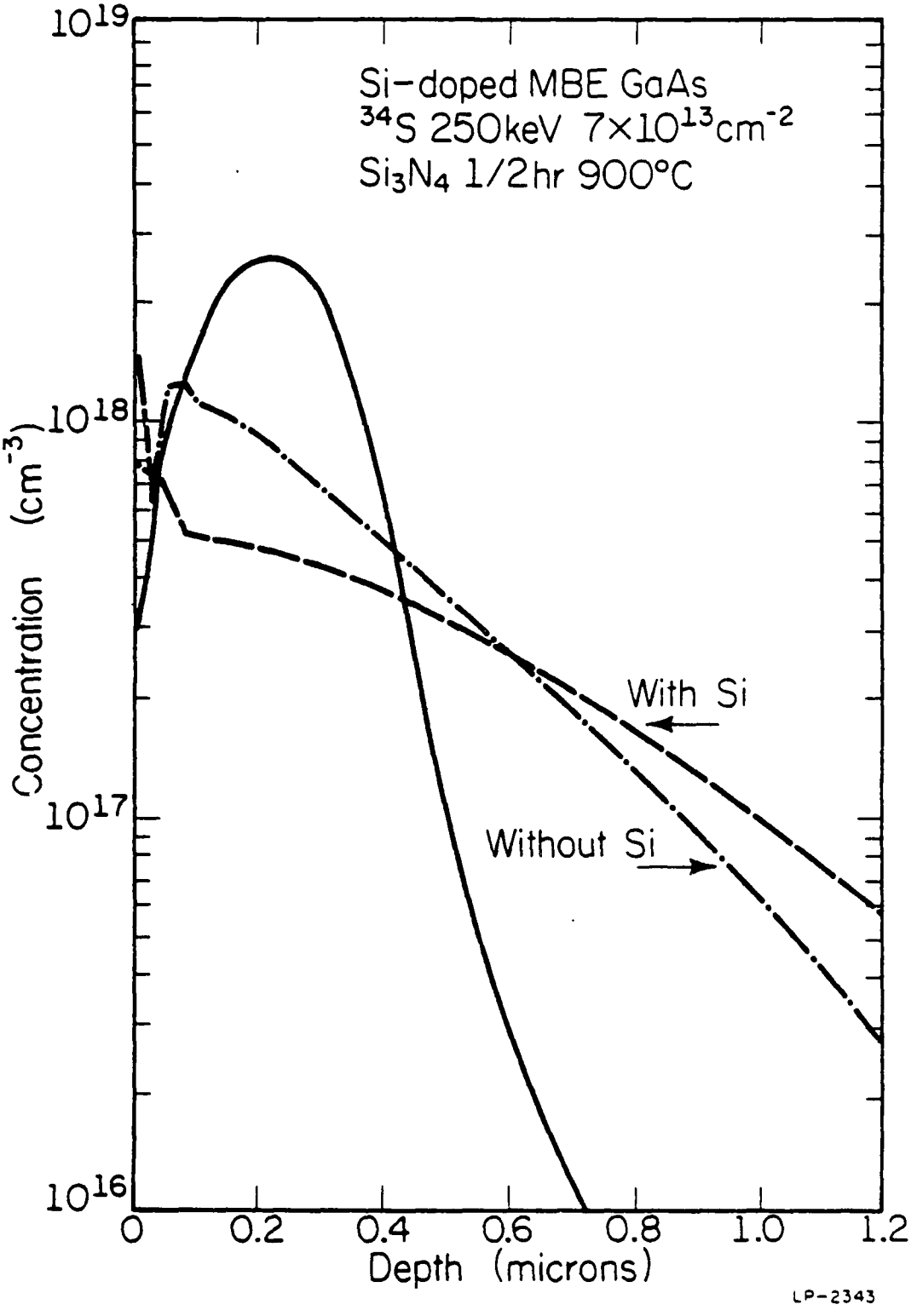


Fig. 5.12 SIMS profile of $^{34}S$ due to a $7 \times 10^{13}$ $cm^{-2}$ $^{34}S$ implant into heavily Si-doped (Nd ≈ $2.2 \times 10^{18}$ $cm^{-3}$) MBE GaAs annealed at 900°C ("With Si"). Shown also for comparison is the SIMS profile of $^{34}S$ if the Si-doping is absent ("Without Si").

formation of a secondary peak at around 0.6 μm. The next factor to be examined is, therefore, the additional implantation damage associated with the Si co-implants.

To simulate the damage due to the Si co-implants, Ar is co-implanted with S at 250 keV and to the same doses as the Si co-implants ($R_p$ = 0.17 μm for Ar). In the case of a $7 \times 10^{13}$ $cm^{-2}$ S implant and a $3 \times 10^{14}$ $cm^{-2}$ Ar co-implant, the amount of S diffusion at 800°C annealing is observed to be even somewhat less than if a Si co-implant were used (Fig. 5.13). When the annealing temperature is raised to 900°C, no secondary peak is formed. Instead, an approximately gaussian tail appears which largely coincides with the tail of the secondary peak found with the Si co-implant of the same dose (Fig. 5.14). It therefore appears that the presence of Si is necessary for the formation of the secondary peak observed in Fig. 5.3.

For the same S dose ($7 \times 10^{13}$ $cm^{-2}$), when the dose of the Ar co-implant is raised to $5 \times 10^{14}$ $cm^{-2}$ (well above the estimated amorphization limit of $\sim 1.5 \times 10^{14} cm^{-2}$ [ref. 31, extrapolated]) very little S diffusion is observed for 800°C annealing (Fig. 5.15). At 900°C somewhat more diffusion is observed, but the redistribution is much less than in single S implants or even S + Si dual implants (Fig. 5.16). Again, no secondary peak is formed.

When the dose of the Ar co-implant is lowered to $3.5 \times 10^{13}$ $cm^{-2}$, damage enhanced diffusion is observed (Figs. 5.17-5.19) in much the same way as with the corresponding low dose Si co-implant.

It may be concluded that a large density of implantation damage actually inhibits the diffusion of S while a low level of damage enhances it. This helps to explain the dose dependent trends of the redistribution

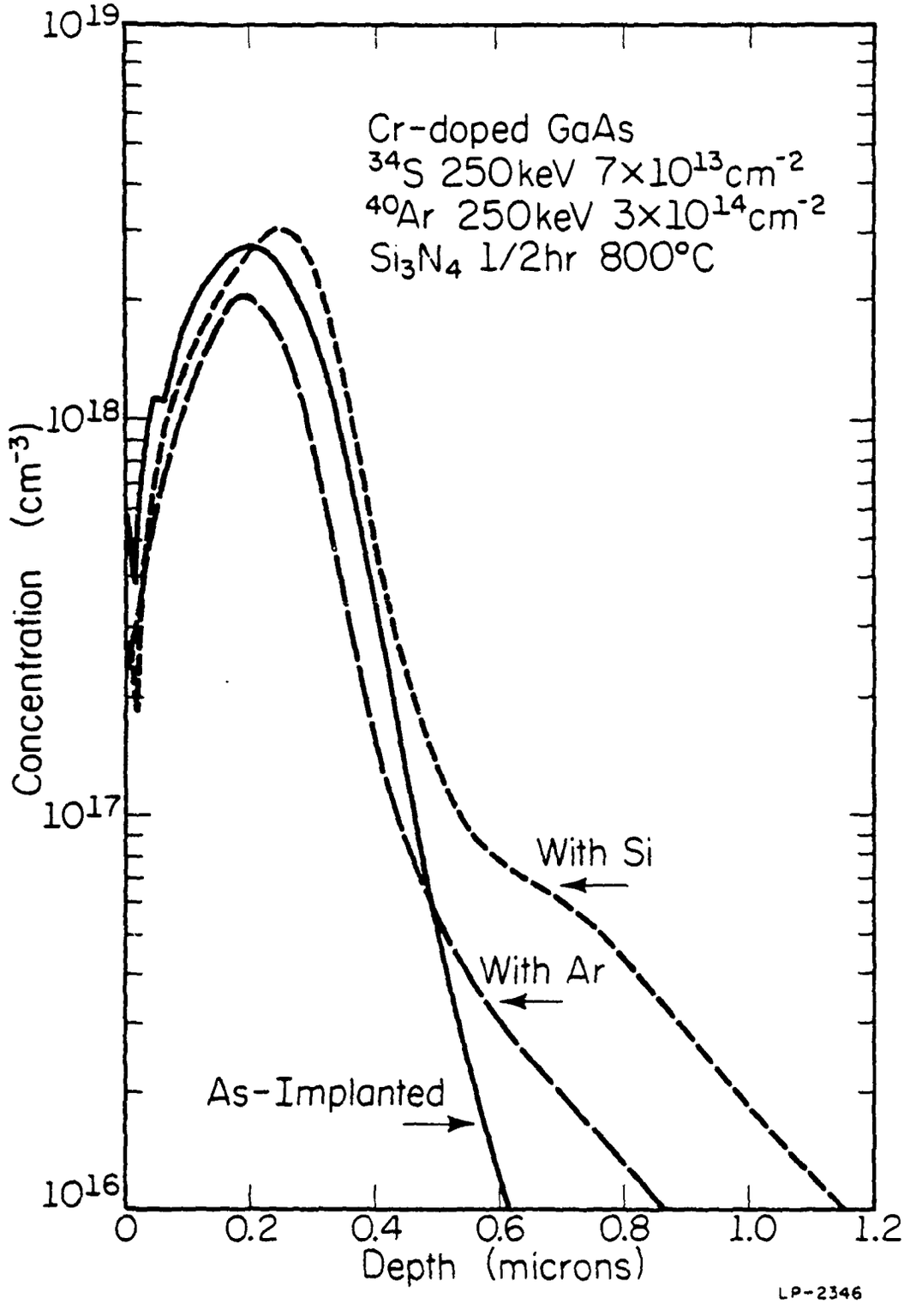


Fig. 5.13 SIMS profile of $^{34}S$ due to a $7 \times 10^{13}$ $cm^{-2}$, 250 keV $^{34}S$ implant in the presence of a $3 \times 10^{14}$ $cm^{-2}$, 250 keV $^{40}Ar$ co-implant and annealed at 800°C ("With Ar"). Shown also for comparison is the SIMS profile of $^{34}S$ due to the same $^{34}S$ implant in the presence of a $3 \times 10^{14}$ $cm^{-2}$, 220 keV $^{28}Si$ implant annealed at the same temperature ("With Si").

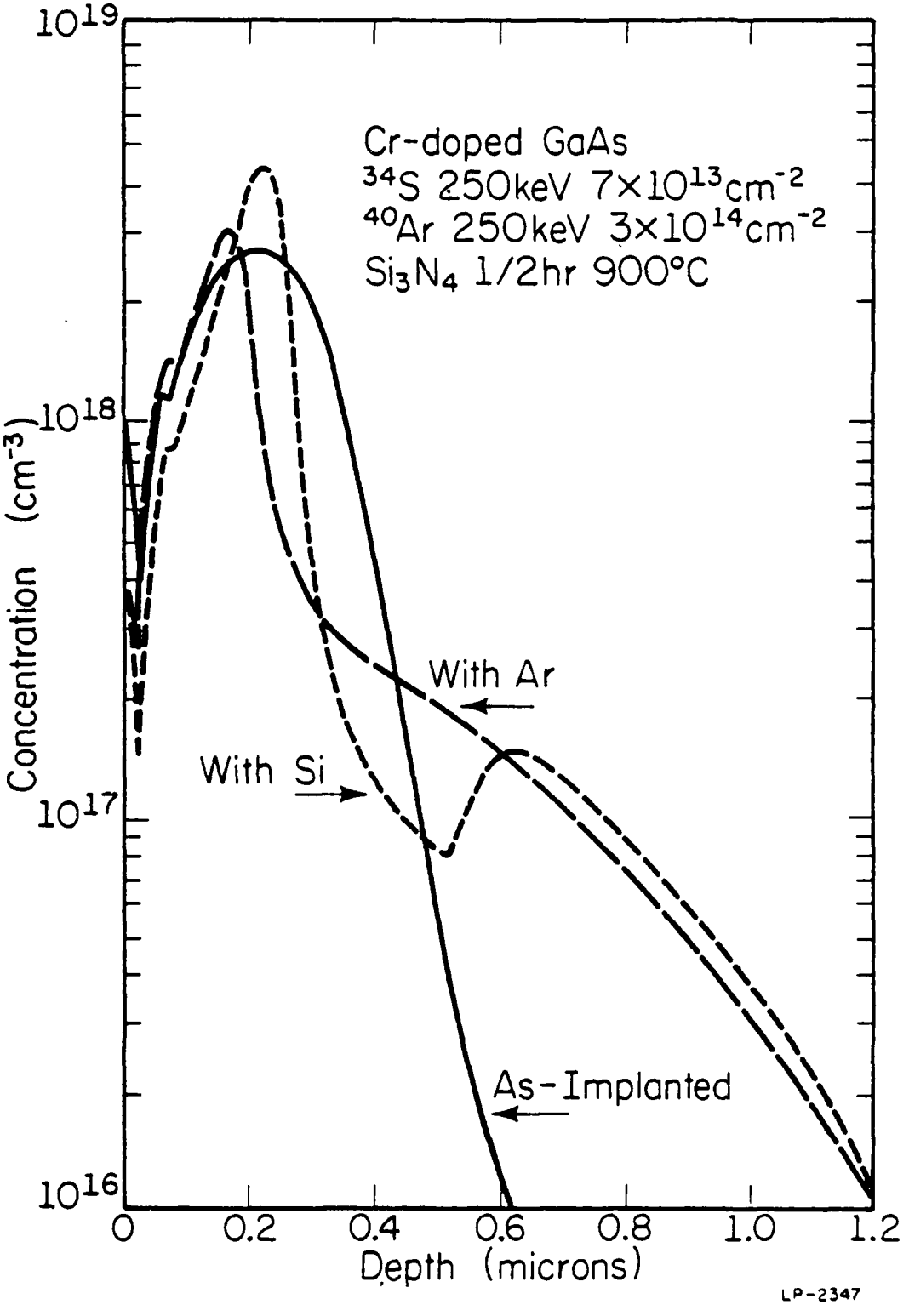


Fig. 5.14 SIMS profile of $^{34}S$ due to a $7 \times 10^{13}$ $cm^{-2}$, 250 keV $^{34}S$ implant in the presence of a $3 \times 10^{14}$ $cm^{-2}$, 250 keV $^{40}Ar$ co-implant and annealed at 900°C ("With Ar"). Shown also for comparison is the SIMS profile of $^{34}S$ due to the same $^{34}S$ implant in the presence of a $3 \times 10^{14}$ $cm^{-2}$, 220 keV $^{28}Si$ implant annealed at the same temperature ("With Si").

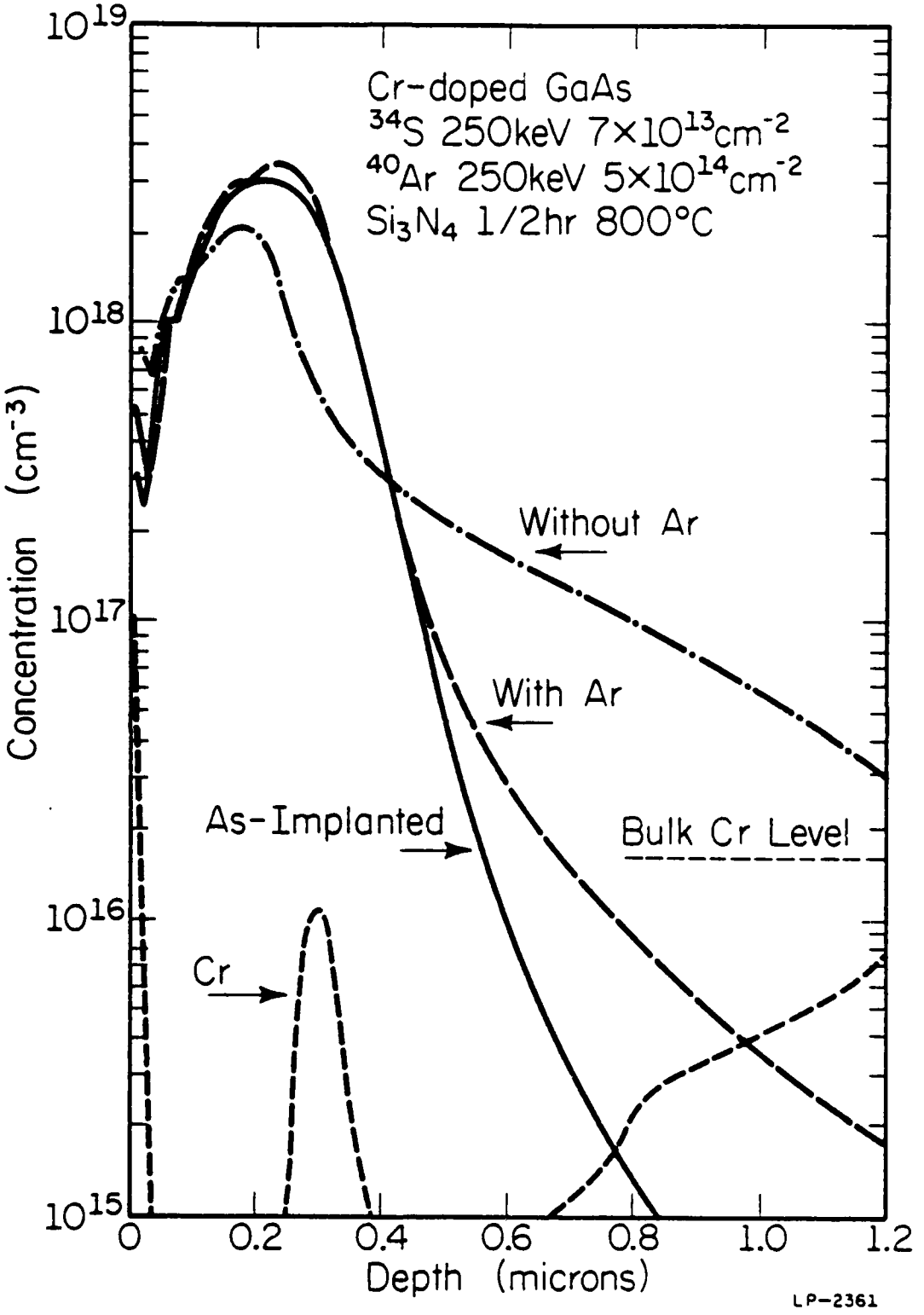


Fig. 5.15 SIMS profile of $^{34}S$ due to a $7 \times 10^{13}$ cm$^{-2}$, 250 keV $^{34}S$ implant in the presence of an amorphizing $5 \times 10^{14}$ cm$^{-2}$, 250 keV $^{40}Ar$ co-implant and annealed at 800°C ("With Ar"). Shown also for comparison is the SIMS profile of $^{34}S$ if the $^{40}Ar$ co-implant is absent ("Without Ar") and the Cr distribution in the dual implant.

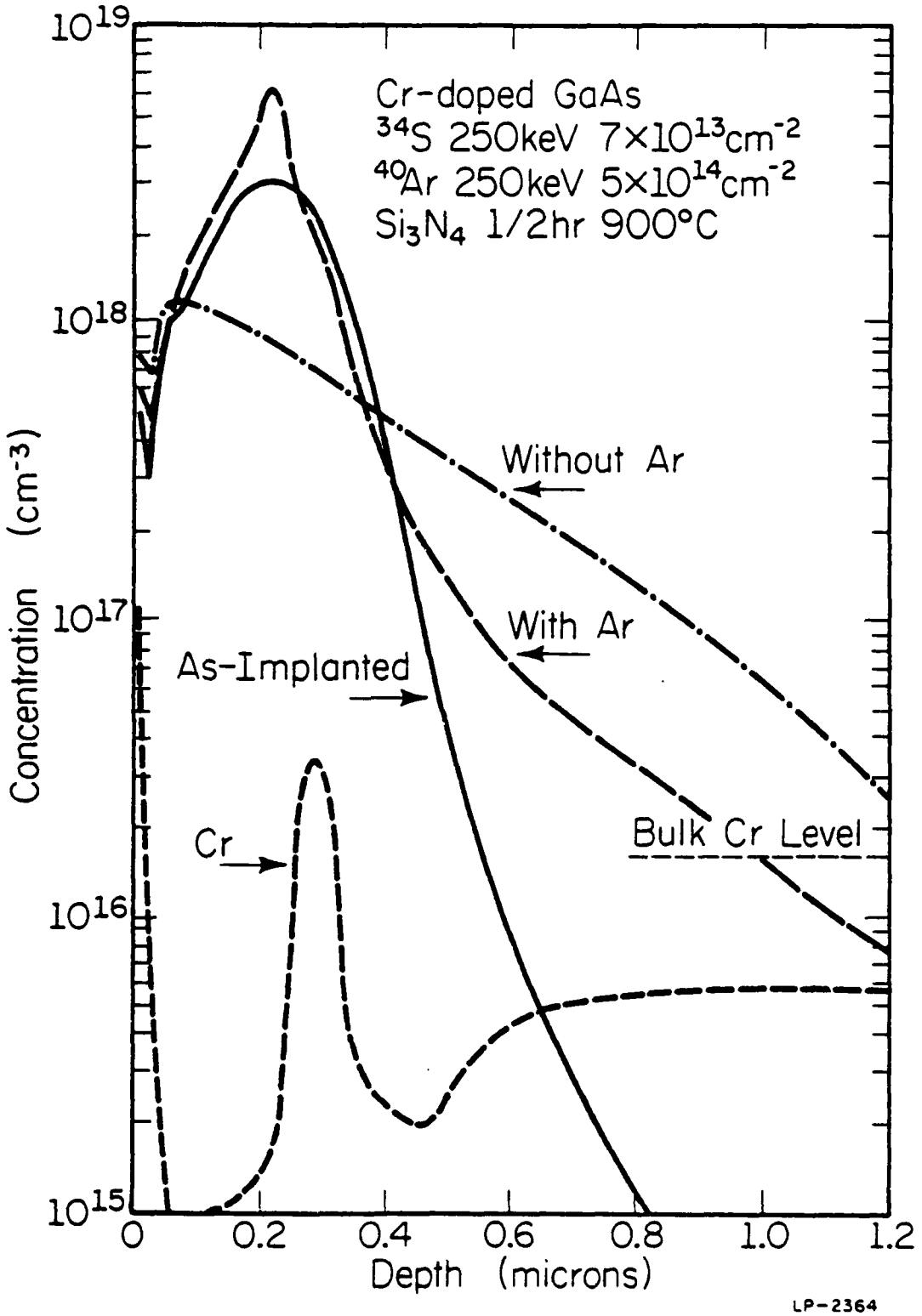


Fig. 5.16 SIMS profile of $^{34}S$ due to a $7 \times 10^{13}$ $cm^{-2}$, 250 keV $^{34}S$ implant in the presence of an amorphizing $5 \times 10^{14}$ $cm^{-2}$, 250 keV $^{40}Ar$ co-implant and annealed at 900°C ("With Ar"). Shown also for comparison is the SIMS profile of $^{34}S$ if the $^{40}Ar$ co-implant is absent ("Without Ar") and the Cr distribution in the dual implant.

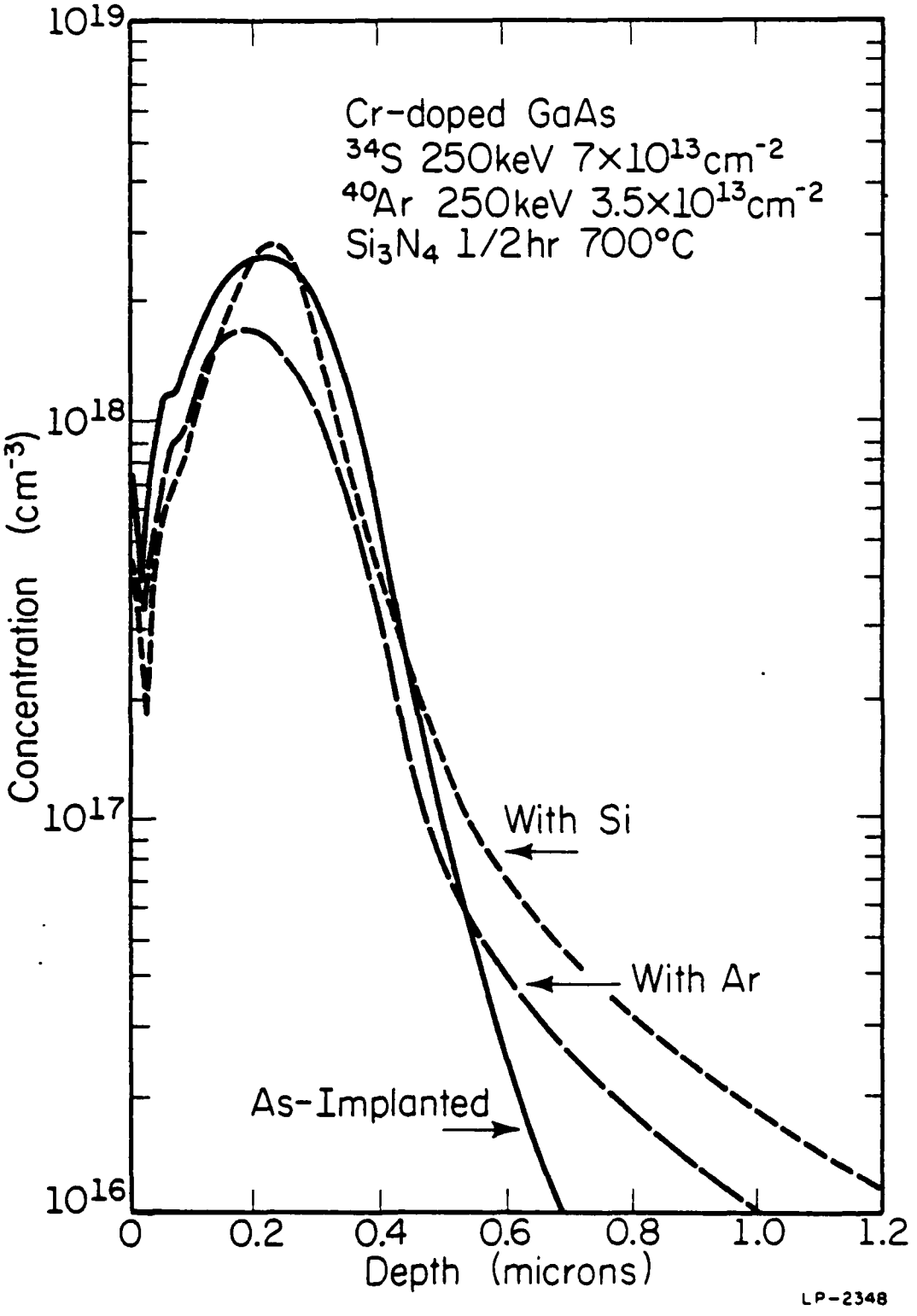


Fig. 5.17 SIMS profile of $^{34}S$ due to a $7 \times 10^{13}$ cm$^{-2}$, 250 keV $^{34}S$ implant in the presence of a $3.5 \times 10^{13}$ cm$^{-2}$, 250 keV $^{40}Ar$ co-implant and annealed at 700°C ("With Ar"). Shown also for comparison is the SIMS profile of $^{34}S$ if the $^{40}Ar$ co-implant is replaced by a 220 keV $^{28}Si$ co-implant of the same dose ("With Si").

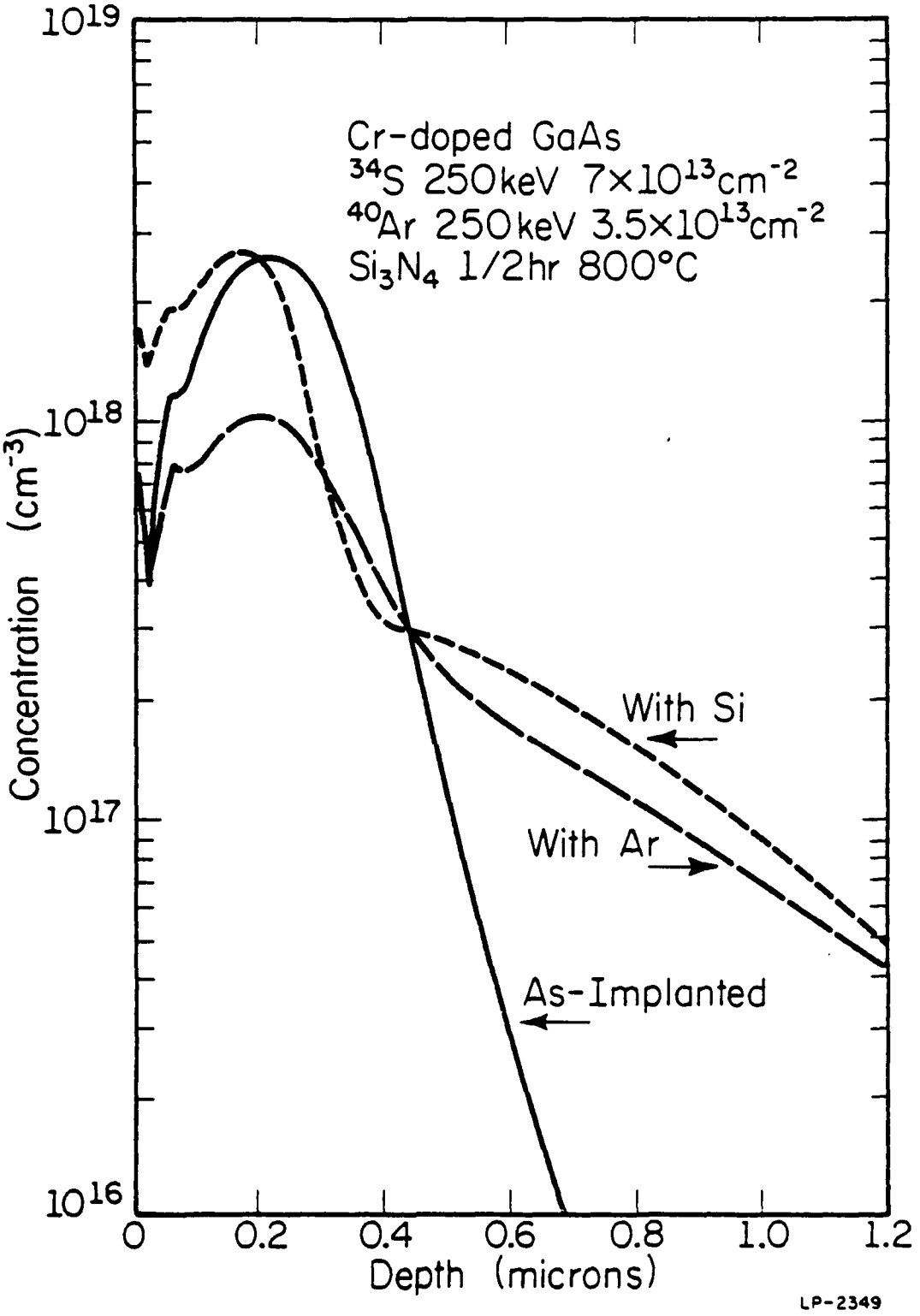


Fig. 5.18 SIMS profile of $^{34}S$ due to a $7 \times 10^{13}$ $cm^{-2}$, 250 keV $^{34}S$ implant in the presence of a $3.5 \times 10^{13}$ $cm^{-2}$, 250 keV $^{40}Ar$ co-implant and annealed at 800°C ("With Ar"). Shown also for comparison is the SIMS profile of $^{34}S$ if the $^{40}Ar$ co-implant is replaced by a 220 keV $^{28}Si$ co-implant of the same dose ("With Si").

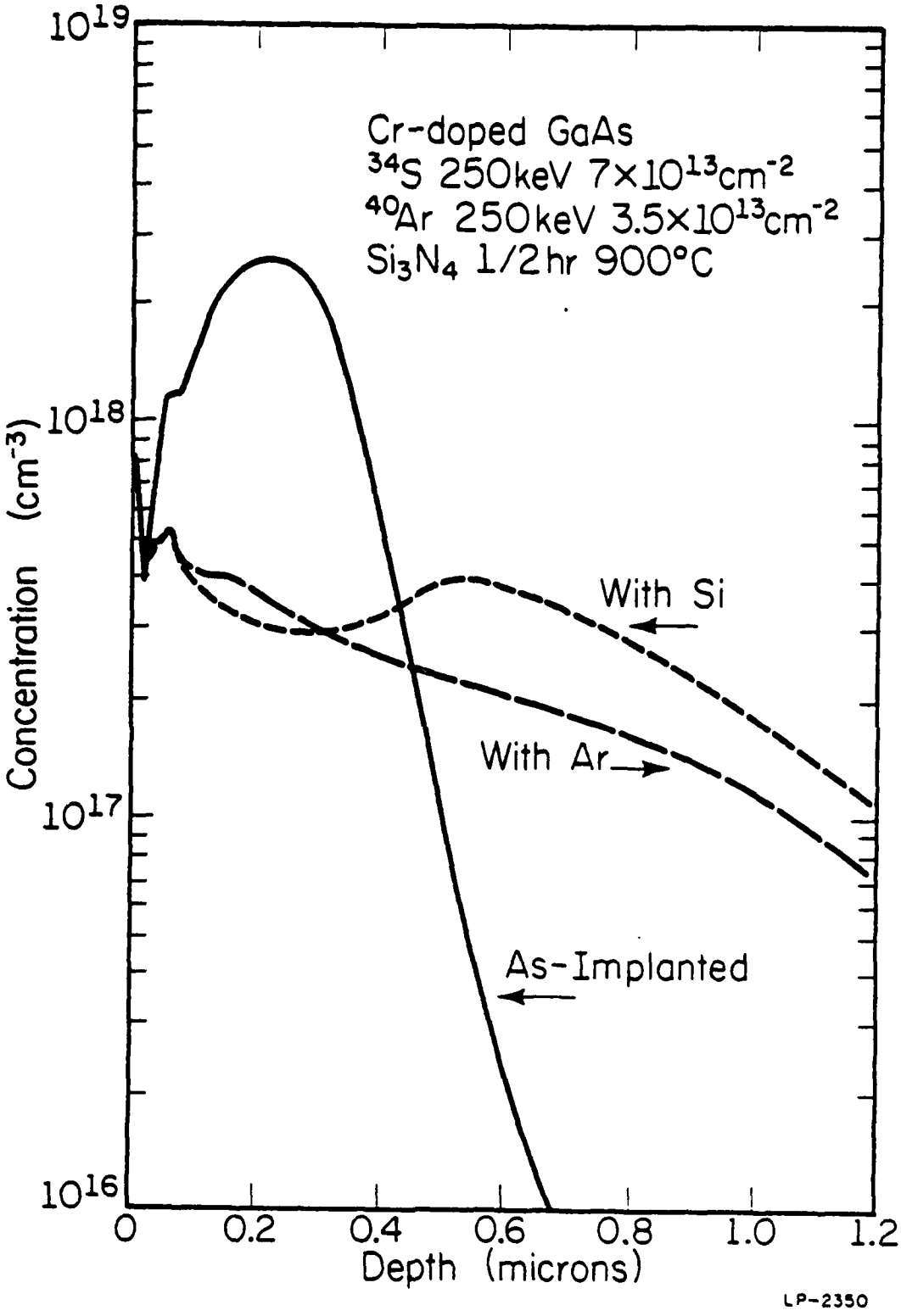


Fig. 5.19 SIMS profile of $^{34}S$ due to a $7 \times 10^{13}$ cm$^{-2}$, 250 keV $^{34}S$ implant in the presence of a $3.5 \times 10^{13}$ cm$^{-2}$, 250 keV $^{40}Ar$ co-implant and annealed at 900°C ("With Ar"). Shown also for comparison is the SIMS profile of $^{34}S$ if the $^{40}Ar$ co-implant is replaced by a 220 keV $^{28}Si$ co-implant of the same dose ("With Si").

of single S implants. As the dose is increased, the increased level of radiation damage in the vicinity of the projected range reduces the broadening of the as-implanted peak upon annealing. However, away from the region of maximum implantation damage, the lower levels of defect densities result in the formation of penetrating tails, apparently due to defect enhanced diffusion. Finally, far away from the projected range, normal diffusion takes place and the extremities of the diffusion tails assume a gaussian shape.

In the S + Si dual implants using a medium dose ($7 \times 10^{13}$ $cm^{-2}$) of S and a larger dose ($> 10^{14}$ $cm^{-2}$) of Si, both the Si and the additional implantation damage due to the Si co-implant seem to have a part in reducing the diffusion of S during annealing. The origin of the secondary peak found after 900°C annealing in this case (Fig. 5.3) is still undetermined, but is possibly due to a complex interplay between Si trapping, inhibited S diffusion in regions of high implantation damage and enhanced diffusion in regions of low level damage. Christel and Gibbons [82] have presented calculations which show that local stoichiometric disturbances due to the different rates of energy transfer from the incident ions to the different types of substrate atoms (in this case Ga and As) can result in regions of excess As followed by a deeper region of excess Ga, with a transition region in between (Fig. 5.20). There is some experimental evidence that the Ga divacancy ($V_{Ga}V_{Ga}$) plays a significant role in aiding the diffusion of S in crystalline GaAs [49]. Hence, the region of excess Ga can be expected to be also a region of reduced S diffusivity, and a local depletion of S can occur at the transition region if the diffusivity of S in the region of excess As is also much reduced due to the presence of a sufficient concentration of Si and implantation damage.

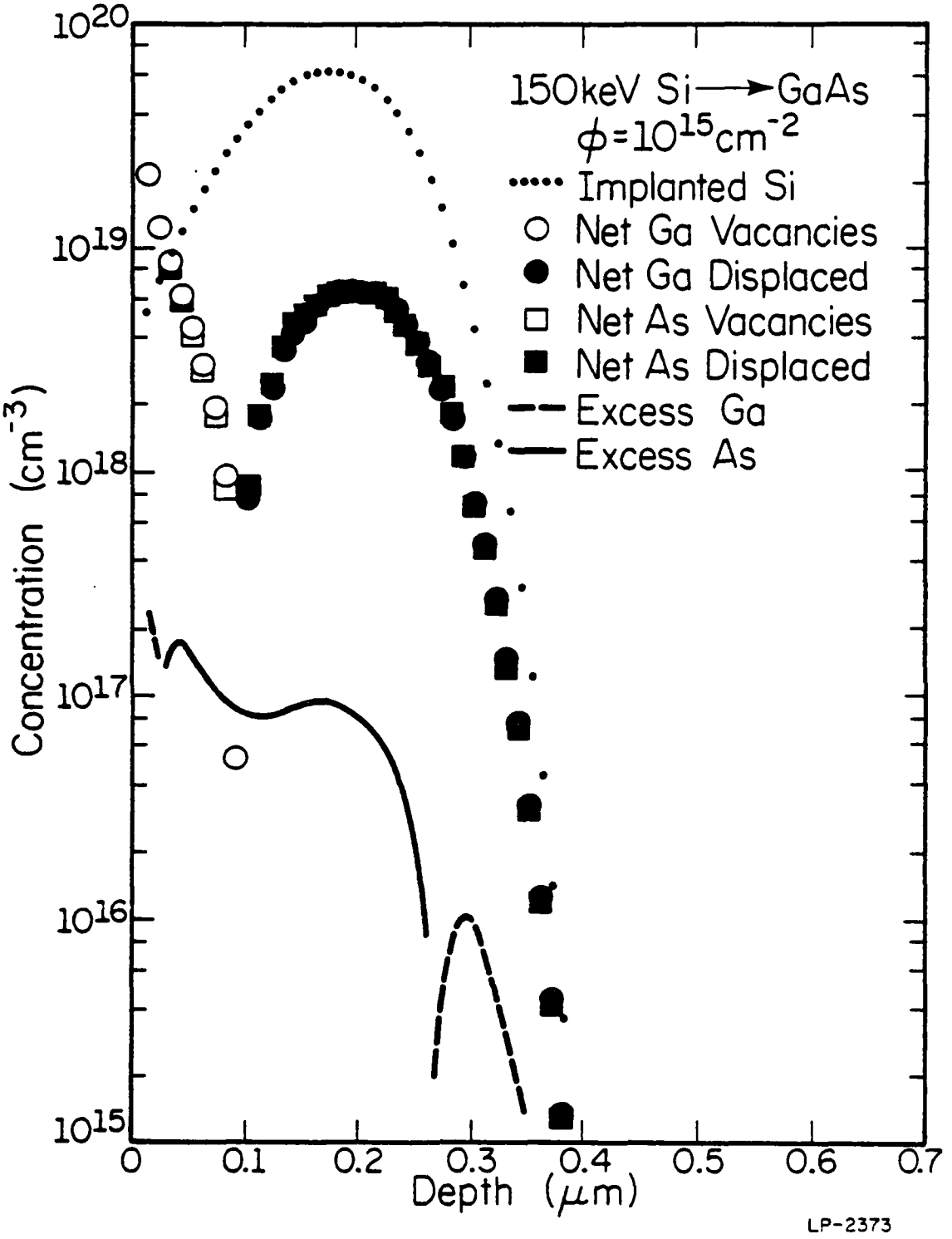


Fig. 5.20 Calculated stoichiometric distribution in GaAs implanted with 150 keV Si to a dose of $10^{15}$ $cm^{-2}$ [82].

## 5.4. Electrical Properties of the Dual Implants

The S + Si dual implants which reduce the diffusion of S can also have possible advantages in electrical activation. The tendency of a fraction of the implanted Si taking up acceptor (As) sites reduces the effective doping efficiency of high dose Si implants. S, being a column VI element, goes preferentially onto As sites. Hence its presence will reduce the availability of As sites to Si and increase the overall doping efficiency by decreasing the Si compensation ratio. The greatly retarded diffusion of S in the presence of amorphizing Ar implants seems attractive for situations in which the doping effects of Si co-implants are undesirable, provided that the amorphized substrate recovers sufficiently upon annealing. The electrical characteristics of such dual implants will be discussed in this section.

Shown in Fig. 5.21 are the carrier concentration and mobility profiles due to a dual implant of $7 \times 10^{13}$ $cm^{-2}$ S and $3 \times 10^{14}$ $cm^{-2}$ Si annealed at 800°C. Shown also in comparison (dashed line) is the carrier concentration profile due to a $3.7 \times 10^{14}$ $cm^{-2}$ single Si implant at 220 keV annealed at the same temperature. The activation efficiency of the dual implant is clearly better than that of the single Si implant of the same equivalent dose. The peak electron concentration in the dual implant is 45% higher ($\sim 1.55 \times 10^{18}$ $cm^{-3}$ vs $1.05 \times 10^{18}$ $cm^{-3}$) while the sheet carrier concentration is 50% higher ($\sim 3.4 \times 10^{13}$ $cm^{-2}$ vs. $2.2 \times 10^{13}$ $cm^{-2}$). A surface inactive layer of $\sim 0.25$ um exists in both cases and is presumably due to incomplete lattice recovery from implantation damage. The rapidly falling tail of the carrier concentration profile of the dual implant is consistent with the reduced diffusivity of S.

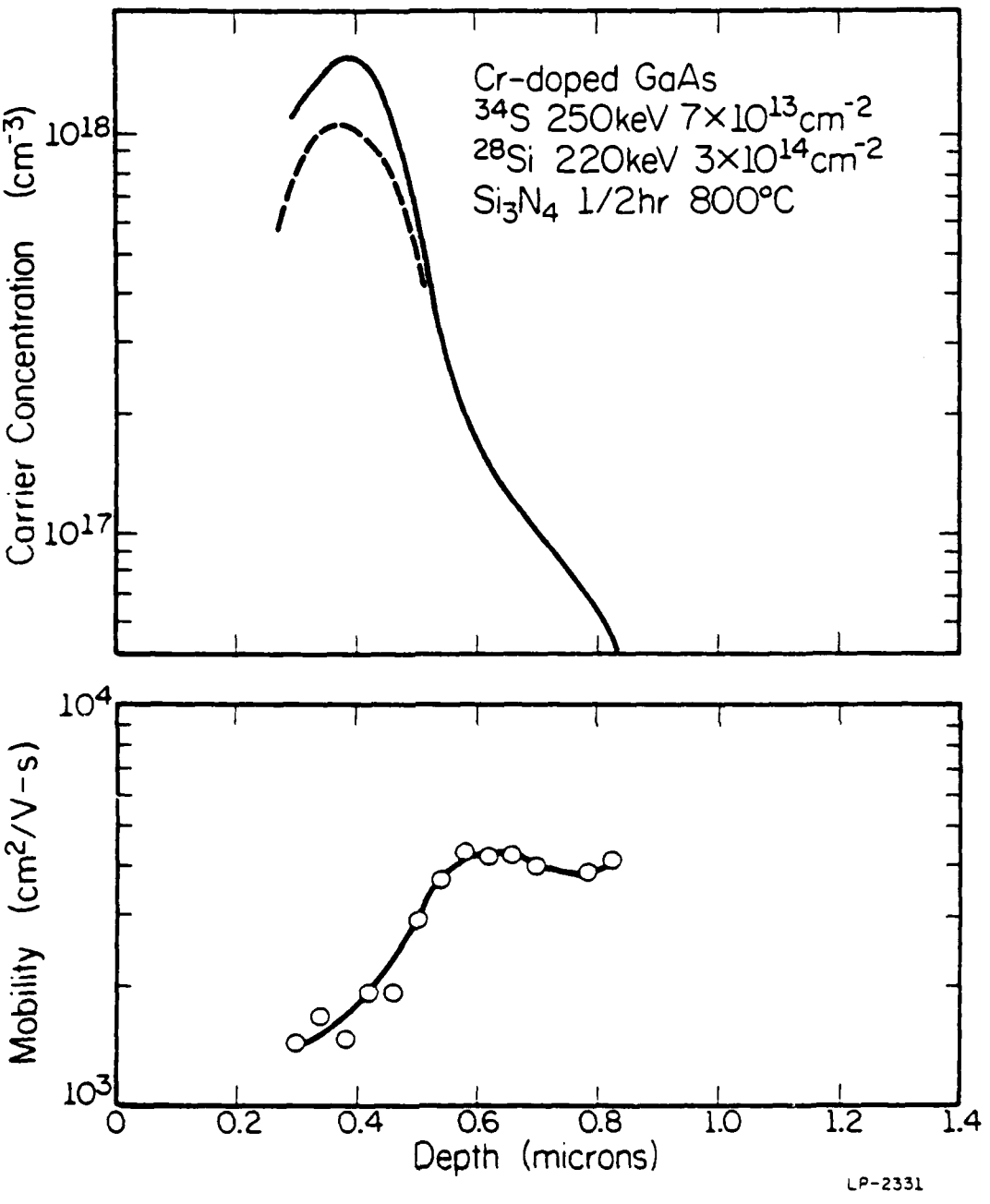


Fig. 5.21 Carrier concentration and mobility profiles due to a dual implant of $7 \times 10^{13}$ $cm^{-2}$ $^{34}S$ at 250 keV and $3 \times 10^{14}$ $cm^{-2}$ $^{28}Si$ at 220 keV annealed at 800°C. The dashed line is the carrier concentration profile due to a $3.7 \times 10^{14}$ $cm^{-2}$ $^{28}Si$ implant at 220 keV annealed at the same temperature.

Electrical measurements on S + Ar dual implants with $7 \times 10^{13}$ $cm^{-2}$ S at 250 keV and $5 \times 10^{14}$ $cm^{-2}$ Ar at 250 keV fail to detect any electrical activity after the samples are annealed at 800°C. Possible explanations for this include the following: 1) the amorphized GaAs does not recover sufficiently by annealing at 800°C to support any electrical activity; 2) damage gettering of Cr from the bulk creates such a level of Cr accumulation that the electrical activity of any S donors are completely compensated; 3) formation of thermally stable but electrically inactive complexes between S and defects.

Figures 5.15-5.16 also show the Cr distributions associated with the S + Ar dual implant. It is seen that for both 800°C and 900°C annealing there is a general Cr depletion region extending deep into the substrate, with a local accumulation in the vicinity of projected ranges of the implants. However, the Cr level in the local accumulation does not exceed $1.5 \times 10^{16}$ $cm^{-3}$ for 800°C annealing and is therefore insufficient to completely compensate the implanted S.

In another experiment, Cr-doped GaAs is amorphized by a $5 \times 10^{14}$ $cm^{-2}$ Ar implant at 250 keV. The sample is encapsulated with $Si_3N_4$ and annealed at 800°C for 15 min. The $Si_3N_4$ cap is then removed, and the sample is implanted with $7 \times 10^{13}$ $cm^{-2}$ S at 250 keV. Annealing is again performed with a $Si_3N_4$ cap for an additional 15 min at 800°C. The radiation damage associated with the amorphizing Ar implant is therefore annealed for a total time of 30 min, while the damage associated with the S implant is only annealed for 15 min. The results of SIMS measurements of the S distribution and electrical measurements after such a two-step anneal are shown in Fig. 5.22. It is obvious that the implanted layer recovers sufficiently to give a significant carrier concentration and a

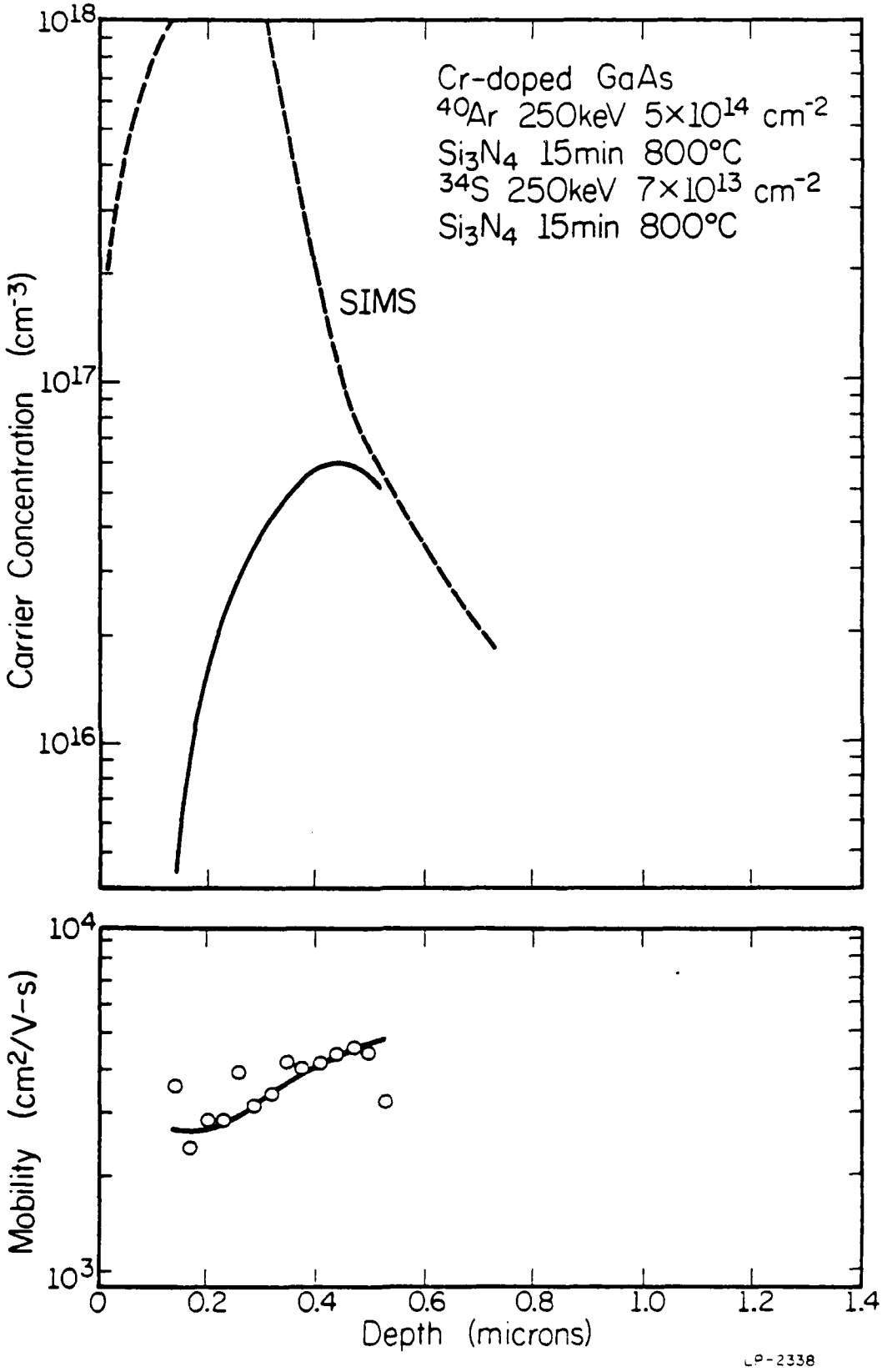


Fig. 5.22 Carrier concentration and mobility profiles after a two-step anneal at 800°C of a dual implant of an amorphizing $^{40}Ar$ implant and a $7 \times 10^{13}$ $cm^{-2}$ $^{34}S$ implant. The SIMS profile of $^{34}S$ is also shown for comparison.

relatively high mobility. It appears that the total compensation of the S impurities occurs only when they are annealed in the presence of a very large density of defects.

Hence, the complete lack of electrical activity in the S + Ar dual implants mentioned above is probably due to the formation of thermally stable but electrically inactive complexes between S and a high density of defects. It is entirely possible that these complexes are S-defect clusters which are too large to diffuse. Thus the lack of S diffusivity in these dual implants is unfortunately accompanied by a lack of electrical activity, and this limits the application of such dual implants to situations where selected areas with S donors are to be deactivated. This also suggests another reason why in the case of high dose ($10^{15}$ $cm^{-2}$) S implants very few carriers are found in the peak regions of the atomic S distributions where little S diffusion is observed: the peak regions of the atomic profiles are also regions of maximum implantation damage, and hence the formation of S-defect complexes is a distinct possibility.

## 5.5. Summary

Implanted S has been found to interact with Si co-implants or Si-doping at sufficiently high Si concentrations resulting in a decreased diffusivity of S. The S + Si dual implants also result in a higher activation efficiency over that obtainable by Si single implants of an equivalent dose. The observed S-Si interaction breaks down at 900°C.

Implanted S exhibits defect-enhanced diffusion at low levels of implantation damage and inhibited diffusion at high levels of damage. Unfortunately, in the case of damage inhibited diffusion, the electrical activity of S is lost at the same time. It is probable that annealing S

implants in the presence of a high density of implantation damage results in the formation of thermally stable but electrically inactive S-defect complexes which are too large to diffuse effectively.

# 6. CONCLUSIONS

The diffusion and electrical properties of implanted S in GaAs with or without co-implants have been investigated with SIMS and Hall effect measurements. The diffusivity has been found to be high and is affected by the presence of Si and implantation damage.

For single S implants, a dose dependent diffusion during annealing is observed. The shape of the as-implanted S distribution is best preserved in high dose ($10^{15}$ $cm^{-2}$) implants, but penetrating tails are formed in all cases. For low doses ($7 \times 10^{12}$ $cm^{-2}$), the diffusion tails are approximately gaussian and the estimated diffusion coefficients at the tail regions are $9 \times 10^{-13}$ $cm^2/sec$, $10^{-12}$ $cm^2/sec$ and $8 \times 10^{-12}$ $cm^2/sec$ for 700°C, 800°C and 900°C, respectively. These values are much higher than the values obtained from S indiffusion experiments into crystalline GaAs, and probably represent enhanced diffusion effects due to defects outdiffusing from the implanted region. For high doses ($10^{15}$ $cm^{-2}$), the shape of the as-implanted profile is largely preserved even after annealing at 900°C, but extremely long diffusion tails ($\geq$ 2 μm) which decay slower than an exponential function are formed. Outdiffusion into the $Si_3N_4$ cap is significant for all doses.

Electrical measurements are made for annealing temperatures up to 800°C since the Cr-doped substrates used type convert at 900°C. The activation efficiencies of the low dose ($7 \times 10^{12}$ $cm^{-2}$) and medium dose ($7 \times 10^{13}$ $cm^{-2}$) implants are at best fair, being 26% and 36% respectively after annealing at 800°C, and only 2.3% for high dose ($10^{15}$ $cm^{-2}$) implants annealed at the same temperature. For the medium dose implants, only a fraction of the implanted S in the vicinity of the peak of the

atomic profile is electrically active, while the activation efficiency at the tail of the atomic profile is practically 100% (for 800°C annealing). For high dose implants, almost none of the implanted S around the peak of the atomic distribution is electrically active, and most of the conductivity is contributed by the tail of the atomic profile, which also shows a very high activation efficiency. It appears that as the implantation dose is increased, the diffusivity of S around the peak regions of the atomic distribution is decreased, but the electrical activation in the same regions is decreased as well.

Implanted S has been found to interact with Si-doping, resulting in a reduced S diffusivity if the Si concentration is sufficiently high. The Si can be introduced during crystal growth or by co-implantation. S + Si dual implants give a higher electrical activation efficiency and a higher peak carrier concentration than single Si implants of the same total dose. The presence of S (which occupies As sites) probably forces a larger fraction of the implanted Si to occupy Ga sites, thereby increasing its doping efficiency by decreasing the compensation ratio. Reduction in S diffusivity due to S-Si interactions is observed up to annealing temperatures of 800°C. At 900°C, thermal processes again prevail, and the diffusivity is again very high unless other factors (as described below) are present.

Implanted S exhibits damage enhanced diffusion in the presence of low levels of implantation damage, as evidenced by its increased diffusivity in the presence of low dose ($3.5 \times 10^{13}$ $cm^{-2}$, 250 keV) Ar co-implants. However, in the presence of an amorphizing dose of Ar ($5 \times 10^{14}$ $cm^{-2}$, 250 keV), diffusion is dramatically reduced, to a degree even less than that observed for S-Si interactions. In addition,

the reduction in diffusivity persists even if the annealing temperature is raised to 900°C. Unfortunately, no appreciable electrical activity is found in these cases for annealing temperatures up to 800°C. Comparison with control experiments indicates that the crystal structure recovers sufficiently to support electrical activity and the total lack of carriers is probably due to the formation of thermally stable but electrically inactive S-defect complexes which are too large to diffuse. Such complexes are also likely to be the cause of the lack of S diffusivity and electrical activity of high dose ($10^{15}$ $cm^{-2}$) implants in regions where the implantation damage has been concentrated.

In conclusion, the high diffusivity of S will limit its use in device applications. S + Si dual implants can be used advantageously for selective $n^+$ doping with better doping efficiency, higher carrier concentrations, and reduced diffusivity of S. The applications of S + Ar dual implants (with amorphizing doses of Ar) will be limited to situations where selected areas with S-doping are to be deactivated, e.g., for electrical isolation purposes. Other impurity pairs can also be investigated for possible interactions that can be utilized advantageously for device fabrication.

# REFERENCES


1. H. Winston, "Semi-Insulating Gallium Arsenide Substrates for High-Frequency FET and IC Fabrication," Solid State Technology, vol. 26, no. 1, pp. 145-150, 1983.

2. A. M. Huber, G. Morillot, N. T. Linh, P. N. Favennec, B. Deveaud and B. Toulouse, "Chromium Profiles in Semi-Insulating GaAs after Annealing with a $Si_3N_4$ Encapsulant," Appl. Phys. Lett., vol. 34, pp. 858-859, 1979.

3. V. Eu, M. Feng, W. B. Henderson, H. B. Kim and J. M. Whelan, "Cr Profiles in Semi-Insulating GaAs after Annealing with and without $SiO_2$ Encapsulants in a $H_2$- $As_4$ Atmosphere," Appl. Phys. Lett., vol. 37, pp. 473-475, 1980.

4. H. Kanber, M. Feng, V. K. Eu, R. C. Rush and W. B. Henderson, "Correlation between Chemical and Electrical Profiles in $Si^+$, $Se^+$ and $S^+$ Implanted Bulk and Epitaxial GaAs," J. Electron. Mater., vol. 11, pp. 1083-1114, 1982.

5. P. K. Vasudev, R. G. Wilson and C. A. Evans, Jr., "Chromium Redistribution during Thermal Annealing of Semi-Insulating GaAs as a Function of Encapsulant and Implant Fluence," Appl. Phys. Lett., vol. 36, pp. 837-840, 1980.

6. P. M. Asbeck, J. Tandon, B. M. Welch, C. A. Evans, Jr. and V. R. Deline, "Effects of Cr Redistribution on Electrical Characteristics of Ion-Implanted Semi-Insulating GaAs," IEEE Electron Device Lett., vol. EDL-1, pp. 35-37, 1980.

7. S. Y. Chiang and G. L. Pearson, "Properties of Vacancy Defects in GaAs Single Crystals," J. Appl. Phys., vol. 46, pp. 2986-2991, 1975.

8. P. K. Chatterjee, K. V. Vaidyanathan, M. S. Durschlag and B. G. Streetman, "Photoluminescence Study of Native Defects in Annealed GaAs," Solid State Commun., vol. 17, pp. 1421-1424, 1975.

9. E. M. Swiggard, S. H. Lee and F. W. Von Batchelder, "GaAs Synthesized in Pyrolytic Boron Nitride (PBN)," in Gallium Arsenide and Related Compounds (St. Louis) 1976, edited by L. F. Eastman, Conf. Ser. 33b, Institute of Physics, Bristol and London, 1977, pp. 23-27.

10. R. L. Henry and E. M. Swiggard, "LEC Growth of InP and GaAs Using PBN Crucibles," in Gallium Arsenide and Related Compounds (St. Louis) 1976, edited by L. F. Eastman, Conf. Ser. 33b, Institute of Physics, Bristol and London, 1977, pp. 28-36.

11. T. R. AuCoin, R. L. Ross, M. J. Wade and R. O. Savage, "Liquid Encapsulated Compounding and Czochralski Growth of Semi-Insulating Gallium Arsenide," Solid State Technology, vol. 22, no. 1, pp. 59-62, p. 67, 1979.

12. D. E. Holmes, R. T. Chen, K. R. Elliott and C. G. Kirkpatrick, "Stoichiometry-Controlled Compensation in Liquid Encapsulated Czochralski GaAs," Appl. Phys. Lett., vol. 40, pp. 46-48, 1982.

13. J. Lagowski, H. C. Gatos, J. M. Parsey, K. Wada, M. Kaminska and W. Walakiewicz, "Origin of the 0.82-eV Electron Trap in GaAs and Its Annihilation by Shallow Donors," Appl. Phys. Lett., vol. 40, pp. 342-344, 1982.

14. S. Makram-Ebeid, D. Gautard, P. Devillard and G. M. Martin, "Outdiffusion of the Main Electron Trap in Bulk GaAs due to Thermal Treatment," Appl. Phys. Lett., vol. 40, pp. 161-163, 1982.

15. L. B. Ta, H. M. Hobgood, A. Rohatgi and R. N. Thomas, "Effects of Stoichiometry on Thermal Stability of Undoped, Semi-Insulating GaAs," J. Appl. Phys., vol. 53, pp. 5771-5775, 1982.

16. Y. Nanishi, S. Ishida, T. Honda, H. Yamazaki and S. Miyazawa, "Inhomogeneous GaAs FET Threshold Voltages Related to Dislocation Distribution," Jpn. J. Appl. Phys., part 2, vol. 21, pp. L335-L337, 1982.

17. S. Miyazawa, T. Mizutani and H. Yamazaki, "Leakage Current $I_L$ Variation Correlated with Dislocation Density in Undoped, Semi-Insulating LEC-GaAs," Jpn. J. Appl. Phys., part 2, vol. 21, pp. L542-L544, 1982.

18. P. M. Asbeck, C. G. Kirkpatrick, M. J. Sheets, E. J. Babcock, B. M. Welch and R. Zucca, "Reproducibility of FET Channel Implants for GaAs Digital ICs," presented at GaAs IC Symp., (San Diego, CA), 1981, unpublished.

19. A. Lidow, J. F. Gibbons, V. R. Deline and C. A. Evans, Jr., "Ion-Implanted Selenium Profiles in GaAs as Measured by Secondary Ion Mass Spectrometry," Appl. Phys. Lett., vol. 32, pp. 15-17, 1978.

20. J. P. Donnelly, "Ion Implantation in GaAs," in Gallium Arsenide and Related Compounds (St. Louis) 1976, edited by L. F. Eastman, Conf. Ser. 33b, Institute of Physics, Bristol and London, 1977, pp. 166-170.

21. F. H. Eisen, J. S. Harris, B. Welch, R. D. Pashley, D. Sigurd and J. W. Mayer, "Properties of Tellurium Implanted Gallium Arsenide," in Ion Implantation in Semiconductors and Other Materials, edited by B. L. Crowder. New York: Plenum Press, 1973, pp. 631-640.

22. D. E. Davies, S. Roosild and L. Lowe, "The Role of Elevated Temperatures in the Implantation of GaAs," Solid-State Electron., vol. 18, pp. 733-736, 1975.

23. M. Takai, K. Gamo, K. Masuda and S. Namba, "Effects of Implantation Temperature on Lattice Location of Tellurium Implanted in Gallium Arsenide," Jpn. J. Appl. Phys., vol. 12, pp. 1926-1930, 1973.

24. J. M. Woodcock, J. M. Shannon and D. J. Clark, "Electrical and Cathodoluminescence Measurements on Ion Implanted Donor Layers in GaAs," Solid-State Electron., vol. 18, pp. 267-275, 1975.

25. D. H. Lee and R. M. Malbon, "Ion-Implanted Silicon Profiles in GaAs," Appl. Phys. Lett., vol. 30, pp. 327-329, 1977.

26. H. Rupprecht, J. M. Woodall, K. Konnerth and D. G. Pettit, "Efficient Electroluminescence from GaAs Diodes at 300°K," Appl. Phys. Lett., vol. 9, pp. 221-223, 1966.

27. H. Kressel, J. U. Dunse, H. Nelson, F. Z. Hawrylo, "Luminescence in Silicon-Doped GaAs Grown by Liquid-Phase Epitaxy," J. Appl. Phys., vol. 39, pp. 2006-2011, 1968.

28. T. Morizumi and K. Takahashi, "Si- and Ge-Doped GaAs p-n Junctions," Jpn. J. Appl. Phys., vol. 8, pp. 348-357, 1969.

29. J. P. Donnelly, W. T. Lindley and C. E. Hurwitz, "Silicon- and Selenium- Ion-Implated GaAs Reproducibly Annealed at Temperatures up to 950°C," Appl. Phys. Lett., vol. 27, pp. 41-43, 1975.

30. S. G. Liu, E. C. Douglas, C. P. Wu, C. W. Magee, S. Y. Narayan, S. T. Jolly, F. Kolondra and S. Jain, "Ion Implantation of Sulfur and Silicon in GaAs," RCA Rev., vol. 41, pp. 227-262, 1980.

31. J. D. Sansbury and J. F. Gibbons, "Properties of Ion Implanted Silicon, Sulfur, and Carbon in Gallium Arsenide," Rad. Eff., vol. 6, pp. 269-276, 1970.

32. R. G. Hunsperger and O. J. Marsh, "Electrical Properties of Cd, Zn and S Ion-Implanted Layers in GaAs," Rad. Eff., vol. 6, pp. 263-268, 1970.

33. F. H. Eisen and M. B. Welch, "Radiotracer Profiles in Sulfur Implanted GaAs," in Ion Implantation in Semiconductors 1976, edited by F. Chernow, J. A. Borders and D. K. Brice. New York: Plenum Press, 1977, pp. 97-106.

34. M. Fujimoto, H. Yamazaki and T. Honda, "Sulfur Ion Implantation in Gallium Arsenide," in Ion Implantation in Semiconductors 1976, edited by F. Chernow, J. A. Borders and D. K. Brice. New York: Plenum Press, 1977, pp. 89-96.

35. H. Müller, J. Gyulai, J. W. Mayer, F. H. Eisen and B. Welch, "Anodic Oxidation and Profile Determination of Ion Implanted Semi-Insulating GaAs," in Ion Implantation in Semiconductors, edited by S. Namba. New York: Plenum Press, 1975, pp. 19-25.

36. R. M. Malbon, D. H. Lee and J. M. Whelan, "Annealing of Ion Implanted GaAs in a Controlled Atmosphere," J. Electrochem. Soc., vol. 123, pp. 1413-1415, 1976.

37. R. G. Wilson and D. M. Jamba, "Dependence of Implanted Se and S Profiles on GaAs Implantation Temperature and Crystallinity," Appl. Phys. Lett., vol. 39, pp. 715-717, 1981.

38. Y. K. Yeo, Y. S. Park and R. Kwor, "Correlation of Electrical Carrier and Atomic Profiles of S Implants in GaAs," J. Appl. Phys., vol. 53, pp. 1815-1817, 1982.

39. R. Kwor, Y. K. Yeo and Y. S. Park, "Electrical Properties and Distribution of S Implants in GaAs," J. Appl. Phys., vol. 53, pp. 4786-4792, 1982.

40. P. Baruch, "Radiation Defects and Impurity Diffusion in Silicon," in Radiation Effects in Semiconductors 1976, edited by N. B. Urli and J. W. Corbett, Conf. Ser. 31, Institute of Physics, Bristol and London, 1977, pp. 126-143.

41. E. B. Stoneham and J. F. Gibbons, "Control of Zinc Diffusivity in $GaAs_{0.6}P_{0.4}$ by Multiple Implantation," J. Appl. Phys., vol. 48, pp. 5086-5091, 1977.

42. W. V. McLevige, "Annealing Studies of Beryllium in Gallium Arsenide and Gallium Arsenide Phosphide," Ph.D. thesis, U. of Illinois, 1978.

43. A. Lidow, J. F. Gibbons, V. R. Deline and C. A. Evans, Jr., "Fast Diffusion of Elevated-Temperature Ion-Implanted Se in GaAs as Measured by Secondary Ion Mass Spectrometry," Appl. Phys. Lett., vol. 32, pp. 149-151, 1978.

44. B. J. Masters and E. F. Gorey, "Proton-Enhanced Diffusion and Vacancy Migration in Silicon," J. Appl. Phys., vol. 49, pp. 2717-2724, 1978.

45. E. B. Stoneham and J. F. Gibbons, "The Effects of Ion-Implanted Ga, As and P on the Subsequent Diffusion of Ion-Implanted Zn in $GaAs_{0.6}P_{0.4}$," in Ion Implantation in Semiconductors, edited by S. Namba. New York: Plenum Press, 1975, pp. 57-63.

46. D. Lecrosnier, J. Paugam, G. Pelous, F. Richou and M. Salvi, "Gold Gettering in Silicon by Phosphorus Diffusion and Argon Implantation: Mechanisms and Limitations," J. Appl. Phys., vol. 52, pp. 5090-5097, 1981.

47. A. J. N. Houghton and B. Tuck, "Diffusion of Zinc into Ion-Implanted Gallium Arsenide," Solid-State Electron., vol. 25, pp. 441-448, 1982.

48. P. N. Favennec, M. Gauneau, H. L'Haridon, B. Deveaud, C. A. Evans, Jr. and R. J. Blattner, "Chromium Gettering in GaAs by Oxygen Implantation," Appl. Phys. Lett., vol. 38, pp. 271-273, 1981.

49. A. B. Young and G. L. Pearson, "Diffusion of Sulfur in Gallium Phosphide and Gallium Arsenide," J. Phys. Chem. Solids, vol. 31, pp. 517-527, 1970.

50. M. N. Yoder, "Complexes and their Effects on III-V Compounds," Semi-Insulating III-V Materials Conference, University of Nottingham, April 14-16, 1980.

51. J. G. Oakes and J. E. Degenford, GaAs Monolithic Microwave Subsystem Technology, Base Report N00014-78-C-0268, Westinghouse Electric, 1980.

52. J. Lindhard and A. Winther, "Stopping Power of Electron Gas and Equipartition Rule," Mat. Fys. Medd. Dan. Vid. Selsk., vol. 34, pp. 1-21, 1964.

53. O. B. Firsov, "A Qualitative Interpretation of the Mean Excitation Energy in Atomic Collisions," J. Exper. Theoret. Phys., vol. 36, pp. 1517-1523, 1959.

54. J. Lindhard, M. Scharff and H. Schiott, "Range Concepts and Heavy Ion Ranges," Mat. Fys. Medd. Dan. Vid. Selsk., vol. 33, pp. 1-39, 1963.

55. J. F. Gibbons, W. S. Johnson and S. W. Mylroie, Projected Range Statistics, Semiconductors and Related Materials, 2nd edition. Stroudsburg, Pennsylvania: Dowden, Hutchinson and Ross, 1975.

56. S. T. Picraux, "Vaporisation of Ion-Implanted GaAs," in Ion Implantation in Semiconductors and Other Materials, edited by B. L. Crowder. New York: Plenum Press, 1973, pp. 641-654.

57. D. H. Lee, R. M. Malbon and J. M. Whelan, "Characteristics of Implanted N-type Profiles in GaAs Annealed in a Controlled Atmosphere," in Ion Implantation in Semiconductors 1976, edited by F. Chernow, J. A. Borders and D. K. Brice. New York: Plenum Press, 1977, pp. 115-122.

58. J. Kasahara, M. Arai and N. Watanabe, "Suppression of Thermal Conversion in Cr-Doped Semi-Insulating GaAs," J. Appl. Phys., vol. 50, pp. 8229-8231, 1979.

59. J. C. C. Fan, R. L. Chapman, J. P. Donnelly, G. W. Turner and C. O. Bozler, "Beam Annealing of Ion-Implanted GaAs and InP," in Laser and Electron-Beam Solid Interactions and Materials Processing, edited by J. F. Gibbons, L. D. Hess and T. W. Sigmon. New York: Elsevier North Holland, 1981, pp. 261-274.

60. J. L. Tandon and F. H. Eisen, "Pulsed Annealing of Implanted Semi-Insulating GaAs," in Laser-Solid Interactions and Laser Processing - 1978, edited by S. D. Ferris, H. J. Leamy and J. M. Poate, Conf. Proc. No. 50, American Institute of Physics, 1979, pp. 616-622.

61. S. S. Kular and B. J. Sealy, "Laser Annealing of Capped and Uncapped GaAs," Electron. Lett., vol. 15, pp. 413-414, 1979.

62. T. Yu, K. J. Soda and B. G. Streetman, "Annealing of Nitrogen-Implanted $GaAs_{1-x}P_x$ by a Swept Line Electron Beam," J. Appl. Phys., vol. 51, pp. 4399-4404, 1980.

63. N. J. Shah, H. Ahmed, I. R. Sanders and J. F. Singleton, "Activation of Low Dose Silicon Implants in GaAs by Multiply Scanned Electron Beams," Electron. Lett., vol. 16, pp. 433-434, 1980.

64. M. Kuzuhara, H. Kohzu and Y. Takayama, "Infrared Rapid Thermal Annealing of Si-Implanted GaAs," Appl. Phys. Lett., vol. 41, pp. 755-758, 1982.

65. R. L. Chapman, J. C. C. Fan, J. P. Donnelly, B-Y. Tsaur, "Transient Annealing of Selenium-Implanted Gallium Arsenide Using a Graphite Strip Heater," Appl. Phys. Lett., vol. 40, pp. 805-807, 1982.

66. K. V. Vaidyanathan, M. J. Helix, D. J. Wolford, B. G. Streetman, R. J. Blattner and C. A. Evans, Jr., "Study of Encapsulants for Annealing GaAs," J. Electrochem. Soc., vol. 124, pp. 1781-1784, 1977.

67. M. J. Helix, K. V. Vaidyanathan and B. G. Streetman, "Properties of Be-Implanted Planar GaAs p-n Junctions," IEEE J. Solid-State Circuits, vol. SC-13, pp. 426-429, 1978.

68. M. J. Helix, K. V. Vaidyanathan, B. G. Streetman, H. B. Dietrich and P. K. Chatterjee, "R.F. Plasma Deposition of Silicon Nitride Layers," Thin Solid Films, vol. 55, pp. 143-148, 1978.

69. Cameca Instruments Inc., Technical Information, 1979.

70. C. A. Evans, Jr., "Ion Probe Mass Spectrometry: Overview," Thin Solid Films, vol. 19, pp. 11-19, 1973.

71. M. L. Yu, "Work-Function Dependence of Negative-Ion Production during Sputtering," Phys. Rev. Lett., vol. 40, pp. 574-577, 1978.

72. C. A. Andersen, "Progress in Analytic Methods for the Ion Microprobe Mass Analyzer," Int. J. Mass. Spectrom. Ion Phys., vol. 2, pp. 61-74, 1969.

73. L. J. van der Pauw, "A Method of Measuring Specific Resistivity and Hall Effect of Discs of Arbitrary Shape," Philips Res. Repts., vol. 13, pp. 1-9, 1958.

74. W. V. McLevige, P. K. Chatterjee and B. G. Streetman, "Versatile Double A.C. Hall Effect System for Profiling Impurities in Semiconductors," J. Phys. E: Sci. Instrum., vol. 10, pp. 335-337, 1977.

75. D. R. Myers, "Properties of Silicon Implanted with Arsenic through Silicon Dioxide," Ph.D. thesis, U. of Illinois, 1977.

76. D. L. Kendall, "Diffusion," in Semiconductors and Semimetals, vol.4, edited by R. K. Willardson and A. C. Beer. New York: Academic Press, 1968, pp. 163-259.

77. P. K. Chatterjee, K. V. Vaidyanathan, W. V. McLevige and B. G. Streetman, "Photoluminescence from Be-Implanted GaAs," Appl. Phys. Lett., vol. 27, pp. 567-569, 1975.

78. W. V. McLevige, M. J. Helix, K. V. Vaidyanathan and B. G. Streetman, "Electrical Profiling and Optical Activation Studies of Be-Implanted GaAs," J. Appl. Phys., vol. 48, pp. 3342-3346, 1977.

79. T. Hirao, K. Inoue, S. Takayanagi and Y. Yaegashi, "Annealing Behaviors of Phosphorus Implanted in Silicon," in Ion Implantation in Semiconductors 1976, edited by F. Chernow, J. A. Borders and D. K. Brice. New York: Plenum Press, 1977, pp. 1-9.

80. J. A. Davies and P. Jespersgard, "Anomalous Penetration of Xenon in Tungsten Crystals--a Diffusion Effect," Can. J. Phys., vol. 44, pp. 1631-1638, 1966.

81. W. Rothemund and C. R. Fritzsche, "Radiation Damage in Ion-Implanted GaP and $GaAs_{0.6}P_{0.4}$," Appl. Phys. Lett., vol. 33, pp. 435-437, 1978.

82. L. A. Christel and J. F. Gibbons, "Stoichiometric Disturbances in Ion Implanted Compound Semiconductors," J. Appl. Phys., vol. 52, pp. 5050-5055, 1981.

# VITA

Siu Sing Chan attended the University of Illinois at Urbana-Champaign as an undergraduate in the Department of Electrical Engineering from Fall 1973 to Spring 1976. He graduated with a B.S. degree in Electrical Engineering with Highest Honors in May 1976 and was given the Bronze Tablet Award. He continued at the University of Illinois for his graduate work on ion implantation in semiconductors and obtained his M.S. degree in January, 1980. Currently he is a Ph.D. candidate in the Department of Electrical Engineering. Mr. Chan is a member of Tau Beta Pi and Eta Kappa Nu.